Self-Assembly of Brush Polymers

Thesis by
Benjamín Ragnar Sveinbjörnsson

In Partial Fulfillment of the Requirements for the degree
of
Doctor of Philosophy

CALIFORNIA INSTITUTE OF TECHNOLOGY
Pasadena, California
2014
Defended April 29th, 2014

ACKNOWLEDGEMENTS

First, I would like to thank my advisor, Professor Robert H. Grubbs, for the opportunity to do my graduate research within his group and for his guidance throughout my studies here at Caltech. I could not imagine a better advisor or a better group to work in. At times when I needed motivation to concentrate on chemistry, he provided great advice and help in finding the motivation again and developing strategies for keeping on track, and for that I am extremely grateful.

I would also like to thank my whole thesis committee, Professor David Tirrell, Professor Harry Gray, and Professor Dennis Dougherty. I have thoroughly enjoyed all of my meetings with them and appreciate the advice they have given me concerning both my research and future career.

I have had the pleasure of collaborating with many scientists, both here at Caltech and elsewhere, and I would like to thank the following for their collaborations on various projects: Dr. Garret Miyake, Raymond Weitekamp, Dr. Robert Macfarlane, Dr. Chris Bates, Dr. Yan Xia, Dr. Guangbin Dong, Melody Morris, Ricky Barz, Professor Harry A. Atwater, Dr. Laura Pavelka, Bingyin Jiang, Professor Robert B. Grubbs, Weiyin Gu, Gajin Jeong, Dr. Sung Woo Hong, Professor Thomas Russell, Dr. Lei Fang, and Professor Zhenan Bao. I would also like to thank Dr. David VanderVelde for NMR guidance and Dr. Mona Shahgholi and Naseem Torian for mass spectrometry analysis.

I've also enjoyed working with so many great people in the Grubbs group. Linda Syme has been really helpful with so many organizational aspects during my graduate career. I've overlapped with many great grad students, postdocs, and other group members during these past five years: Dr. Paul Clark, Dr. Jean Li, Dr. Chris Daeffler, Dr. Benjamin Keith Keitz, Dr. Matthew van Wingerden, Dr. Renee Thomas, Myles Herbert, Brendan Quigley, Zachary Wickens, Carl Blumenfeld, Nicholas Swisher, Anton Toutov, Julian Edwards, Lauren Rosebrugh, Alice Chang, Tonia Ahmed, Dr. A. J. Boydston, Alan Burts, Dr. Alexey Fedorov, Ali Sullivan, Dr. Bahar Bingol, Dr. Bill Morandi, Dr. Choon Woo Lee, Hidenori Someya, Hiroshi Miyazaki, Dr. Hoyong Chung, Dr. Ian Stewart, Dr. Jeff Cannon, Dr. Jeremiah Johnson, Dr. John Hartung, Dr. Josh Palmer, Dr. Keary Engle, Dr. Koji Endo, Dr. Melanie Pribisko Yen, Dr. Nanditha Nair, Dr. Pablo Guzman, Dr. Paresma Patel, Dr. Peili Teo, Dr. Peter Dornan, Dr. Rosemary Conrad, Dr. Sarah Bronner, Dr. Shane Mangold, Dr. Taek-soo Kim, Dr. Vanessa Marx, Dr. Victoria Piunova, Dr. Vincent LaVallo, Dr. Vlad Iluc, Dr. Weibin Li, Yong-Guen Yu, and Yusuke Hibi.

There are more invaluable people in the chemistry department that I would like to thank for their help through the years: Agnes Tong, Joe Drew, Scott Virgil, Anne Penney, Rick Gerhart, Anthony Solyom, and Steve Gould.

In grad school there have been times when the research has been quite tough and the results not what I was hoping for, and at times I have been temporarily lost concerning what went wrong and consequently bummed out. At those times there have been certain groups and friends that have been there for me to help brighten the day and help me re-energize in order to get back on track and keep going. For those times I would like to thank the following groups and all of my friends that I've met there: TACIT/EXPLiCIT, the Caltech Toastmasters, the JPL Rovers, and Vatnaskógur (efnafræðilega jafnast ekkert á við skúffukökurnar í Vatnaskógi). There are also certain friends here that have been especially supportive to me, and there have been times where it would have been really tough to keep going if it had not been for them: Dr. Amit Lakhanpal, Dr. Crystal Dilworth, and Teagan Wall, you all are amazing and I cannot thank you enough for having been there for me during those tough times! I also want to thank two of the coolest people I know, who I am privileged to call my friends: Marty Gibbons and Anne Hyvarinen.

Last but not least I would like to thank my family for their endless love, support, and understanding. Elsku mamma, pabbi, Guðlaug María, Davíð Örn, Fjóla Dögg og Salómon Blær. Þið eruð lang best í heimi og ég er ykkur óendanlega þakklátur fyrir þann skilning og stuðning sem að þið hafið sýnt mér þessi ár mín í doktorsnáminu. Ég get ekki þakkað ykkur nóg fyrir allt sem þið hafið gert fyrir mig, hvort sem það er að hlusta á röfl í mér, lesa yfir hitt og þetta, eða bara spila og/eða kjafta saman um hitt og þetta, bæði á Skype og þegar við höfum getað eytt tíma með hvoru öðru. Ég elska ykkur öll ótrúlega mikið og bið Guð um áframhaldandi blessun fyrir ykkur öll!

ABSTRACT

The unique structure and properties of brush polymers have led to increased interest in them within the scientific community. This thesis describes studies on the self-assembly of these brush polymers.

Chapter 2 describes a study on the rapid self-assembly of brush block copolymers into nanostructures with photonic bandgaps spanning the entire visible spectrum, from ultraviolet to near infrared. Linear relationships are observed between the peak wavelengths of reflection and polymer molecular weights. This work enables "bottom-up" fabrication of photonic crystals with application-tailored bandgaps, through synthetic control of the polymer molecular weight and the method of self-assembly.

Chapter 3 details the analysis of the self-assembly of symmetrical brush block copolymers in bulk and thin films. Highly ordered lamellae with domain spacing ranging from 20 to 240 nm are obtained by varying molecular weight of the backbone. The relationship between degree of polymerization and the domain spacing is reported, and evidence is provided for how rapidly the brush block copolymers self-assemble and achieve thermodynamic equilibrium.

Chapter 4 describes investigations into where morphology transitions take place as the volume fraction of each block is varied in asymmetrical brush block copolymers. Imaging techniques are used to observe a transition from lamellar to a cylindrical morphology as the volume fraction of one of the blocks exceeds 70%. It is also shown that the asymmetric brush block copolymers can be kinetically trapped into undulating lamellar structures by drop casting the samples.

Chapter 5 explores the capability of macromolecules to interdigitate into densely grafted molecular brush copolymers using stereocomplex formation as a driving force. The stereocomplex formation between complementary linear polymers and brush copolymers is demonstrated, while the stereocomplex formation between complementary brush copolymers is shown to be restricted.

TABLE OF CONTENTS

Chapter 1

INTRODUCTION

BRUSH POLYMERS

Assemblies of polymer chains that are bound by one end to planar or spherical surfaces, or bound to linear polymer chains, are referred to as polymer brushes.[1] When the polymer side chains are bound to a linear polymer the steric crowding of the side chains forces the polymer backbone to be more extended, resulting in a cylindrical worm-like structure[1,2] that can reach lengths up to a few hundred nanometers.[3–6] These polymers also show little evidence of any entanglement even at ultra-high molecular weights. The structural characteristics of brush polymers has led to increased interest in their utilization for applications such as drug delivery,[7,8] templates for inorganic particles,[9–11] molecular actuators,[12] and as precursors for various carbon nanostructures.[13,14]

There are three general methods of synthesizing brush polymers: the "grafting from", the "grafting onto", and the "grafting through", or the macromonomer (MM) approach (**Figure 1-1**).[15] In the "grafting from" method, the side chains are polymerized from initiators sites on the polymeric backbone.[16–18] This method provides good control of main chain polydispersity (PDI), but gives only intermediate control over the side chain PDI and the grafting density due to the high density of initiation sites on the backbone.[19–21] In the "grafting onto" method, the polymer side chains are coupled onto the polymer backbone.[15,22–24] This method allows for good main chain PDI and side chain PDI, but lacks control over the grafting density due to growing steric difficulties for the side chains to access and couple to the backbone as the conversion increases.[19,25] In the "grafting through" or MM approach, the side chains are synthesized with a polimerizable end group, which is then polymerized to make the brush polymer.[26,27] This method provides good side chain PDI and guarantees complete grafting of the polymer. However, some polymerization methods lack good control over the main chain length and PDI with this approach.[19] Recent studies have shown that ruthenium catalyzed ring-opening metathesis polymerization (ROMP) of norbornene end functionalized MMs can help overcome the limitations of the MM approach, and has been used to yield brush polymers with excellent PDI values (<1.10) while reaching ultra-high molecular weights (MWs) (up to 1880×10^3 g/mol).[3,28]

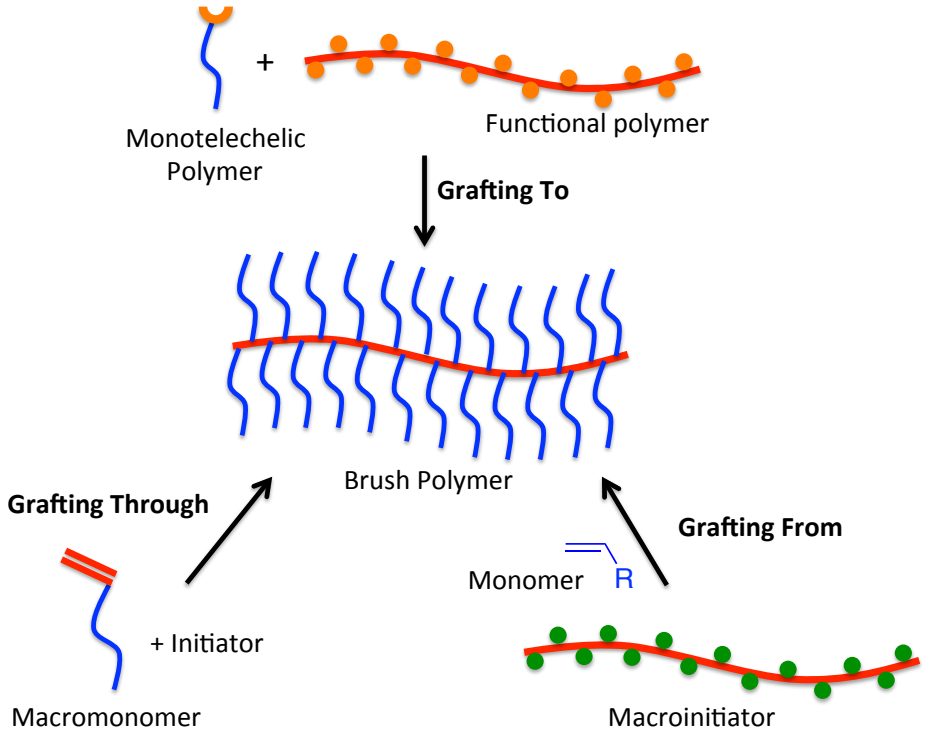

Figure 1-1. Schematic illustration of the three pathways to synthesizing brush polymers.

OLEFIN METATHESIS

Olefin metathesis is an extremely versatile and well-reviewed reaction where a carbon-carbon double bond undergoes scission and rearrangement (**Scheme 1-1**).[29] The development of efficient catalysts has led to the widespread use of this reaction for applications such as insect pheromones, waxes, plasticizers, and baseball bats.[30,31]

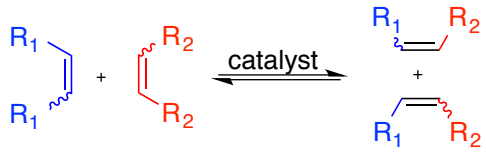

Scheme 1-1. A general scheme for olefin metathesis.

The mechanism of olefin metathesis starts with an olefin coordinating to the metal carbene complex, followed by a [2+2] cycloaddition with the metal carbene double bond to yield a metalla cyclobutane. Next, a cycloreversion takes place, where cleavage of the newly formed bonds results

in the starting material, but the cleavage of the other two bonds in the metallocyclobutane yields a new olefin coordinated to a new metal carbene. The newly formed olefin can then dissociate from the metal center to give the desired product and a new metal carbene that can re-enter the catalytic cycle **(Scheme 1-2)**.

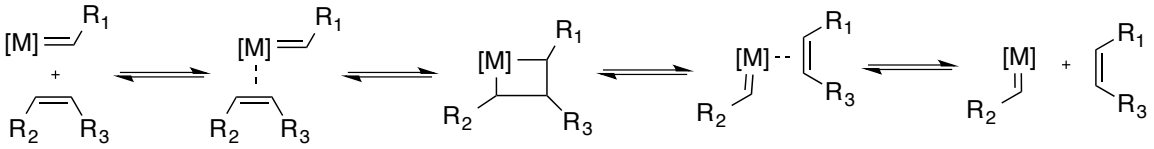

Scheme 1-2. A general scheme for the mechanism of olefin metathesis.

Depending on the chemical structure of the desired product, several types of olefin metathesis reactions are possible. When building small molecules, the main types of metathesis used are cross metathesis (CM), ring-closing metathesis (RCM), and ring-opening cross metathesis (ROCM) (**Figure 1-2**). In cross metathesis, two terminal alkenes undergo transalkylidenation to yield the desired product and ethylene. Ring-closing metathesis involves an α,ω-diolefin that closes to form a ring, usually releasing ethylene in the process. Ring-opening cross metathesis involves a cyclic olefin that reacts with a linear olefin to open up the ring.

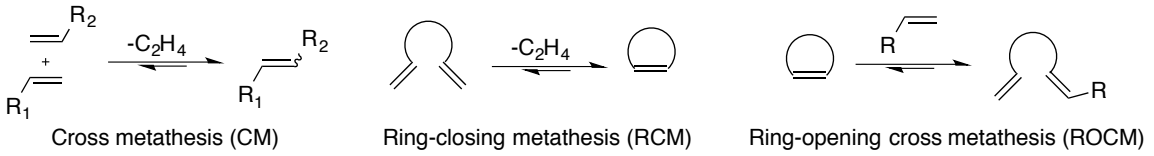

Figure 1-2. General reaction schemes for cross metathesis (left), ring-closing metathesis (center), and ring-opening cross metathesis (right).

Olefin metathesis has also proven effective in synthesizing polymers via either acyclic diene metathesis polymerization (ADMET) or the previously mentioned ROMP (**Figure 1-3**). In ADMET a diene undergoes repeated cross metathesis to give the polymer in a step polymerization. ADMET reactions are generally run under conditions of high concentration and often involve the active removal of ethylene. ROMP, on the other hand, is a chain polymerization, where the catalyst acts as an initiator for the polymerization. It is similar to ROCM, where a cyclic olefin is opened, but instead of reacting with a linear alkene to release the molecule from the catalyst, the newly opened ring reacts with another cyclic olefin to grow a polymer chain.

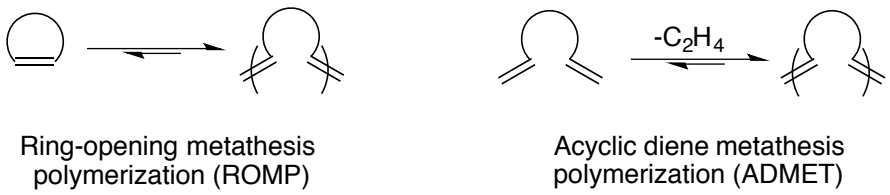

Figure 1-3. General reaction schemes for ring-opening metathesis polymerization (left) and acyclic diene metathesis polymerization (right).

In order to obtain well defined, narrowly dispersed polymers with high molecular weights via ROMP, it is important that the catalyst used exhibits both fast initiation and high reactivity. Since MMs are challenging monomers, this has been especially important when attempting to synthesize brush polymers via ROMP. Recently, it was found that the bis-pyridine derivative of the second generation Grubbs catalyst[32] (**Figure 1-4**) shows fast initiation, high reactivity, and high functional group tolerance, even in the ROMP of MMs, making it a pivotal tool to advance our studies of brush polymers and their self-assembly.[3,28,33]

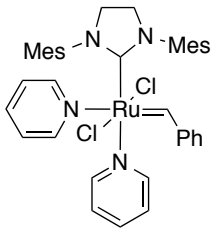

Figure 1-4. The chemical structure of the bis-pyridine derivative of the second-generation Grubbs catalyst.

BRUSH COPOLYMER SELF-ASSEMBLY

Utilizing the highly reactive and fast-initiating bis-pyridine derivative of the second-generation Grubbs catalyst, Xia *et al.* started exploring the self-assembly of both random and block brush copolymers (**Figure 1-5**) using small-angle X-ray scattering (SAXS) and atomic force microscopy (AFM).[3] The brush copolymers used were synthesized from poly lactide (PLA) and poly (*n*-butyl acrylate) (P*n*BA) based MMs.

The brush random copolymers showed close to identical domain spacing (as measured by SAXS) regardless of the degree of polymerization (DP) of the backbone, suggesting a microphase

segregation of the side chains, with the poly norbornene backbone localized at the interface between the PLA and P*n*BA domains (**Figure 1-6 top**).[3]

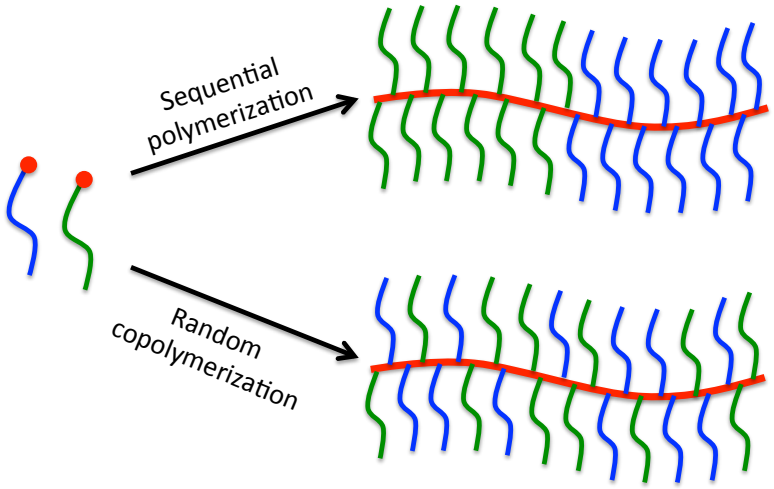

Figure 1-5. Schematic illustration of a block brush copolymer (top) and a brush random copolymer (bottom) synthesized from MMs.

The brush block copolymers (BCPs), on the other hand, showed the domain spacing to be dependent on the backbone length. The observed length was close to the expected length given a fully extended backbone. It was inferred from these results that the brush BCPs gave interdigitated packing of the polymers in a lamellar structure (**Figure 1-6 bottom**). Furthermore, Xia *et al.* found that these brush BCPs could reach domain spacing large enough to reflect visible light.[3]

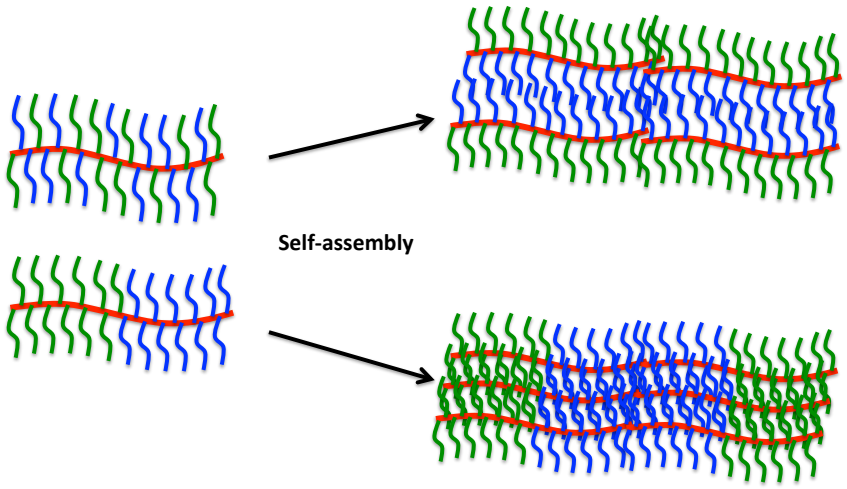

Figure 1-6. Proposed self-assembly of a brush random copolymer (top) and a brush block copolymer (bottom).

This thesis describes further studies on the self-assembly of brush polymers. *Chapter 2* discusses the self-assembly of brush BCPs into tunable photonic crystals that reflect light from the ultraviolet (UV) region and into the near infrared (NIR) region.[34] *Chapter 3* reports on studies on the self-assembly of symmetrical brush BCPs in bulk and thin films.[35,36] These studies were done in collaboration with the Russell group at University of Massachusetts - Amherst, where we synthesized all the materials and they conducted the SAXS measurements and the imaging of the self-assembled samples. *Chapter 4* describes initial investigations on the self-assembly of asymmetrical brush BCPs. Finally, *Chapter 5* discusses studies on the capability of macromolecules to interdigitate into densely grafted brush copolymers using stereocomplexation as a driving force for the macromolecule/brush copolymer interactions.[37]

REFERENCES:

(1) Zhang, M.; Müller, A. H. E. *J. Polym. Sci. Part A Polym. Chem.* **2005**, *43*, 3461.

(2) Sheiko, S. S.; Möller, M. *Chem. Rev.* **2001**, *101*, 4099.

(3) Xia, Y.; Olsen, B. D.; Kornfield, J. A.; Grubbs, R. H. *J. Am. Chem. Soc.* **2009**, *131*, 18525.

(4) Runge, M. B.; Bowden, N. B. *J. Am. Chem. Soc.* **2007**, *129*, 10551.

(5) Runge, M. B.; Lipscomb, C. E.; Ditzler, L. R.; Mahanthappa, M. K.; Tivanski, A. V.; Bowden, N. B. *Macromolecules* **2008**, *41*, 7687.

(6) Rzayev, J. *Macromolecules* **2009**, *42*, 2135.

(7) Johnson, J. A.; Lu, Y. Y.; Burts, A. O.; Xia, Y.; Durrell, A. C.; Tirrell, D. A.; Grubbs, R. H. *Macromolecules* **2010**, *43*, 10326.

(8) Johnson, J. A.; Lu, Y. Y.; Burts, A. O.; Lim, Y.; Finn, M. G.; Koberstein, J. T.; Turro, N. J.; Tirrell, D. A.; Grubbs, R. H. *J. Am. Chem. Soc.* **2011**, *133*, 559.

(9) Zhang, M.; Estournès, C.; Bietsch, W.; Müller, A. H. E. *Adv. Funct. Mater.* **2004**, *14*, 871.

(10) Djalali, R.; Li, S.-Y.; Schmidt, M. *Macromolecules* **2002**, *35*, 4282.

(11) Zhang, M.; Drechsler, M.; Muller, A. H. E. *Chem. Mater.* **2004**, *16*, 537.

(12) Li, C.; Gunari, N.; Fischer, K.; Janshoff, A.; Schmidt, M. *Angew. Chem. Int. Ed.* **2004**, *43*, 1101.

(13) Huang, K.; Rzayev, J. *J. Am. Chem. Soc.* **2009**, *131*, 6880.

(14) Cheng, C.; Qi, K.; Khoshdel, E.; Wooley, K. L. *J. Am. Chem. Soc.* **2006**, *128*, 6808.

(15) Hadjichristidis, N.; Pitsikalis, M.; Pispas, S.; Iatrou, H. *Chem. Rev.* **2001**, *101*, 3747.

(16) Beers, K. L.; Gaynor, S. G.; Matyjaszewski, K.; Sheiko, S. S.; Moller, M. *Macromolecules* **1998**, *31*, 9413.

(17) Börner, H. G.; Beers, K.; Matyjaszewski, K.; Sheiko, S. S.; Möller, M. *Macromolecules* **2001**, *34*, 4375.

(18) Cheng, G.; Böker, A.; Zhang, M.; Krausch, G.; Muller, A. H. E. *Macromolecules* **2001**, *34*, 6883.

(19) Neiser, M. W.; Okuda, J.; Schmidt, M. *Macromolecules* **2003**, *36*, 5437.

(20) Neugebauer, D.; Sumerlin, B. S.; Matyjaszewski, K.; Goodhart, B.; Sheiko, S. S. *Polymer* **2004**, *45*, 8173.

(21) Sumerlin, B. S.; Neugebauer, D.; Matyjaszewski, K. *Macromolecules* **2005**, *38*, 702.

(22) Deffieux, A.; Schappacher, M. *Macromolecules* **1999**, *32*, 1797.

(23) Schappacher, M.; Deffieux, A. *Science* **2008**, *319*, 1512.

(24) Schappacher, M.; Deffieux, A. *Macromolecules* **2005**, *38*, 7209.

(25) Gao, H.; Matyjaszewski, K. *J. Am. Chem. Soc.* **2007**, *129*, 6633.

(26) Rizmi, A. C. M.; Khosravi, E.; Feast, W. J.; Mohsin, M. A.; Johnson, A. F. *Polymer* **1998**, *39*, 6605.

(27) Heroguez, V.; Breunig, S.; Gnanou, Y.; Fontanille, M. *Macromolecules* **1996**, *29*, 4459.

(28) Xia, Y.; Kornfield, J. A.; Grubbs, R. H. *Macromolecules* **2009**, *42*, 3761.

(29) Trnka, T. M.; Grubbs, R. H. *Acc. Chem. Res.* **2001**, *34*, 18.

(30) Giardello, M. New Developments in the Commercialization of Olefin Metathesis Technology http://www.isom17.com/summaries/Giardello, Mike-ISOM XVII.pdf (accessed Apr 10, 2014).

(31) Herbert, M. B.; Marx, V. M.; Pederson, R. L.; Grubbs, R. H. *Angew. Chem. Int. Ed.* **2013**, *52*, 310.

(32) Sanford, M. S.; Love, J. A.; Grubbs, R. H. *Organometallics* **2001**, *20*, 5314.

(33) Love, J. A.; Morgan, J. P.; Trnka, T. M.; Grubbs, R. H. *Angew. Chem. Int. Ed.* **2002**, *41*, 4035.

(34) Sveinbjörnsson, B. R.; Weitekamp, R. A.; Miyake, G. M.; Xia, Y.; Atwater, H. A.; Grubbs, R. H. *Proc. Natl. Acad. Sci. USA* **2012**, *109*, 14332.

(35) Gu, W.; Huh, J.; Hong, S. W.; Sveinbjornsson, B. R.; Park, C.; Grubbs, R. H.; Russell, T. P. *ACS Nano* **2013**, *7*, 2551.

(36) Hong, S. W.; Gu, W.; Huh, J.; Sveinbjornsson, B. R.; Jeong, G.; Grubbs, R. H.; Russell, T. P. *ACS Nano* **2013**, *7*, 9684.

(37) Sveinbjornsson, B. R.; Miyake, G. M.; El-Batta, A.; Grubbs, R. H. *ACS Macro Lett.* **2014**, *3*, 26.

C h a p t e r 2

BRUSH POLYMER APPLICATIONS: PHOTONIC CRYSTALS

Reproduced in part with permission from:
Sveinbjörnsson, B. R.; Weitekamp, R. A.; Miyake, G. M.; Xia, Y.; Atwater, H. A.; Grubbs, R. H. *Proc. Natl. Acad. Sci. U.S.A.* **2012**, *109*, 14332-14336.

ABSTRACT

This chapter describes a study on the self-assembly of brush block copolymers into photonic crystals. The reduced chain entanglement of brush polymers over their linear analogs drastically lowers the energetic barriers to reorganization. Herein, the rapid self-assembly of brush block copolymers to nanostructures with photonic bandgaps spanning the entire visible spectrum, from ultraviolet (UV) to near infrared (NIR), is demonstrated. Linear relationships were observed between the peak wavelengths of reflection and polymer molecular weights. This work enables "bottom-up" fabrication of photonic crystals with application-tailored bandgaps through synthetic control of the polymer molecular weight and the method of self-assembly. These polymers could be developed into NIR-reflective paints to combat the "urban heat island effect" due to NIR photon thermalization.

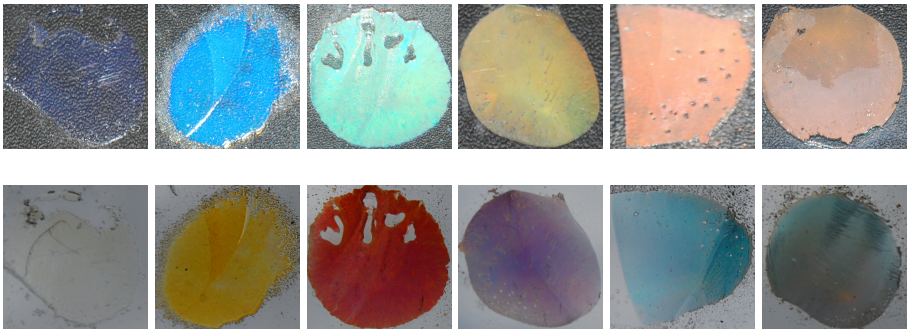

INTRODUCTION

The self-assembly of block copolymers (BCPs) into a variety of morphologies,[1–4] as well as their potential to selectively incorporate additives,[5] has earned them increased interest for many applications, including construction of photonic crystals. Photonic crystals are materials with periodic structures of different refractive indices, resulting in reflection of specific ranges of electromagnetic waves, thus creating a photonic band gap.[6,7] In order to tune these materials for specific purposes, such as for optical materials, telecommunications, and in the energy field, it is important to be able to control the range of the light these materials reflect. IR-reflecting materials are of special appeal for energy conservation purposes, since there is a substantial amount of thermal energy in IR light and these materials could therefore be used, e.g. in window coatings to reduce energy costs.[8–10] Photonic crystals are also seen in nature, contributing to the colors of butterfly wings, bird feathers, and opals.[6] The ability to synthetically mimic these properties is therefore of fundamental interest.

Despite their desirability, critical challenges must be addressed before BCPs can be broadly utilized as photonic crystals. Obtaining BCPs with the large domain sizes required to reflect the wavelengths of interest is a critical limitation.[9,11,12] The high molecular weights required make the synthesis of these polymers difficult, and chain entanglement also retards the self-assembly process. To the best of our knowledge, the self-assembly of linear BCPs has not yet been used successfully to form photonic crystals that can reach far into the visible spectra without the need for additional techniques, such as swelling the material with additives, including small molecules, inorganic nanoparticles, or other polymers.[5,8,9,12–14] While other approaches, such as layer-by-layer stacking,[15,16] electrochemical etching,[17,18] laser-beam-scanning chemical vapor deposition,[19] holographic lithography,[20,21] and self-assembly of monodisperse colloidal particles,[22,23] have been used successfully to yield well-defined photonic crystals, these methods often require expensive apparatus and complex processes.

However, brush polymers have recently shown potency as a platform material for photonic crystals. High molecular weight brush BCPs have been shown to self-assemble into domain sizes of over 100 nm,[24–28] as well as self-assembling into photonic material reflecting blue and even green light.[25,27,28] The steric crowding of the side chains forces the main chain to be in an extended conformation, yielding cylindrical structures.[29] Brush polymers also show less entanglement

compared to their linear analogs, resulting in rapid self-assembly.[28,30] In this chapter, we describe a successful approach to synthesizing brush BCPs, and fabricate them in a simple manner into an array of well-controlled photonic crystals that reflect wavelengths into the NIR region.

RESULTS AND DISCUSSION

In order to find a convenient model system to work with, a variety of different macromonomer (MM) systems were tested to observe roughly what degrees of polymerizations would be required for the brush BCPs to reflect light in the visible region. All the polymers used were based on MMs with a norbornene (NB) backbone that was polymerized via ring-opening metathesis polymerization (ROMP) using a ruthenium-based catalyst (**Figure 2-1**). The side chains of the different systems used were (1) polylactide (PLA) ($M_w \approx 4.4 \times 10^3$ g/mol) and a dodecanyl group (C12), (2) PLA ($M_w \approx 4.4 \times 10^3$ g/mol) and a "wedge" side chain, (3) poly *tert*-butyl acrylate (P*t*BA) and polystyrene (PS) side chains ($M_w \approx 5.1 \times 10^3$ g/mol), and (4) PLA ($M_w \approx 4.4 \times 10^3$ g/mol) and PS side chains ($M_w \approx 5.1 \times 10^3$ g/mol).

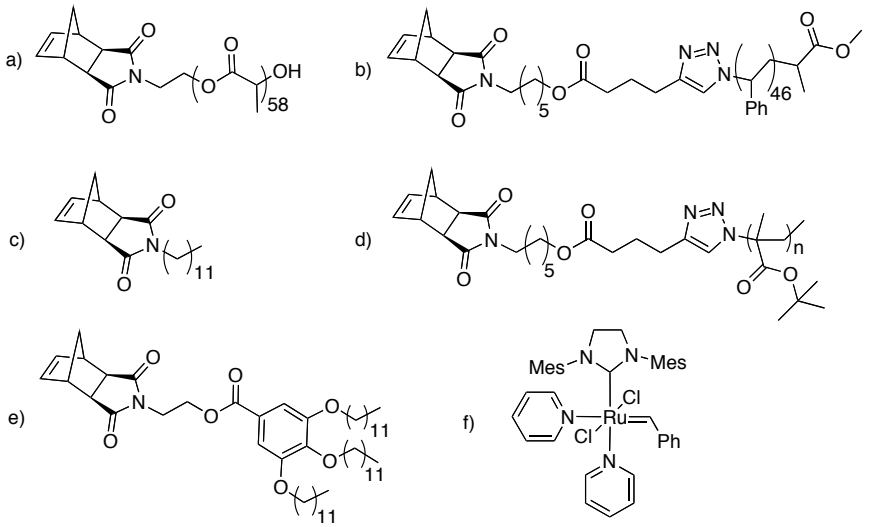

Figure 2-1. Chemical structure of the macromonomers tested and the catalyst used: a) Norbornene-polylactide (NB-PLA), b) norbornene-polystyrene (NB-PS), c) dodecanyl norbornene (NB-C12), d) norbornene *tert*-butyl acrylate (NB-*t*BA), e) norbornene wedge (NB-wedge), and f) ruthenium based metathesis catalyst used in ring-opening metathesis polymerizations.

The different combinations of MMs were copolymerized in various ratios, mainly asymmetrical, but in the case of the NB-tPBA/NB-PS as well as the NB-PLA/NB-PS copolymerizations, the MMs were also copolymerized in symmetrical ratios (**Table 2-1**).

Table 2-1. Preliminary tests of several combinations of macromonomers.

Test #	Side chain A	Side chain B	A:B:catalyst ratio	Observed color
1	PLA	C12	200:1000:1	Dark blue
2	PLA	C12	200:1500:1	Light blue
3	PLA	C12	200:2000:1	-
4	PLA	Wedge	200:1000:1	Blue
5	PLA	Wedge	200:2000:1	Green
6	PLA	PS	400:200:1	Dark blue
7	PLA	PS	400:400:1	Green
8	PtBA	PS	400:400:1	-

After the ROMP, the samples were purified, dried, and isolated as white solids. Then they were annealed by controlled evaporation from tetrahydrofuran (THF) or dichloromethane (DCM) to yield colored films. In most of the cases the color was easily observed (**Figure 2-2**), but the copolymerization of PLA and PS, which reached green color when polymerized at a ratio of 400:400:1 (PLA:PS:catalyst), was deemed the most convenient system to use for a more detailed study.

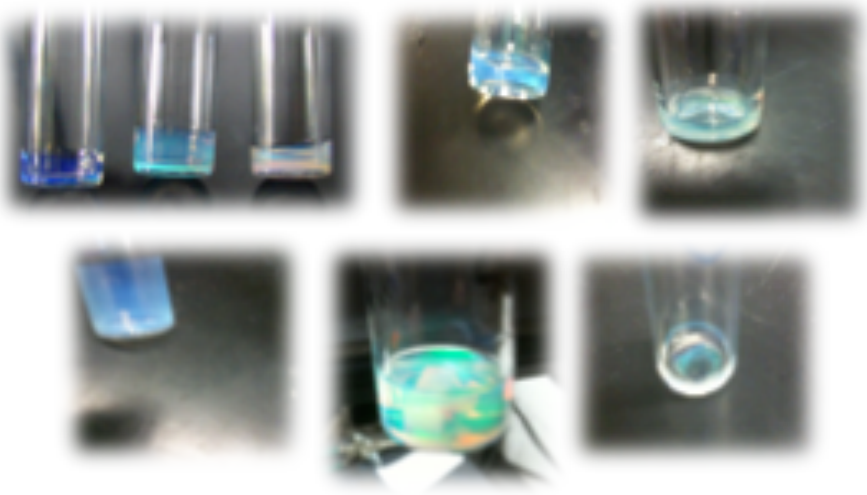

Figure 2-2. Images of the preliminary tests of self-assembled brush block copolymers from Table 2-1: Entries #1-3 are shown from left to right (top left), as well as entry #4 (top center), entry #5 (top right), entry #6 (bottom left), entry #7 (bottom center), and entry #8 (bottom right).

The racemic PLA and PS based MMs employed in this study were synthesized from *exo*-norbornene functionalized initiators, suited for the ring opening polymerization of lactide and the controlled radical polymerization of styrene. The MMs were synthesized with similar molecular weights (MWs) and narrow polydispersity indices (PDIs) (PLA: $M_n = 6.1 \times 10^3$ g/mol, PDI = 1.20; PS: $M_n = 5.7 \times 10^3$ g/mol, PDI = 1.02). More importantly, the advantageous characteristics (*i.e.* livingness, stability, functional group, and steric tolerance) of Ru-mediated ROMP enabled the sequential polymerization of the MMs to brush BCPs in high yields with controlled MWs and narrow MWDs (**Figure 2-3**). The MW of the brush BCPs were controlled by the MM to Ru ratio, and ranged from 1.08×10^6 to 6.64×10^6 g/mol, while maintaining relatively narrow MWDs (PDI = 1.07-1.58) considering the ultra-high MWs, highlighting the robustness of ROMP. For this study, we targeted blocks with near equal weight ratios with the goal of achieving lamellar nanostructures (**Table 2-2**).

Table 2-2. Molecular weight information about the (polynorbornene-*g*-polystyrene)-*b*-(polynorbornene-*g*-polylactide) polymer series. a) The molar ratios used in the synthesis of these brush block copolymers of the catalyst (C) and the MMs. b) Molecular weight and polydispersity indices as measured by GPC. c) Approximation of the size of each block as calculated using NMR and GPC results (discussed later).

Sample	C:PLA:PS [a]	$M_{n,theo}$ ($\times 10^6$ g/mol)	M_n ($\times 10^6$ g/mol)[b]	PDI (M_w/M_n)[b]	DP PLA [c]	DP PS [c]
A	1:74:78	0.90	1.08	1.07	84	98
B	1:99:105	1.20	1.53	1.09	116	142
C	1:126:132	1.52	1.99	1.12	153	182
D	1:136:144	1.65	2.38	1.22	187	215
E	1:135:142	1.63	2.68	1.16	206	246
F	1:150:158	1.81	2.94	1.17	225	271
G	1:157:166	1.90	3.19	1.26	246	292
H	1:174:183	2.10	3.32	1.29	252	309
I	1:198:210	2.40	4.02	1.34	289	391
J	1:223:237	2.71	4.21	1.36	319	391
K	1:246:262	2.99	5.80	1.5	436	543
L	1:273:288	3.30	6.64	1.58	497	624

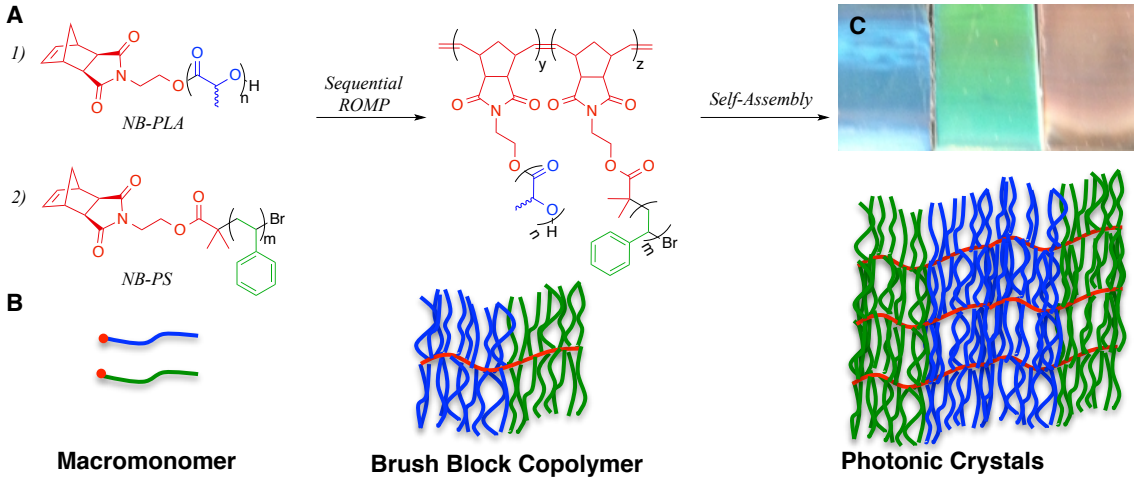

Figure 2-3. (**A**) PS and PLA based MMs were sequentially polymerized by ROMP to brush BCPs. (**B**) A schematic representation depicts the brush BCPs, and their assembly into ordered lamellar nanostructures. (**C**) Different annealing techniques render unique photonic crystals for the same brush BCP, as shown in this photograph.

After preparing a series of well-defined brush BCPs with a broad range of MWs, we investigated a number of simple self-assembly methods to yield thin, solid films. Our annealing methods included controlled evaporation from DCM and THF solutions, before and after thermal annealing, as well as direct thermal annealing of the solid polymer powder under compression between two glass substrates. The drastic effect of the assembly method on the resulting nanostructures is most starkly visualized by a single brush BCP (M_n = 2.94 × 10^6 g/mol), which appeared blue when cast from DCM, green when cast from THF, and red after thermally annealing of the green film cast from THF (**Figure 2-4**). Quantitative reflection measurements were performed on a spectrophotometer equipped with an 'integrating sphere' diffuse reflectance accessory. The reflection spectra confirm the large differences between samples prepared by different annealing procedures (**Figure 2-4A**). For the sample shown in **Figure 2-4**, the first (longest wavelength) peak of reflection shifts by hundreds of nanometers, depending on the method of film preparation. The difference in color is not due to residual solvent; the films were completely dry and we did not observe any color change upon placing a sample in high vacuum for more than 50 hours.

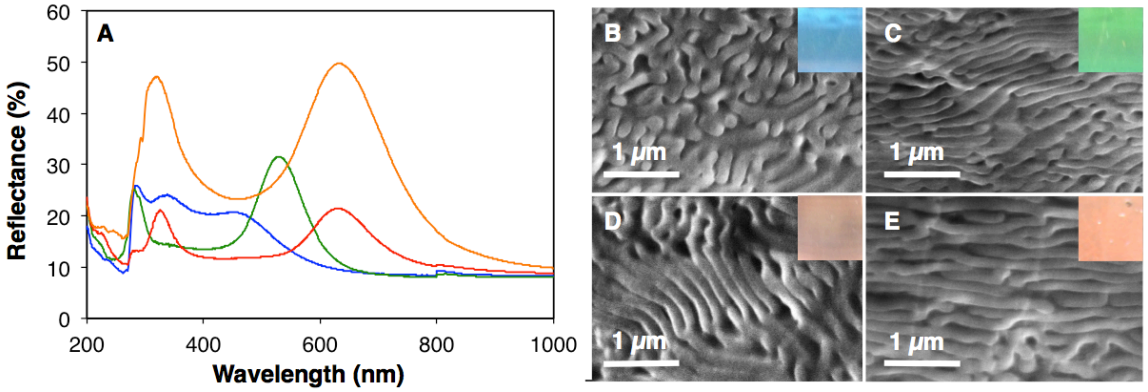

Figure 2-4. (**A**) Reflection spectra are plotted for the brush BCP (M_n = 2.94 × 10^6 g/mol) films prepared from the controlled evaporation from DCM (blue), or THF, before (green), and after (red) thermal treatment, as well as via thermal annealing under compression (orange). SEM cross-sections reveal the morphology of the middle of the brush BCP films prepared from the controlled evaporation from DCM (**B**), THF before (**C**) and after (**D**) thermal annealing, as well as by direct thermal annealing under compression (**E**). The insets show photographs of each sample.

Scanning electron micrograph (SEM) cross-sections were used to directly image the film morphologies to further investigate causes of the observed reflection spectra. Although the thermally annealed samples must be composed of larger domain sizes than the films prepared via controlled evaporation (as suggested by the greater λ_{max}), we were curious as to why the film cast from DCM provided the markedly altered reflection spectra. SEM images provided insight into the self-assembly of the films from different techniques, clearly visualizing the polymer morphologies and domain sizes (**Figure 2-4 B-E**). For this polymer, all of the films, except those prepared from DCM, showed the expected stacked lamellar morphology for symmetric BCPs. In the case of the film cast from DCM, a disordered morphology was observed in the SEM image. The evaporative self-assembly process is dictated by a number of factors, including the kinetics of evaporation, quality of solvent, PS/PLA interaction parameters, as well as the energetics of the glass/polymer interface. For many samples, the degree of lamellar order decreased as a function of distance from the glass interface. For BCPs with approximately equal volume fractions, the lamellar morphology is the most thermodynamically stable, as it minimizes the interfacial surface energy between the two constituent polymers. THF afforded larger and better ordered domains than DCM, which we attribute to the fact that it is a good solvent for this copolymer system,[31] as well as to its decreased volatility, which allows improved chain mobility to rearrange during evaporation before all the chains enter the glassy state once all solvent is removed. After thermal annealing, these samples become more ordered, with larger domain sizes, as observed in the SEMs and evidenced by the

reflection spectra. Films that were directly thermally annealed from dry polymer powder also formed well-ordered lamellae with long wavelength reflection. The improved reflection coefficient is a consequence of film thickness.

We observed the first order peak of reflection to be a linear function of MW, for all of the self-assembly techniques employed. This is in contrast to a corresponding linear copolymer system, where the domain spacing is proportional to $MW^{0.81}$.[32] Because the peak wavelength and domain spacing are directly related by the equation $\lambda_{max} = 2(n_1x_1 + n_2x_2)$,[9] our results suggest that the brush BCPs studied yield a larger increase in domain spacing per monomer incorporated than a corresponding linear system. Given the high persistence lengths of these brush polymers,[33] we rationalize this observation in terms of the degree of backbone extension enforced by the steric congestion of the brushes. Thus, the brush polymer architecture enables both a large equilibrium scaling for self-assembled structures as well as a very fast equilibration rate, due to the significantly reduced chain entanglement (even at ultra high MW).

Direct thermal annealing of the polymer powders under compression proved to be the most successful assembly technique, in that it enabled ultra-high MW polymers to reach ordered nanostructures with photonic crystal characteristics at NIR wavelengths (**Figure 2-5 E-F**). By contrast, in the case of controlled evaporation, most of the high molecular weight polymers ($M_n > 3 \times 10^6$ g/mol) did not assemble into films with distinct Bragg reflection peaks. The unmatched structural order achieved through thermal annealing is highlighted by the fact that the ultra-high MW polymers possessed photonic bandgaps well into the NIR (up to λ_{max} = 1311 nm), an unprecedented wavelength regime for unswelled BCP photonic crystals. Furthermore, the low energetic barriers to reorganization enable the application of any BCP self-assembly technique to our system to achieve improved lamellar order and optical performance. As NIR dielectric mirrors, these robust solid-state photonic crystals enable a host of exciting applications for BCPs to telecommunications and thermal radiation management.

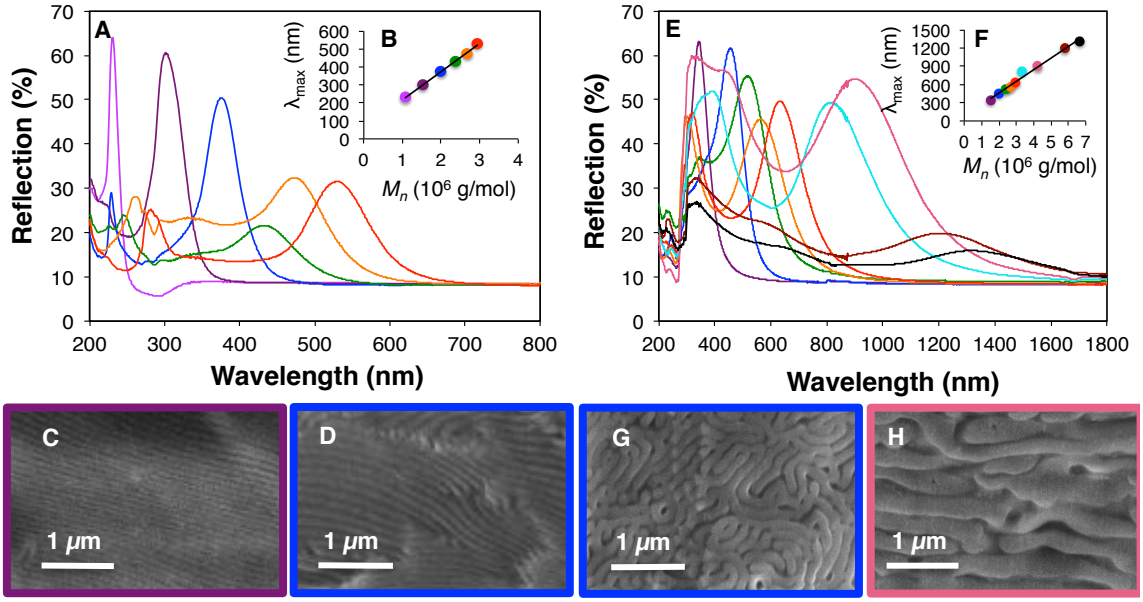

Figure 2-5. (**A**) Reflectance is plotted as a function of wavelength for the films prepared from the controlled evaporation from THF for several different MW polymers. (**B**) λ_{max} is plotted against MW for films prepared from the controlled evaporation of THF. SEM cross-sections are shown for the middle of BCP films with $M_n = 1.53 \times 10^6$ g/mol. Linear fit $R^2 = 0.997$. (**C**) and $M_n = 1.99 \times 10^6$ g/mol (**D**) prepared from the controlled evaporation of THF. (**E**) Reflectance is plotted as a function of wavelength for the films prepared by thermal annealing under compression for several different MW polymers. (**F**) λ_{max} is plotted against MW for films prepared by thermal annealing under compression. SEM cross-sections are shown for the middle of BCP films with $M_n = 1.99 \times 10^6$ g/mol. Linear fit $R^2 = 0.984$. (**G**) and $M_n = 4.21 \times 10^6$ g/mol (**H**) prepared by thermal annealing under compression.

To justify the proposed mechanism of the observed reflection spectra, transfer matrix simulations have been employed to model the reflection spectra of the polymer photonic crystals. Additionally, angle dependent reflection spectra of a well-ordered sample were measured and compared with one-dimensional transfer matrix simulations. Comparison of the experimental data with the simulations showed good agreement and strongly suggested that the observed lamellar nanostructures consist of alternating polymer layers, which represent pseudo-1D photonic crystals.[34]

CONCLUSION

In conclusion, the rapid self-assembly of high-molecular weight brush polymers was shown to work as a facile method for generating ordered nanostructures with large domain sizes, specifically pseudo-1D photonic crystals. The reduced chain entanglement of brush BCPs enables assembly of large nanostructures that reflect long wavelength light without the use of any additives. The linear trend of λ_{max} as a function of MW enables one to synthetically "dial-in" dielectric mirrors with first

order peaks spanning from the UV to NIR. We envision that materials produced through this approach have potential as NIR-reflecting building materials, for use in inhibiting the thermalization of NIR radiation in urban environments. Moreover, the functional flexibility of our approach enables a host of new directions for functional, compliant, and stimuli-responsive photonic elements.

SUPPORTING INFORMATION

Materials

$(H_2IMes)(pyr)_2(Cl)_2RuCHPh$[35] and *N*-(hydroxyethanyl)-*cis*-5-norbornene-*exo*-2,3-di-carboximide[36] were prepared as described previously. All solvents were purchased from VWR or Sigma-Aldrich. Ruthenium tetroxide was purchased form Acros Organics. Ruthenium-based metathesis catalyst was obtained from Materia Inc. and stored in a drybox. Other chemicals were bought from Sigma-Aldrich. Dry solvents were purified by passing them through solvent purification columns. 3,6-dimethyl-1,4-dioxane-2,5-dione was purified by sublimation under vacuum. All other solvents and chemicals were used without further purification unless otherwise stated.

General information

NMR spectra were recorded at room temperature on a Varian Inova 500 (at 500 MHz). The NMR spectra were analyzed on MestReNova software and are reported relative to $CDCl_3$ (δ 7.26). NMR abbreviations: s = singlet, d = doublet, t = triplet, m = multiplet, br = broad, dt = doublet of triblets.

Gel permeation chromatography (GPC) was carried out in THF on two Plgel 10 μm mixed-B LS columns (Polymer Laboratories) connected in series with a miniDAWN TREOS multiangle laser light scattering (MALLS) detector, a ViscoStar viscometer, and Optilab rex differential refractometer (all from Wyatt Technology. The d*n*/dc values used for the polylactide and polystyrene macromonomers were 0.050 and 0.180, respectively. d*n*/dc values for the brush BCPs were obtained for each injection by assuming 100% mass elution from the columns.

High resolution mass spectra (HRMS) were provided by the California Institute of Technology Mass Spectrometry Facility.

SEM images were taken on a ZEISS 1550 VP Field Emission SEM.

Reflection measurements were performed on a Cary 5000 UV/Vis/NIR spectrophotometer equipped with an 'integrating sphere' diffuse reflectance accessory (Internal DRA 1800). All measurements were referenced to a LabSphere Spectralon 99% certified reflectance standard. The samples were illuminated through a Spectralon-coated aperature with a diameter of 1 cm and a beam area of

approximately 0.5 cm^2. The samples were scanned at a rate of 600 nm/min, with a 1 nm data interval, from 1800 to 200 nm, and a detector crossover (InGaAs to PMT) at 800 nm.

Synthesis

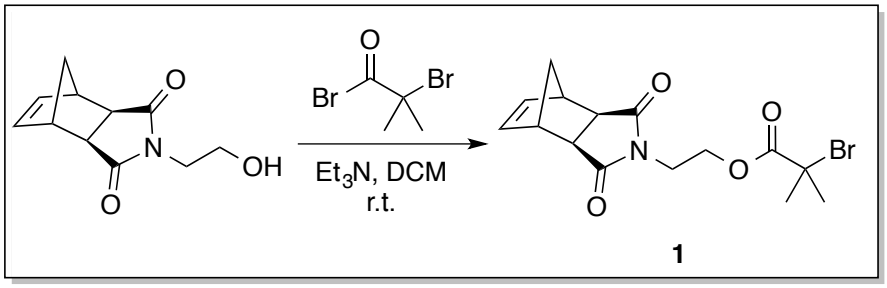

N-(2-bromo-2-methylpropanoylethanyl)-cis-5-norbornene-exo-2,3-dicarboximide (**1**)

A round bottom flask fitted with an addition funnel was flame-dried and subsequently charged with *N*-(hydroxyethanyl)-*cis*-5-norbornene-*exo*-2,3-di-carboximide (2.51 g, 12.1 mmol) and triethylamine (2.3 mL, 16 mmol). Dry dichloromethane (80 mL) was added to the addition funnel and approximately half of it was added to the reaction mixture. To the addition funnel was added 2-bromoisobutyrylbromide (2.2 mL 18 mmol). The reaction flask was submerged in an ice-water bath and the mixture in the addition funnel added drop wise to the reaction flask. When the addition was completed the reaction mixture was allowed to stir at room temperature for 20 hours. The reaction mixture was washed with 0.1 N HCl (25 mL), $NaHCO_3$ (25 mL), and brine (2 × 25 mL), and then dried over $MgSO_4$ and concentrated in vacuo. The product was purified by silica gel chromatography (dichloromethane) to give the product, **1**, as a white solid in 66 % yield (2.87 g, 8.0 mmol). ^{1}H NMR (500 MHz, $CDCl_3$): δ (ppm) 6.28 (t, J = 1.8 Hz, 2H), 4.34-4.32 (m, 2H), 3.82-3.80 (m, 2H), 3.28-3.26 (m, 2H), 2.70 (d, J = 1.4 Hz, 2H), 1.89 (s, 6H), 1.54-1.50 (m, 1H), 1.31 (d, J = 9.9 Hz, 1H). ^{13}C NMR (500 MHz, $CDCl_3$): δ (ppm) 177.7, 171.3, 137.8, 62.6, 55.4, 47.8, 45.2, 42.9, 37.3, 30.6. HRMS (EI+): calcd. for $C_{15}H_{18}O_4NBr$ $[M+H]^+$: *m/z* = 355.0419; found 355.0435. IR (Thin Film, NaCl): 3456, 3065, 2981, 2881, 1774, 1739, 1703, 1464, 1450, 1426, 1392, 1371, 1360, 1328, 1283, 1215, 1192, 1159, 1110, 1037, 1014, 990, 942, 902, 883, 854, 828, 813, 804, 781, 771, 722 cm^{-1}.

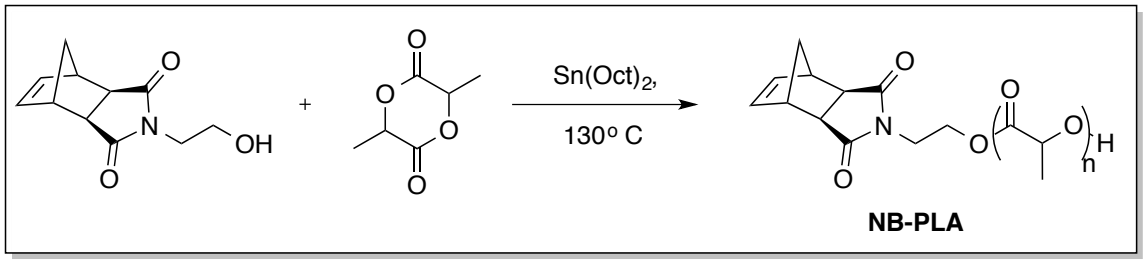

Synthesis of Norbornene-Polylactide (**NB-PLA**)

A flame-dried Schlenck tube was charged with *N*-(hydroxyethanyl)-*cis*-5-norbornene-*exo*-2,3-dicarboximide (233.9 mg, 1.13 mmol) and 3,6-dimethyl-1,4-dioxane-2,5-dione (6.096g, 42.3 mmol) along with tin-(II)-2-ethylhexanoate (≈2 mg, ≈5 μmol). This mixture was put under three vacuum-argon cycles and then allowed to stir at 130° C for 2.5 hours. After cooling to room temperature the product was dissolved in dichloromethane, filtered through a small pad of celite to remove catalyst, and precipitated into cold MeOH. ^{1}H NMR (500 MHz, $CDCl_3$): δ (ppm) 6.28 (br t, 2H), 5.25-5.03 (m, 82 H), 4.40-4.21 (m , 3H), 3.82-3.68 (m, 2H) 3.26 (s, 2H), 2.70 (m, 2H), 1.73-1.39 (m, 247H), 1.23 (br d, J = 8.5 Hz, 1H). M_n = 6.1 kg/mol. GPC-MALLS: M_n = 6.3 kg/mol, M_w/M_n = 1.20.

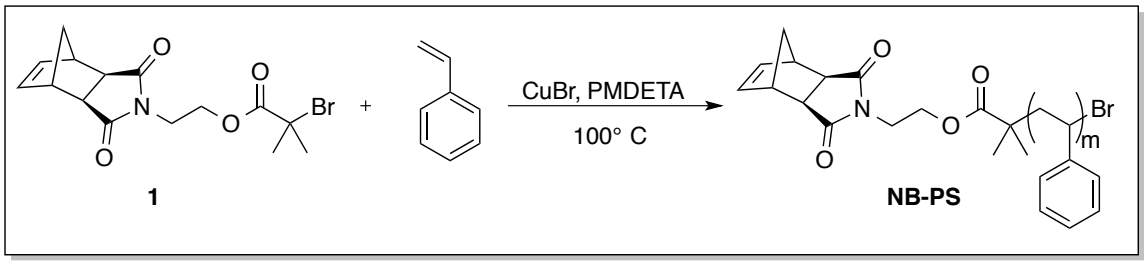

Synthesis of Norbornene-Polystyrene (**NB-PS**)

Styrene (24 mL, 0.209 mol) was passed through basic aluminum oxide and added to an oven-dried Schlenk tube fitted with a septum. Then the styrene underwent three freeze-pump-thaw cycles and was subsequently frozen again. CuBr (77.0 mg, 0.54 mmol) was next added to the frozen styrene under argon. This mixture was put under three vacuum-argon cycles before allowing the styrene to melt under argon. PMDETA (108 μL, 0.52 mmol) was then added to the mixture via a microsyringe and the solution stirred for 5 minutes. The initiator, **1** (670.4 mg, 1.88 mmol), was subsequently added to the Schlenck tube via syringe and the reaction mixture stirred at 100° C. The reaction was

stopped after 4 hours, by cooling it quickly down to room temperature using dry ice and adding THF to the mixture. The product was passed through neutral aluminum oxide to remove catalyst and precipitated into MeOH. The product was purified by repeated precipitations into MeOH until no remaining styrene was observed by NMR and further purified by silica gel chromatography (dichloromethane). ^{1}H NMR (500 MHz, $CDCl_3$): δ (ppm) 7.25-6.29 (br m, 260 H), 6.28 (br s, 2H), 4.59-4.35 (m, 1H), 3.65-3.32 (m, 4H), 3.22 (br s, 2H), 2.62 (br d, J = 6.6 Hz, 2 H), 2.56-1.55 (br m, 105 H), 0.99-0.83 (m, 6H). M_n = 5.8 kg/mol. GPC-MALLS: M_n = 6.1 kg/mol, M_w/M_n = 1.02.

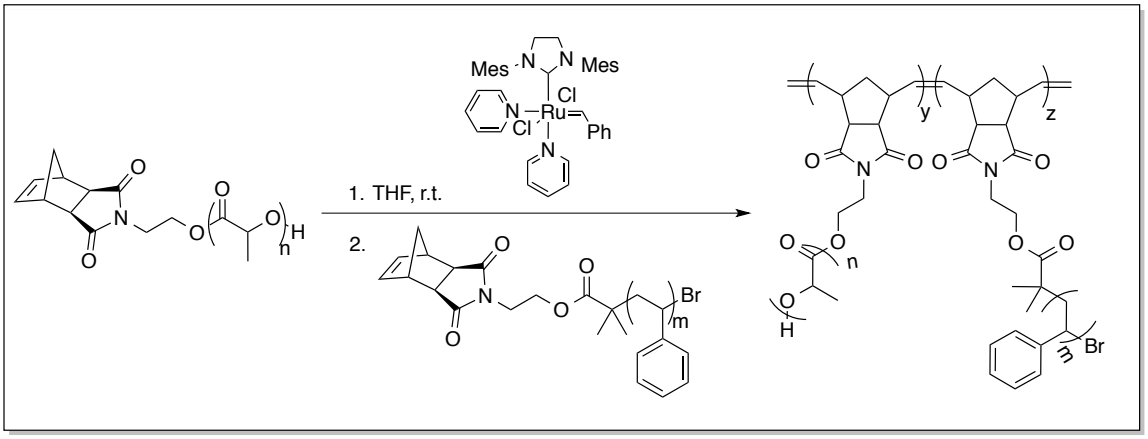

General Procedure for Block Copolymerization of Two Macromonomers via ROMP (**A-L**)

In a typical experiment, 150 mg of each of the macromonomers were added to separate vials. The desired amount of catalyst was added to the third vial. The vials were brought into a drybox and the macromonomers were dissolved in the desired amount of THF ($[M]_0 \approx 0.05$ M), while the catalyst was dissolved in 1.00 mL of THF. The desired amount of catalyst solution was injected via a microsyringe into the solution of the NB-PLA, as it polymerizes faster.[28] When the first macromonomer had polymerized, the solution of the second macromonomer (NB-PS) was added to the reaction mixture. This solution was allowed to stir for an additional 2-3 hours. The reaction was moved out of the dry box, quenched with butyl vinyl ether, and isolated by precipitation into MeOH. Conversion was 100% based on RI traces from the GPC, and isolated yields were generally over 85%.

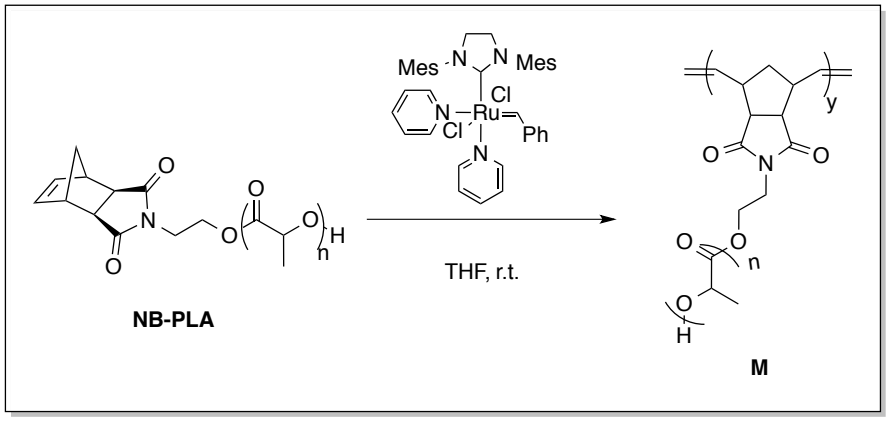

Synthesis of a Polylactide Brush Homopolymer (**M**)

NB-PLA (62.0 mg, 10.2 μmol) was weighed into a vial. The catalyst (2.6 mg, 3.58 μmol) was added to a separate vial. The vials were brought into the drybox and the NB-PLA was dissolved in THF (250 μL), while the catalyst was dissolved in 1.00 mL of THF. The catalyst solution (17 μL, 0.061 μmol) was injected via a microsyringe into the solution of macromonomers and the solution allowed to stir for 2 hours. The reaction was moved out of the dry box, quenched with butyl vinyl ether, and isolated by precipitation into MeOH. GPC-MALLS: M_n = 1.04 x 10^6 g/mol, M_w/M_n = 1.03.

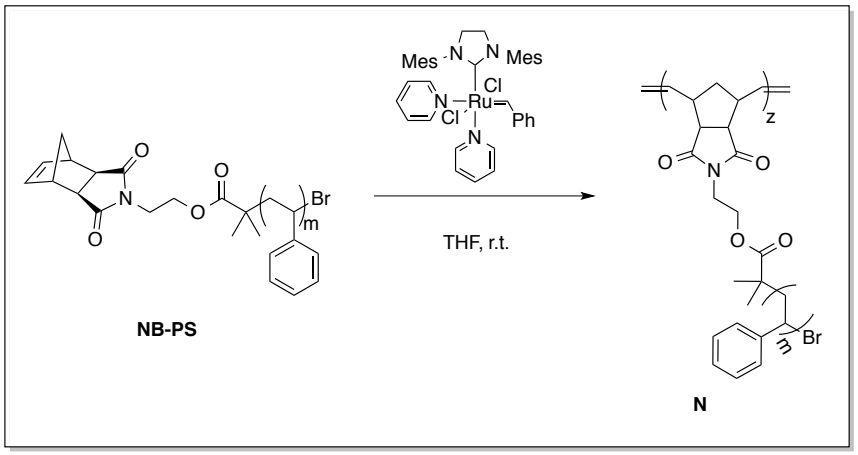

Synthesis of a Polystyrene Brush Homopolymer (**N**)

NB-PS (52.9 mg, 9.12 μmol) was weighed into a vial. The catalyst (2.6 mg, 3.58 μmol) was added to a separate vial. The vials were brought into the drybox and the NB-PS was dissolved in THF

(200 μL), while the catalyst was dissolved in 1.00 mL of THF. The catalyst solution (14.5 μL, 0.052 μmol) was injected via a microsyringe to the solution of macromonomers and the solution allowed to stir for 2 hours. The reaction was moved out of the dry box, quenched with butyl vinyl ether, and isolated by precipitation into MeOH. GPC-MALLS: M_n = 1.14 x 10^6 g/mol, M_w/M_n = 1.04.

Annealing by Slow Evaporation

The solid polymer (≈40-50 mg) was put in a vial and dissolved there in approx. 10 mL of solvent (DCM or THF). Then a glass substrate was put vertically into the vial and the solvent allowed to evaporate at room temperature. The glass substrate could be subsequently annealed at 120°C in an oven for 2 hours.

Thermal annealing between two glass substrates

The solid polymer (≈ 10 mg) was sandwiched between two glass substrates and compressed with a clamp. The glass substrates, now clamped together, are then heated in an oven or a vacuum chamber at 140° C for 30 minutes.

SEM sample preparation

The samples were fractured on glass substrates and exposed to fresh RuO_4 vapor for ≈ 8 minutes.

Calculations

The degree of polymerization (DP) of each MM in the final brush BCPs, shown in **Table 2-2**, was estimated using NMR data. The total molecular weight, measured by GPC-MALLS, was the sum of the molecular weight of each brush times the DP of that brush (**eq. 1**).

$$M_{n,tot} = DP_{PLA} \times M_{n,PLA} + DP_{PS} \times M_{n,PS} \quad \textbf{(1)}$$

The M_n of the PS had been calculated by using the integration value, herein assigned *a*, of the peak at δ 6.29 -7.25ppm to the norbornene olefin peak at δ 6.28 ppm. Likewise, the M_n of the PLA had been calculated by using the integration value, herein assigned *b*, of the peak at δ 5.03-5.25 ppm to the norbornene olefin peak at δ 6.28 ppm. The two MMs did not have any overlapping peaks in that area, so they could be used as identifying peaks in the brush BCPs where the integration value of the PS peak was assigned as *x* and the integration value of the PLA peak was assigned as *y*. The ratio of *x* over *y* remained the same as the ratio of *a* multiplied by the DP of the PS block over *b* multiplied by the DP of the PLA block, as shown in **eq. 2**.

$$\frac{x}{y} = \frac{a \times DP_{PS}}{b \times DP_{PLA}} \quad \textbf{(2)}$$

If we isolate DP_{PS}/DP_{PLA} and assign it the value *c,* we obtain the following equation:

$$c = \frac{DP_{PS}}{DP_{PLA}} = \frac{\frac{x}{y}}{\frac{a}{b}} \quad \textbf{(3)}$$

Then we can add DP_{PLA}/DP_{PLA} to both sides of the equation and obtain:

$$\frac{DP_{PLA} + DP_{PS}}{DP_{PLA}} = 1 + c \quad \textbf{(4)}$$

which can be rearranged to:

$$mol\%\ (PLA) = \frac{DP_{PLA}}{DP_{PLA} + DP_{PS}} = \frac{1}{1+c} \quad \textbf{(5)}$$

to find the mol % of the PLA in the brush block copolymer. The mol % of the PS then becomes:

$$mol\%\ (PS) = \frac{DP_{PS}}{DP_{PLA}+DP_{PS}} = \frac{c}{1+c} \quad \textbf{(6)}$$

With the mol % it becomes simple to calculate the wt % of each MM by multiplying the mol percentages by the molecular weights of their respective MMs:

$$wt\%\ (PS) = \frac{mol\%(PS)\times M_{n,PS}}{mol\%(PS)\times M_{n,PS}+mol\%(PLA)\times M_{n,PLA}} \quad \textbf{(7)}$$

and the DPs can be found by multiplying the weight percentages by the total molecular weight of the brush block copolymer and dividing by molecular weight of the MMs.

$$DP_{PS} = \frac{wt\%(PS)\times M_{n,tot}}{M_{n,PS}} \quad \textbf{(8)}$$

Supplementary Figures

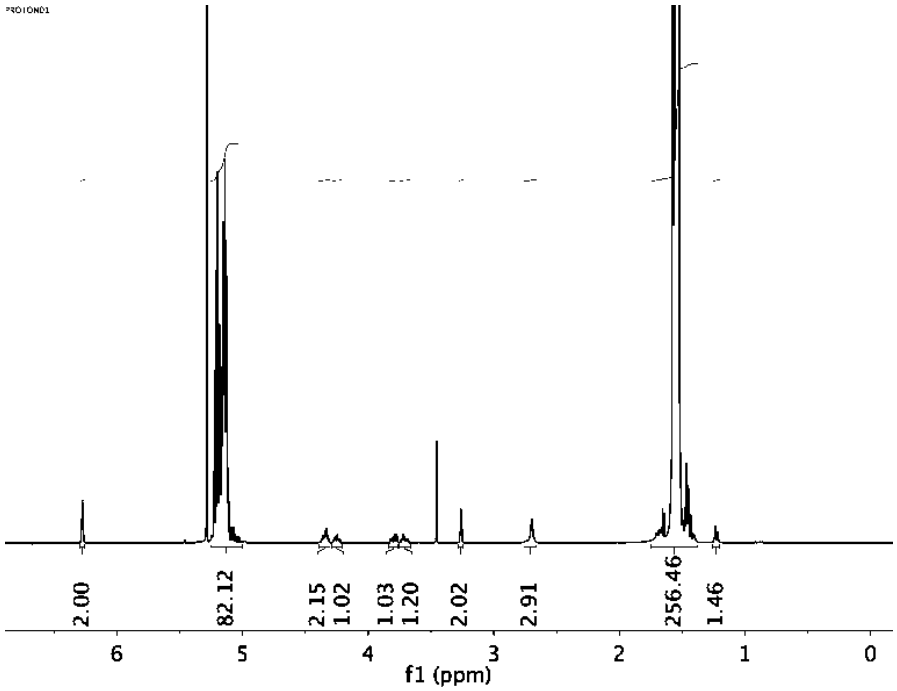

Figure 2-6. ^{1}H NMR spectra of NB-PLA.

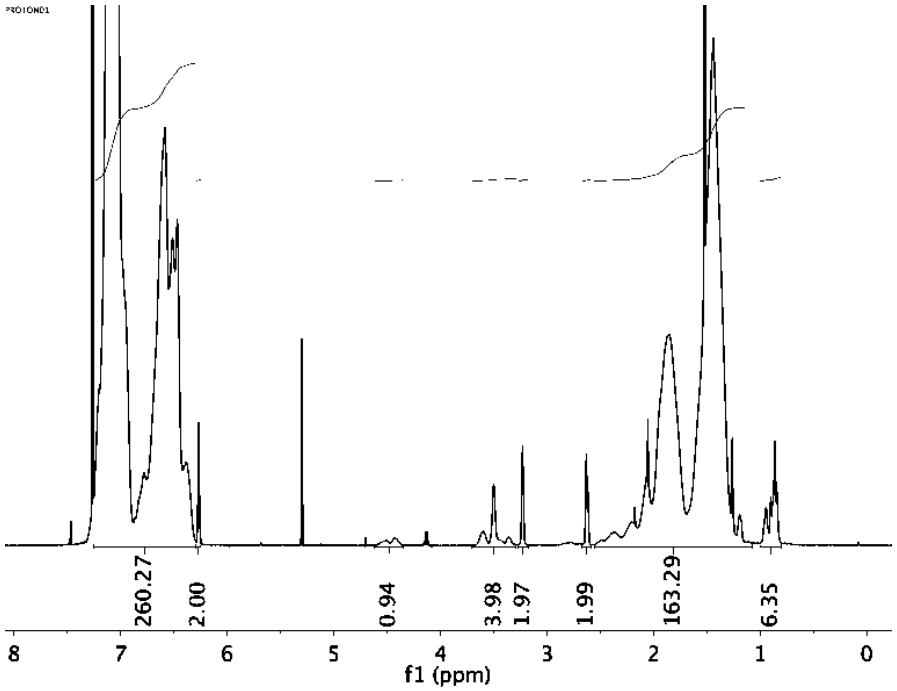

Figure 2-7. ^{1}H NMR spectra of NB-PS.

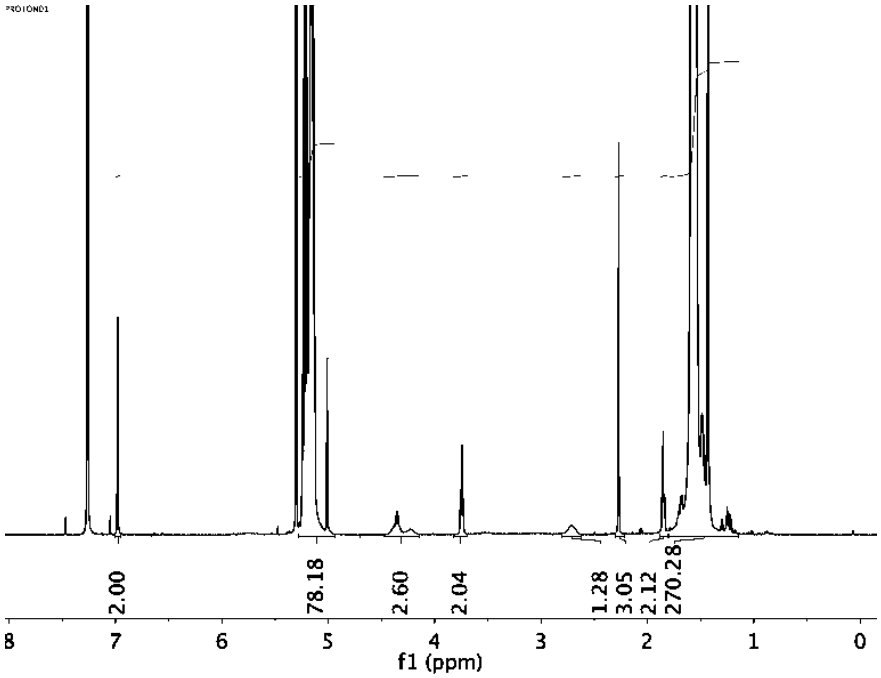

Figure 2-8. ^{1}H NMR spectra of **M** (a polylactide brush homopolymer).

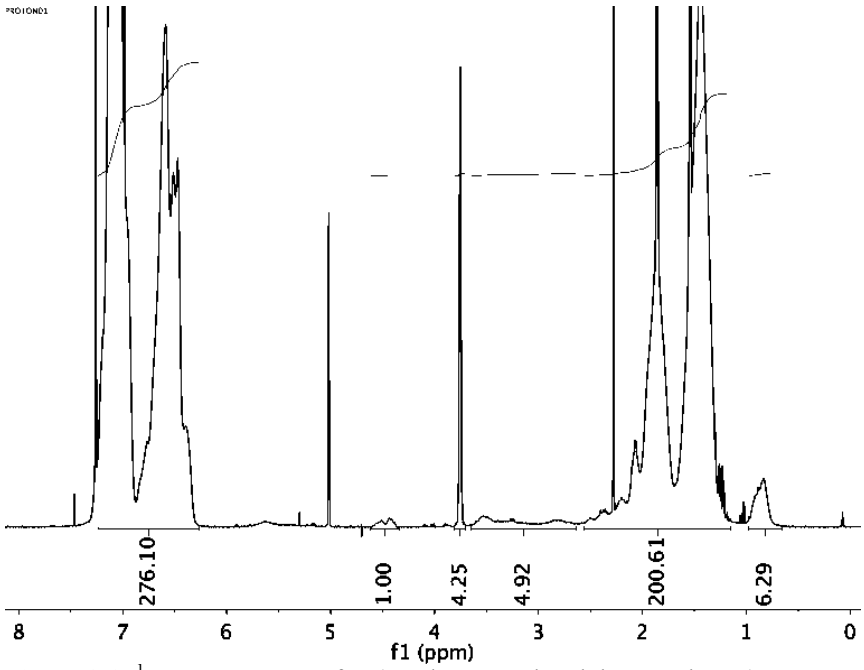

Figure 2-9. ^{1}H NMR spectra of **N** (a polystyrene brush homopolymer).

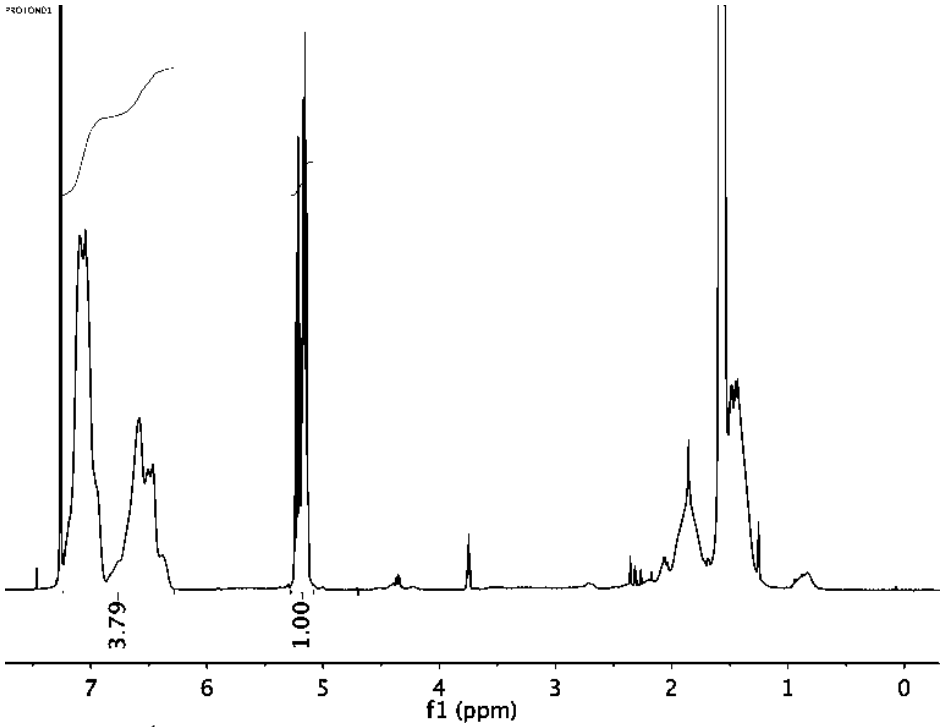

Figure 2-10. ^{1}H NMR spectra of **E** as an example of a brush block copolymer NMR spectra.

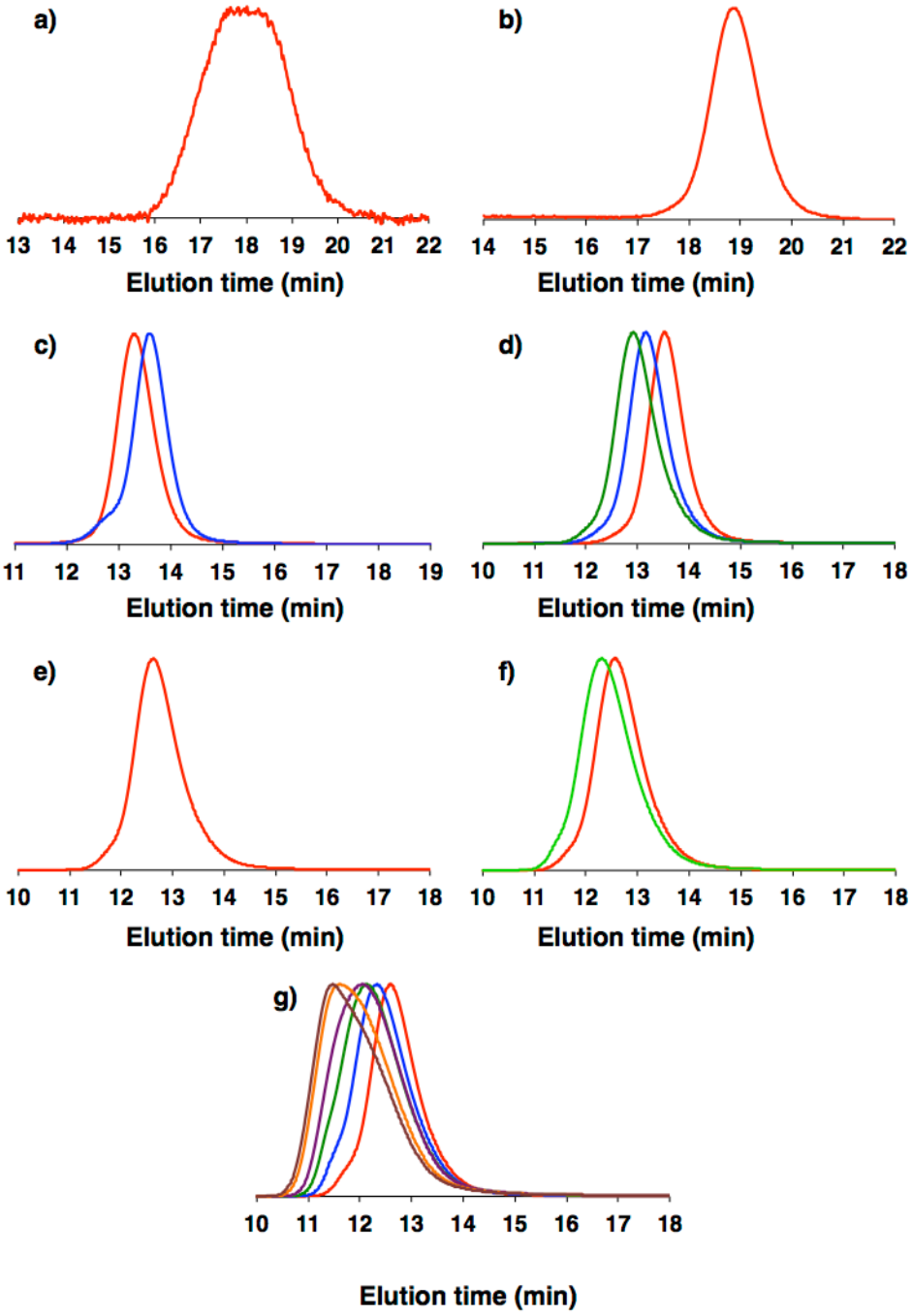

Figure 2-11. GPC RI traces of the polymers synthesized using NB-PLA, NB-PS, or both. All traces were obtained from polymers purified by precipitation into methanol. Each figure represents a single sample or a group of samples that were measured as one sample set. Traces in d-g are from samples in Table 2-2. (a) NB-PLA; (b) NB-PS; (c) red: **M**; blue: **N**; (d) red: **A**; blue: **B**; green: **C**; (e) **E**; (f) red: **D**; green: **G**; (g) red: **F**; blue: **H**; green: **I**; purple: **J**; orange: **K**; brown: **L**.

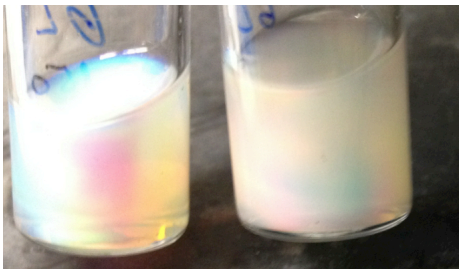

Figure 2-12. A solution of a brush block copolymer reaction solution that turned colored even while it was still in solution.

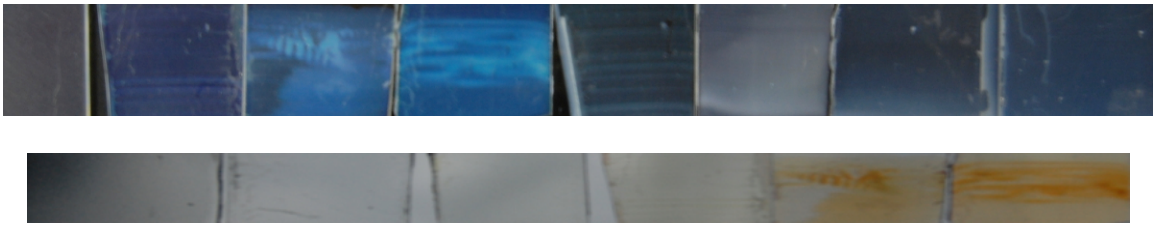

Figure 2-13. Top: Reflection of films of the brush block copolymers made by controlled evaporation from DCM. From left to right are samples **A-H** as described in Table 2-2. Bottom: Transmission of films of the brush block copolymers made by controlled evaporation from DCM. From left to right are samples **A-F** as described in Table 2-2.

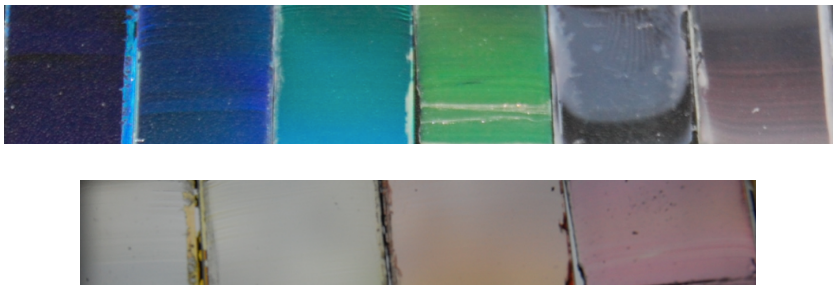

Figure 2-14. Top: Reflection of films of the brush block copolymers made by controlled evaporation from THF. From left to right are samples **C-H** as described in Table 2-2. Bottom: Transmission of films of the brush block copolymers made by controlled evaporation from THF. From left to right are samples **C-F** as described in Table 2-2.

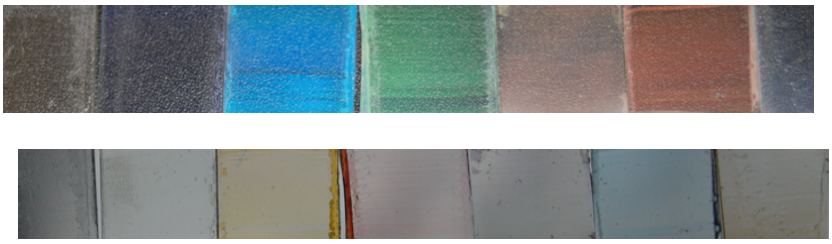

Figure 2-15. Top: Reflection of films of the brush block copolymers made by controlled evaporation from THF after heating. From left to right are samples **A-G** as described in Table 2-2. Bottom: Transmission of films of the brush block copolymers made by controlled evaporation from THF after heting. From left to right are samples **A-G** as described in Table 2-2.

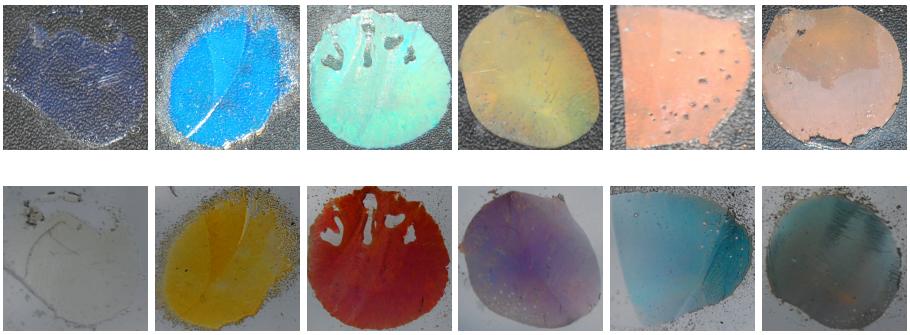

Figure 2-16. Top: Reflection of films of the brush block copolymers made by thermal compression. From left to right are samples **B-G** as described in Table 2-2. Bottom: Transmission of films of the brush block copolymers made by thermal compression. From left to right are samples **B-G** as described in Table 2-2.

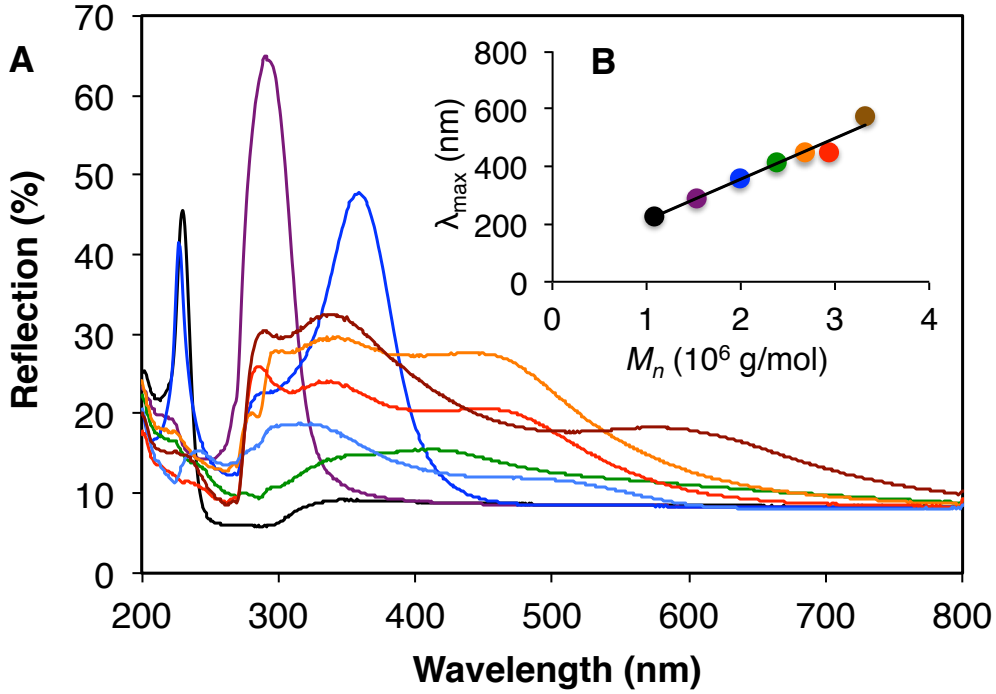

Figure 2-17. A) Plot of reflectance as a function of wavelength for the films prepared from the controlled evaporation from DCM. B) Plot of λ_{max} versus BCP MW for films prepared from the controlled evaporation from DCM.

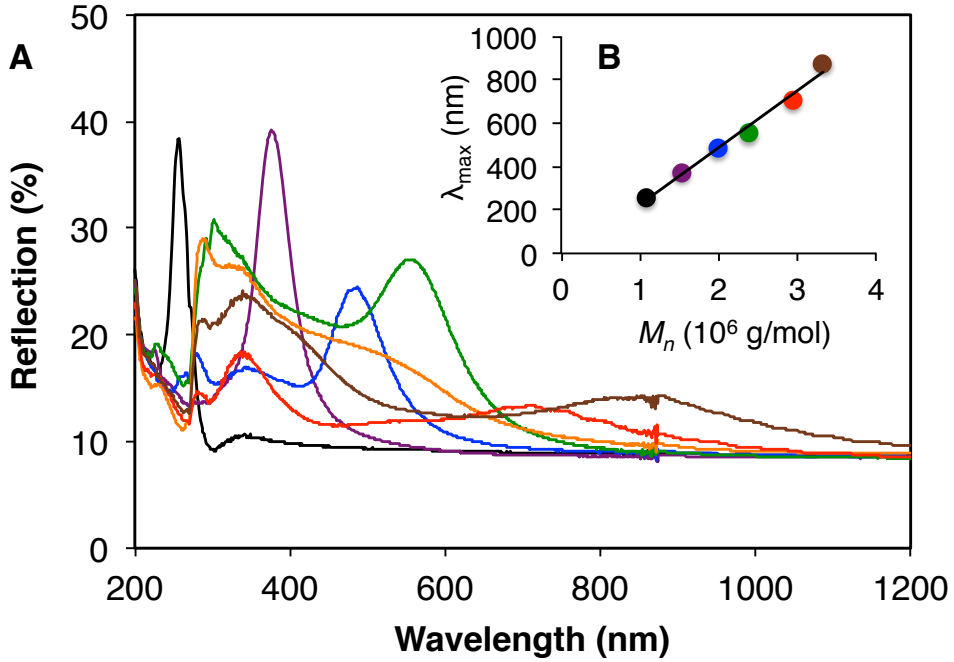

Figure 2-18. A) Plot of reflectance as a function of wavelength for the films prepared from the controlled evaporation from DCM after heating. B) Plot of λ_{max} versus BCP MW for films prepared from the controlled evaporation from DCM after heating.

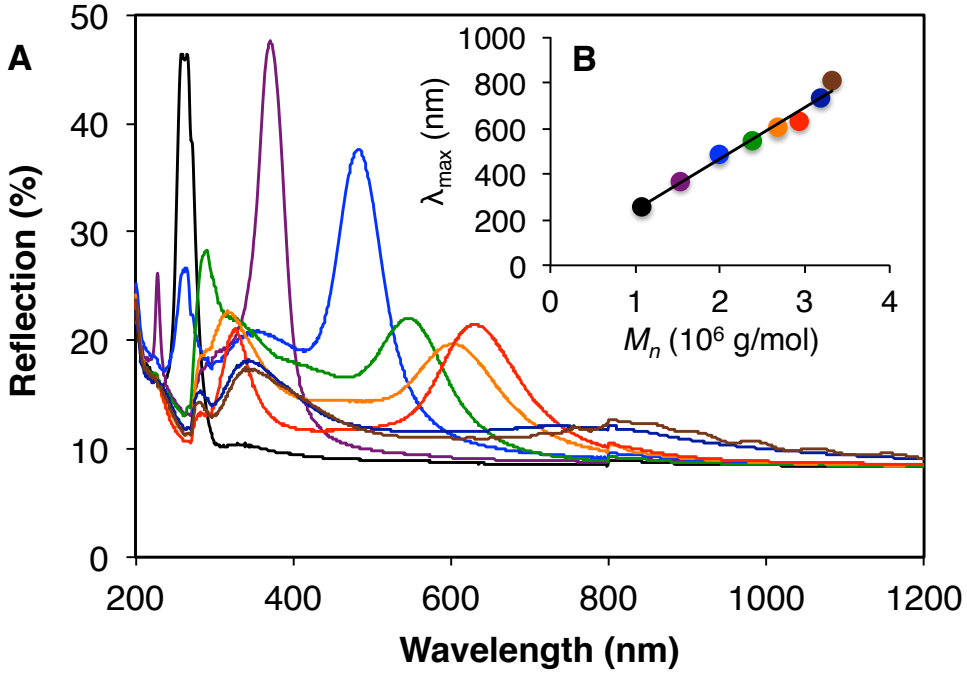

Figure 2-19. A) Plot of reflectance as a function of wavelength for the films prepared from the controlled evaporation from THF after heating. B) Plot of λ_{max} versus BCP MW for films prepared from the controlled evaporation from THF after heating.

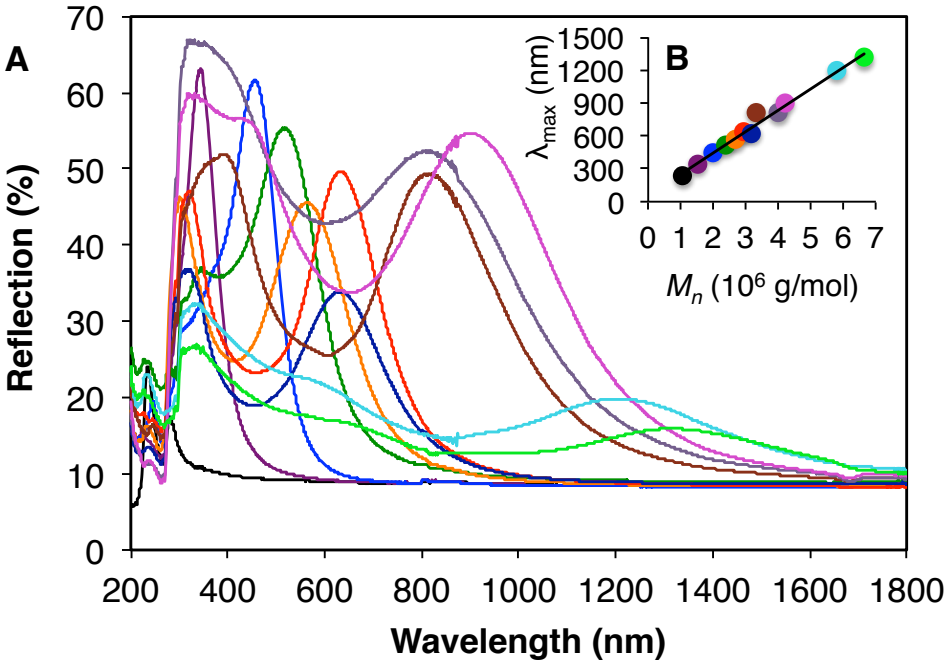

Figure 2-20. A) Plot of the reflectance as a function of wavelength for the polymer side of films prepared from thermal compression. B) Plot of λ_{max} versus BCP MW for the polymer side of films prepared from thermal compression.

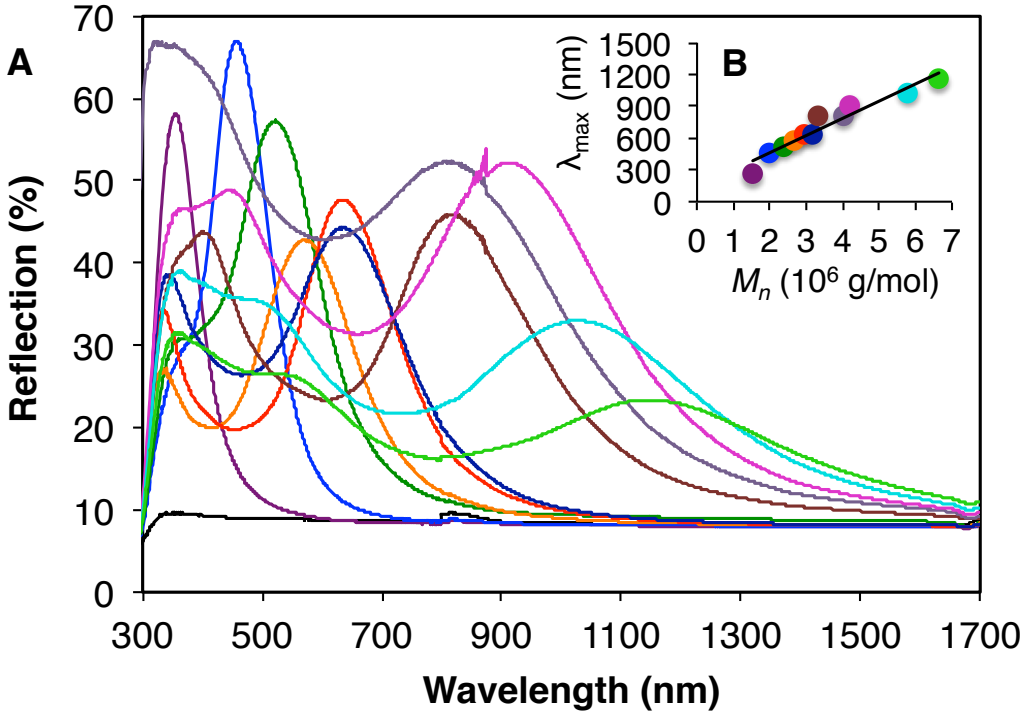

Figure 2-21. A) Plot of the reflectance as a function of wavelength for the glass side of films prepared from thermal compression. B) Plot of λ_{max} versus BCP MW for the glass side of films prepared from thermal compression.

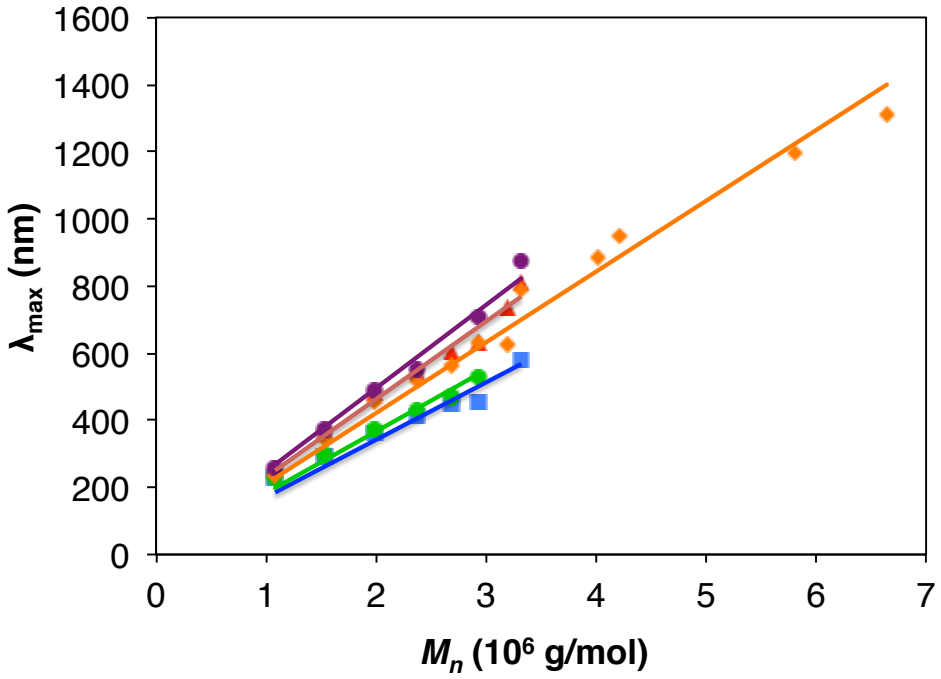

Figure 2-22. Plot of λ_{max} versus BCP MW for the glass side of films prepared from controlled evaporation out of DCM, before (blue) and after (purple) heating, or THF, before (green) and after (red) heating, as well as by thermal compression (orange).

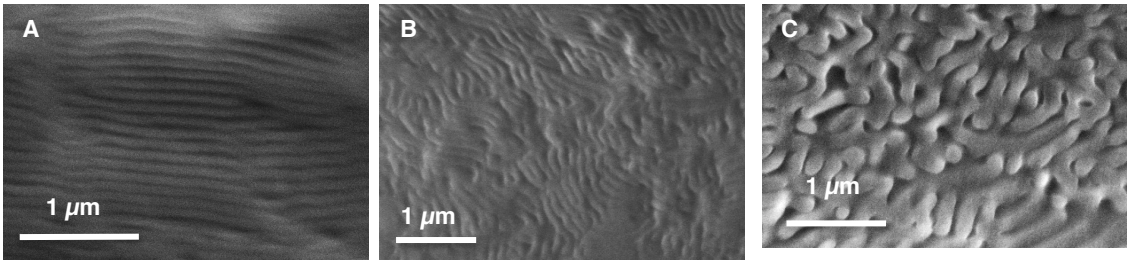

Figure 2-23. SEM image of the center of a cross-section of A) **B** (M_n = 1.53 × 10^6 g/mol) and B) **C** (M_n = 1.99 × 10^6 g/mol) and C) **F** (M_n = 2.94 × 10^6 g/mol) prepared by controlled evaporation from DCM before heating.

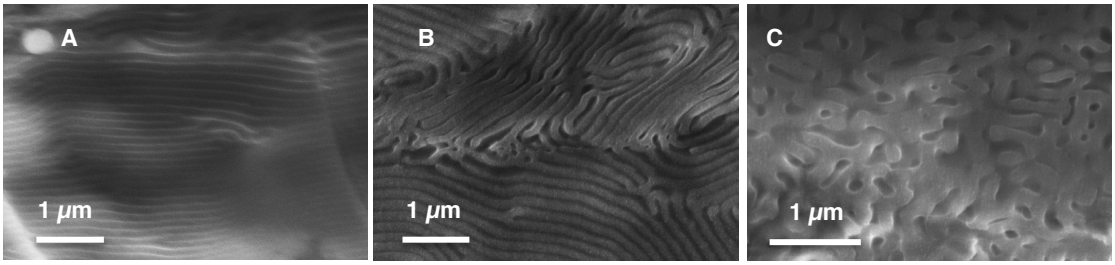

Figure 2-24. SEM image of the center of a cross-section of A) **B** (M_n = 1.53 × 10^6 g/mol) B) **C** (M_n = 1.99 × 10^6 g/mol) and C) **F** (M_n = 2.94 × 10^6 g/mol) prepared by controlled evaporation from DCM after heating.

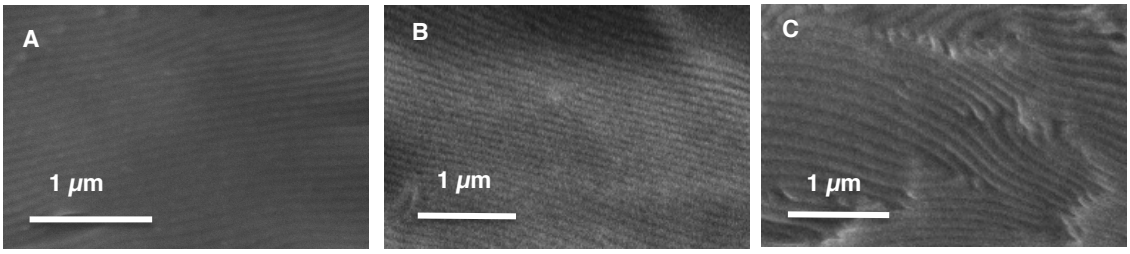

Figure 2-25. SEM image of the center of a cross-section of A) **B** (M_n = 1.53 × 10^6 g/mol) B) **C** (M_n = 1.99 × 10^6 g/mol) and C) **F** (M_n = 2.94 × 10^6 g/mol) prepared by controlled evaporation from THF before heating.

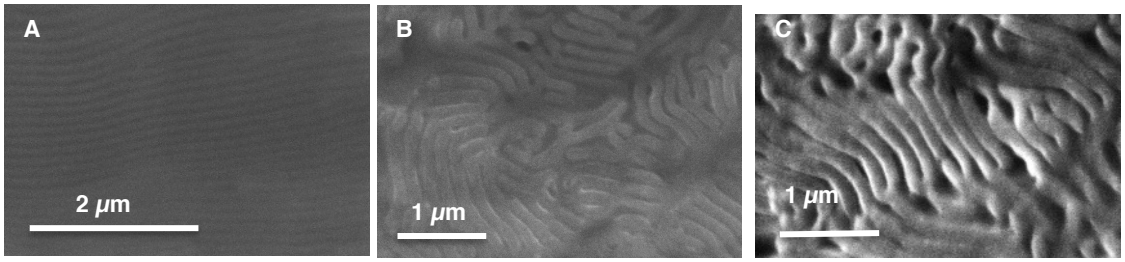

Figure 2-26. SEM image of the center of a cross-section of A) **B** (M_n = 1.53 × 10^6 g/mol) B) **C** (M_n = 1.99 × 10^6 g/mol) and C) **F** (M_n = 2.94 × 10^6 g/mol) prepared by controlled evaporation from THF after heating.

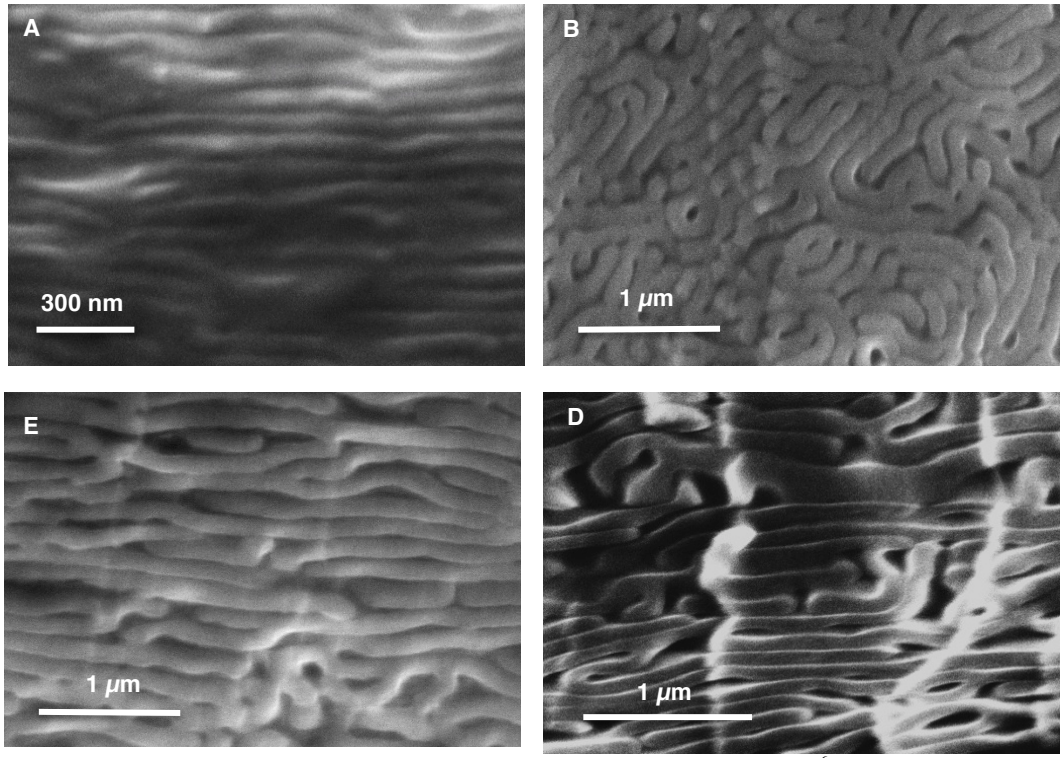

Figure 2-27. SEM image of the center of a cross-section of A) **B** (M_n = 1.53 × 10^6 g/mol) B) **C** (M_n = 1.99 × 10^6 g/mol), C) **F** (M_n = 2.94 × 10^6 g/mol) and D) **K** (M_n = 5.80 × 10^6 g/mol) prepared by controlled evaporation from THF after heating.

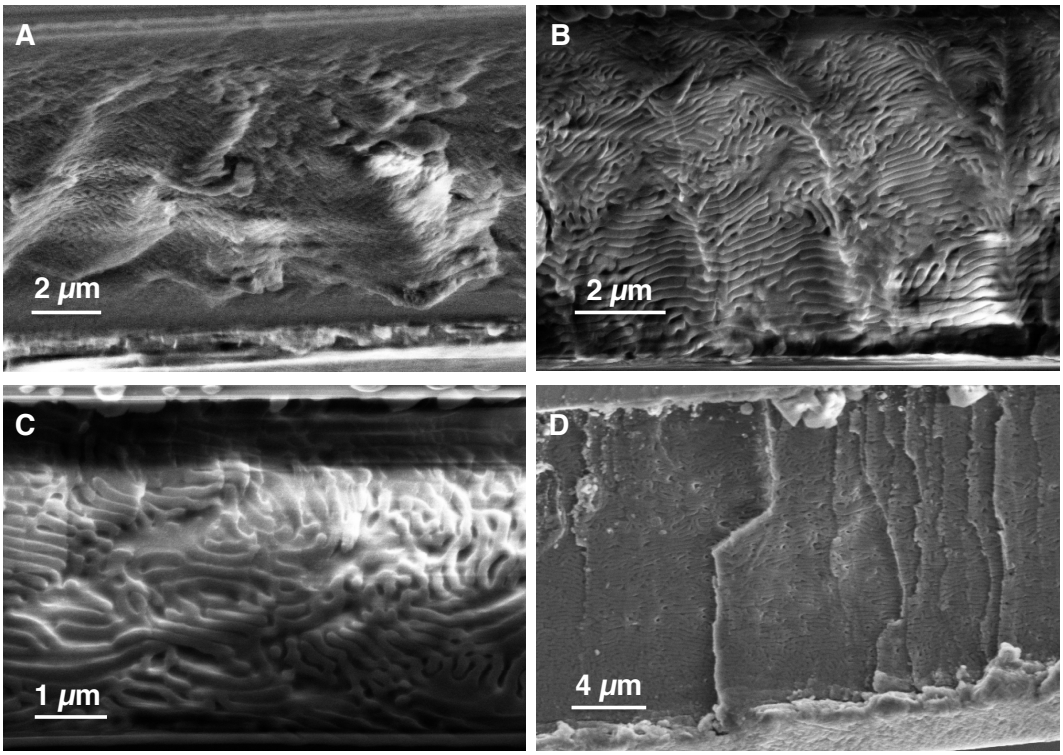

Figure 2-28. SEM image of the thickness of a cross-section of **F** (M_n = 2.94 × 10^6 g/mol) prepared by A) controlled evaporation from DCM, B) controlled evaporation from THF before heating, and C) after heating as well as D) prepared by thermal compression.

This shows that the thermally compressed film is significantly thicker than the films made from controlled evaporation. B) and C) also show that of the samples reflecting light, even the higher molecular weight films prepared by controlled evaporation from THF showed a lamellar orientation.

REFERENCES AND NOTES:

(1) Bates, F. S.; Hillmyer, M. A.; Lodge, T. P.; Bates, C. M.; Delaney, K. T.; Fredrickson, G. H. *Science.* **2012**, *336*, 434.

(2) Fasolka, M. J.; Mayes, A. M. *Annu. Rev. Mater. Res.* **2001**, *31*, 323.

(3) Thomas, E. L.; Lescanec, R. L. *Phil. Trans. R. Soc. Lond. A* **1994**, *348*, 149.

(4) Grubbs, R. B. *J. Polym. Sci. Part A Polym. Chem.* **2005**, *43*, 4323.

(5) Fink, Y.; Urbas, A. M.; Bawendi, M. G.; Joannopoulos, J. D.; Thomas, E. L. *J. Light. Technol.* **1999**, *17*, 1963.

(6) Ge, J.; Yin, Y. *Angew. Chem. Int. Ed.* **2011**, *50*, 1492.

(7) Joannopoulos, J. D. *Photonic Crystals: Molding The Flow of Light*; Princeton University Press, 2008.

(8) Kang, Y.; Walish, J. J.; Gorishnyy, T.; Thomas, E. L. *Nat. Mater.* **2007**, *6*, 957.

(9) Edrington, A. C.; Urbas, A. M.; DeRege, P.; Chen, C. X.; Swager, T. M.; Hadjichristidis, N.; Xenidou, M.; Fetters, L. J.; Joannopoulos, J. D.; Fink, Y.; Thomas, E. L. *Adv. Mater.* **2001**, *13*, 421.

(10) Chow, T.; Li, C.; Lin, Z. *Sol. Energy Mater. Sol. Cells* **2010**, *94*, 212.

(11) Urbas, A.; Fink, Y.; Thomas, E. L. *Macromolecules* **1999**, *32*, 4748.

(12) Urbas, A.; Sharp, R.; Fink, Y.; Thomas, E. L.; Xenidou, M.; Fetters, L. J. *Adv. Mater.* **2000**, *12*, 812.

(13) Parnell, A. J.; Pryke, A.; Mykhaylyk, O. O.; Howse, J. R.; Adawi, A. M.; Terrill, N. J.; Fairclough, J. P. A. *Soft Matter* **2011**, *7*, 3721.

(14) Lee, I.; Kim, D.; Kal, J.; Baek, H.; Kwak, D.; Go, D.; Kim, E.; Kang, C.; Chung, J.; Jang, Y.; Ji, S.; Joo, J.; Kang, Y. *Adv. Mater.* **2010**, *22*, 4973.

(15) Noda, S.; Tomoda, K.; Yamamoto, N.; Chutinan, A. *Science* **2000**, *289*, 604.

(16) Lin, S. Y.; Fleming, J. G.; Hetherington, D. L.; Smith, B. K.; Zubrzycki, W.; Kurtz, S. R.; Bur, J. *Nature* **1998**, *394*, 251.

(17) Masuda, H.; Ohya, M.; Asoh, H.; Nakao, M.; Nohtomi, M.; Tamamura, T. *Jpn. J. Appl. Phys.* **1999**, *38*, L1403.

(18) Birner, A.; Wehrspohn, R. B.; Gösele, U. M.; Busch, K. *Adv. Mater.* **2001**, *13*, 377.

(19) Wanke, M. C.; Lehman, O.; Müller, K.; Wen, Q.; Stuke, M. *Science* **1997**, *275*, 1284.

(20) Shoji, S.; Kawata, S. *Appl. Phys. Lett.* **2000**, *76*, 2668.

(21) Campbell, M.; Sharp, D. N.; Harrison, M. T.; Denning, R. G.; Turberfield, A. J. *Nature* **2000**, *404*, 53.

(22) Braun, P. V; Wiltzius, P. *Nature* **1999**, *402*, 603.

(23) Bertone, J. F.; Jiang, P.; Hwang, K. S.; Mittleman, D. M.; Colvin, V. L. *Phys. Rev. Lett.* **1999**, *83*, 300.

(24) Runge, M. B.; Dutta, S.; Bowden, N. B. *Macromolecules* **2006**, *39*, 498.

(25) Runge, M. B.; Bowden, N. B. *J. Am. Chem. Soc* **2007**, *129*, 10551.

(26) Runge, M. B.; Lipscomb, C. E.; Ditzler, L. R.; Mahanthappa, M. K.; Tivanski, A. V.; Bowden, N. B. *Macromolecules* **2008**, *41*, 7687.

(27) Rzayev, J. *Macromolecules* **2009**, *42*, 2135.

(28) Xia, Y.; Olsen, B. D.; Kornfield, J. A.; Grubbs, R. H. *J. Am. Chem. Soc* **2009**, *131*, 18525.

(29) Sheiko, S. S.; Möller, M. *Chem. Rev.* **2001**, *101*, 4099.

(30) Vlassopoulos, D.; Fytas, G.; Loppinet, B.; Isel, F.; Lutz, P.; Benoit, H. *Macromolecules* **2000**, *33*, 5960.

(31) Vayer, M.; Hillmyer, M. A.; Dirany, M.; Thevenin, G.; Erre, R.; Sinturel, C. *Thin Solid Films* **2010**, *518*, 3710.

(32) Zalusky, A. S.; Olayo-Valles, R.; Wolf, J. H.; Hillmyer, M. A. *J. Am. Chem. Soc.* **2002**, *124*, 12761.

(33) Hu, M.; Xia, Y.; McKenna, G. B.; Kornfield, J. A.; Grubbs, R. H. *Macromolecules* **2011**, *44*, 6935.

(34) Sveinbjörnsson, B. R.; Weitekamp, R. A.; Miyake, G. M.; Xia, Y.; Atwater, H. A.; Grubbs, R. H. *Proc. Natl. Acad. Sci. USA* **2012**, *109*, 14332.

(35) Troparevsky, M. C.; Sabau, A. S.; Lupini, A. R.; Zhang, Z. *Opt. Express* **2010**, *18*, 24715.

(36) Love, J. A.; Morgan, J. P.; Trnka, T. M.; Grubbs, R. H. *Angew. Chem. Int. Ed.* **2002**, *41*, 4035.

C h a p t e r 3

SELF-ASSEMBLY OF SYMMETRIC BRUSH BLOCK COPOLYMERS

Reproduced in part with permission from:
Gu, W.; Huh, J.; Hong, S. W.; Sveinbjornsson, B. R.; Park, C.; Grubbs, R. H.; Russell, T. P. *ACS Nano* **2013**, *7*, 2551-2558.
Hong, S. W.; Gu, W.; Huh, J.; Sveinbjornsson, B. R.; Jeong, G.; Grubbs, R. H.; Russell, T. P. *ACS Nano* **2013**, *7*, 9684-9692

ABSTRACT

Self-assembled structures of brush block copolymers (BCPs) with polylactide (PLA) and polystyrene (PS) side chains were studied in bulk and thin films. The polynorbornene-backbone-based brush BCPs containing approximately equal volume fractions of each block self-assembled into highly ordered lamellae, with domain spacing ranging from 20 to 240 nm by varying molecular weight of the backbone, as revealed by small-angle X-ray scattering (SAXS). The domain size increased approximately linearly with backbone length, which indicated an extended conformation of the backbone in the ordered state. The domain sizes of samples in thin films were found to be consistently larger than the corresponding domain sizes in bulk. The thin film samples were also found to orient perpendicularly to the silica substrate, without modification to the underlying substrate. *In situ* SAXS measurements suggested that the brush BCPs self-assemble in an extremely fast manner that could be attributed to reduced number of entanglements between chains.

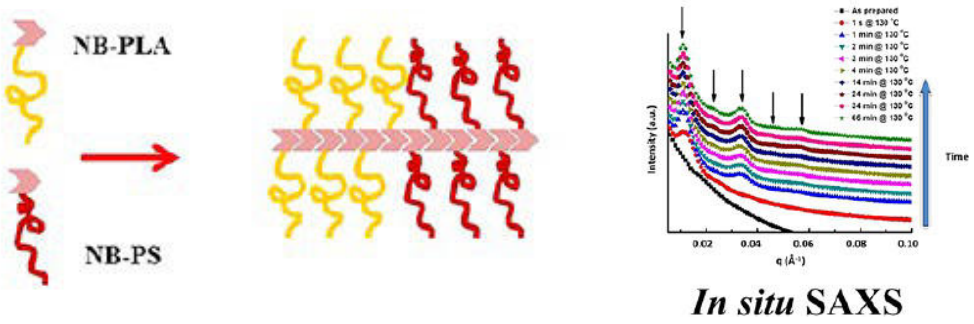

INTRODUCTION

Well-defined, periodic morphologies with features from the nanometer to hundreds of nanometer size scale have received considerable attention, because they can be used as templates and scaffolds for the fabrication of nanodots, nanowires, magnetic storage media, semiconductors, and optical devices, including polarizers and photonic band gap materials.[1–14] The self-assembly of block copolymers (BCPs) is proving to be one of the more promising bottom-up approaches to generating such morphologies in a cost-effective, robust, and scalable manner.[10,12,15–23] While there has been a tremendous drive to continually reduce the size scale of the features (with 3 nm feature sizes being the smallest achieved to date[20]), there are still numerous applications, such as polarizers and photonic bandgap materials, that require feature sizes on the scale of hundreds of nanometers. The use of self-assembly or directed self-assembly of BCPs could significantly reduce the number of steps required to generate features of this size, and therefore lead to a substantial cost savings. Since the period (pitch) of BCP morphologies and the dimensions of microdomains scale approximately with the 2/3 power of the molecular weight (for BCPs comprised of flexible chains in the strong segregation limit), achieving large scale feature requires the use of exceptionally high molecular weight (MW) BCPs. There has not been much, if any, success in using high MW BCPs to achieve large-scale features, because the diffusion of the polymers is exceptionally slow,[24] which significantly retards the self-assembly of the BCPs into highly ordered arrays of microdomains, as well as the elimination of defects in the resultant morphologies. Supercritical carbon dioxide (CO_2) at elevated temperatures has been used to swell BCPs, enhance the diffusion, and to order the BCP microdomains on the 0.1 μm size scale.[25] This still requires prolonged annealing times, and care must be taken to prevent void formation when the CO_2 is removed. Ryu and co-workers reported that polystyrene-*b*-poly(methyl methacrylate) (PS-*b*-PMMA) lamellae with large periods are obtained by solvent annealing sequentially combined with thermal annealing, but this requires multiple steps.[26] In the development of BCPs for photonic bandgap applications, Thomas and co-workers used conventional BCPs and polyelectrolyte-based BCPs with solvents or homopolymer/small molecule additives to achieve periodicities on the scale of 100 nm and larger.[27–29] However, achieving highly ordered structures on the 0.25 μm size scale or larger in an easy and rapid manner with BCPs has been exceedingly difficult.

To the best of our knowledge, there have been relatively few efforts to fabricate and control the ordering and orientation of periodic nanostructures using brush polymers.[30,31] However, the

promising results discussed in *Chapter 2*, where we were able to obtain NIR-reflecting photonic bandgap materials rapidly using the self-assembly of brush BCPs, were a motivation for pursuing further studies on the self-assembly of the brush BCP system. Here we discuss a study on the self-assembly of these brush BCPs, both in the bulk state and in thin film. We also report the scaling relationship between the degree of polymerization (DP) of brush polymers and the domain spacing observed from the self-assembled brush polymers for a few different side chain sizes.

SYNTHESIS OF BRUSH BCPs

The brush BCPs were synthesized using a ruthenium-catalyzed ring-opening metathesis polymerization (ROMP) of polylactide (PLA) and polystyrene (PS) based macromonomers (MMs) in an analogous way to the brush BCPs discussed in *Chapter 2* (**Scheme 3-1**). Four separate series were synthesized with side chains ranging from 2.4×10^3 g/mol to 9.9×10^3 g/mol and total DP of 25 and up to 869 MM units. **Table 3-1** shows the sample codes and characteristics of the brush BCPs used in this study. In the sample code form $[g\text{-}S_x]_p\text{-}b\text{-}[g\text{-}LA_y]_q$, the subscripts x and y are the molecular weights of the side chains of each type (in units of one thousand), and subscripts p and q represent the degree of polymerization of each brush block.

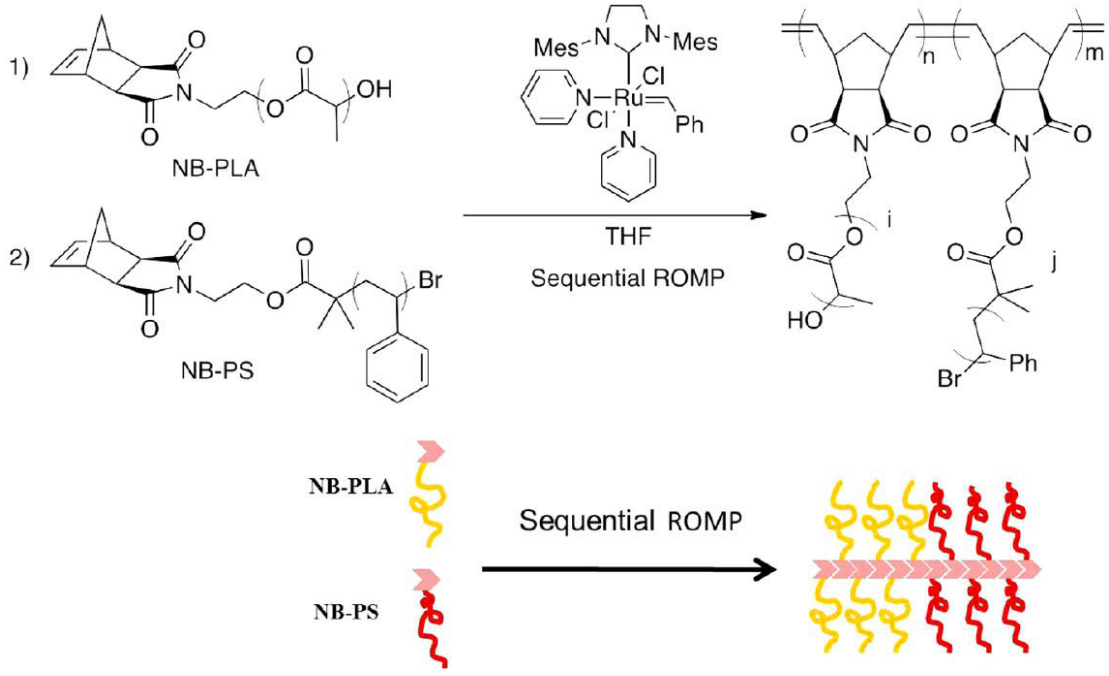

Scheme 3-1. General synthetic route and schematic diagram of brush block copolymers.

Table 3-1. Sample codes and characteristics of symmetric brush block copolymers.

Group	Sample codes	Total M_n [a] ($\times 10^3$ g/mol)	Total DP [b]	L (nm)	
				Bulk [c]	Thin Films [d]
I	$[g\text{-}S_{2.4}]_{19}$-b-$[g\text{-}LA_{2.4}]_{25}$	105	44	19.2	22.0
	$[g\text{-}S_{2.4}]_{35}$-b-$[g\text{-}LA_{2.4}]_{43}$	186	78	33.6	40.0
	$[g\text{-}S_{2.4}]_{51}$-b-$[g\text{-}LA_{2.4}]_{67}$	281	118	54.6	61.0
	$[g\text{-}S_{2.4}]_{98}$-b-$[g\text{-}LA_{2.4}]_{124}$	529	222	91.0	116.0
	$[g\text{-}S_{2.4}]_{189}$-b-$[g\text{-}LA_{2.4}]_{233}$	1007	422	157	215.1
	$[g\text{-}S_{2.4}]_{259}$-b-$[g\text{-}LA_{2.4}]_{381}$	1525	640	[e]	[f]
II	$[g\text{-}S_{4.3}]_{11}$-b-$[g\text{-}LA_{4.5}]_{14}$	104	25	19.8	20.9
	$[g\text{-}S_{4.3}]_{19}$-b-$[g\text{-}LA_{4.5}]_{25}$	192	44	31.2	31.1
	$[g\text{-}S_{4.3}]_{32}$-b-$[g\text{-}LA_{4.5}]_{42}$	320	74	43.9	45.2
	$[g\text{-}S_{4.3}]_{42}$-b-$[g\text{-}LA_{4.5}]_{58}$	432	100	58.7	62.2
	$[g\text{-}S_{4.3}]_{93}$-b-$[g\text{-}LA_{4.5}]_{128}$	954	221	102.9	149.5
	$[g\text{-}S_{4.3}]_{206}$-b-$[g\text{-}LA_{4.5}]_{278}$	2089	484	235[g]	[f]
III	$[g\text{-}S_{5.8}]_{13}$-b-$[g\text{-}LA_{6.1}]_{11}$	140	24	-	-
	$[g\text{-}S_{5.8}]_{30}$-b-$[g\text{-}LA_{6.1}]_{25}$	326	55	-	-
	$[g\text{-}S_{5.8}]_{51}$-b-$[g\text{-}LA_{6.1}]_{46}$	574	97	-	-
	$[g\text{-}S_{5.8}]_{101}$-b-$[g\text{-}LA_{6.1}]_{95}$	1166	196	-	-
	$[g\text{-}S_{5.8}]_{244}$-b-$[g\text{-}LA_{6.1}]_{209}$	2682	452	-	-
	$[g\text{-}S_{5.8}]_{471}$-b-$[g\text{-}LA_{6.1}]_{397}$	5150	869	-	-
IV	$[g\text{-}S_{9.9}]_{13}$-b-$[g\text{-}LA_{9.5}]_{10}$	220	23	-	-
	$[g\text{-}S_{9.9}]_{33}$-b-$[g\text{-}LA_{9.5}]_{25}$	572	59	-	-
	$[g\text{-}S_{9.9}]_{62}$-b-$[g\text{-}LA_{9.5}]_{48}$	1070	110	-	-
	$[g\text{-}S_{9.9}]_{165}$-b-$[g\text{-}LA_{9.5}]_{127}$	2836	292	-	-
	$[g\text{-}S_{9.9}]_{294}$-b-$[g\text{-}LA_{9.5}]_{180}$	4621	474	-	-

[a] Determined by THF GPC using RI and MALLS detectors. [b] Degree of polymerization determined by ^{1}H NMR and THF GPC (as described in *Chapter 2*). [c] The domain spacing L_0 is calculated from the corresponding first-order peak position of the 1-D SAXS profiles ($L_0 = 2\pi/q^*$) unless noted. [d] Center-to-center distance between microdomains determined by GI-SAXS analysis. [e] Peaks are absent during the given experimental condition. [f] Microdomains spacing by GI-SAXS analysis. [g] The first peak value is derived from the higher-order peaks.

SELF-ASSEMBLY OF BRUSH BCPs IN BULK

Bulk samples were prepared in aluminum washers, which were sandwiched by Kapton films and kept in a vacuum oven for 12 hours or longer to achieve thermal equilibrium before SAXS measurements were taken. Circular patterns were observed in the 2D SAXS results from bulk samples of group I and group II (**Figure 3-1 and Figure 3-2**) Samples with low MW in each series showed distinguishable multiple ring patterns (**Figure 3-1 A-D and Figure 3-2 A-E**), indicating

that well-ordered microphase structures were formed isotropically in the bulk state. Meanwhile, the domain spacing of high MW samples (**Figure 3-1 E-F, Figure 3-2 F**) may have been too large and beyond the limit of SAXS, or microdomains may not have been as well-ordered. Profiles of the scattering intensity *versus* scattering vector were also generated from **Figure 3-1** and **Figure 3-2**, and are shown in **Figure 3-3**. A systematic decrease in q^*, the scattering vector of the first-order reflection, was observed from low MW brush BCP to high MW brush BCP, indicating the anticipated increase of the domain spacing ranging from 19.2 to 235 nm (**Table 3-1**). Strong reflections were also seen at integral multiples of q^* in most cases, indicating the lamellar nature of the microdomains with long-range lateral ordering, as expected due to the near symmetric volume fractions of the PS and PLA segments.

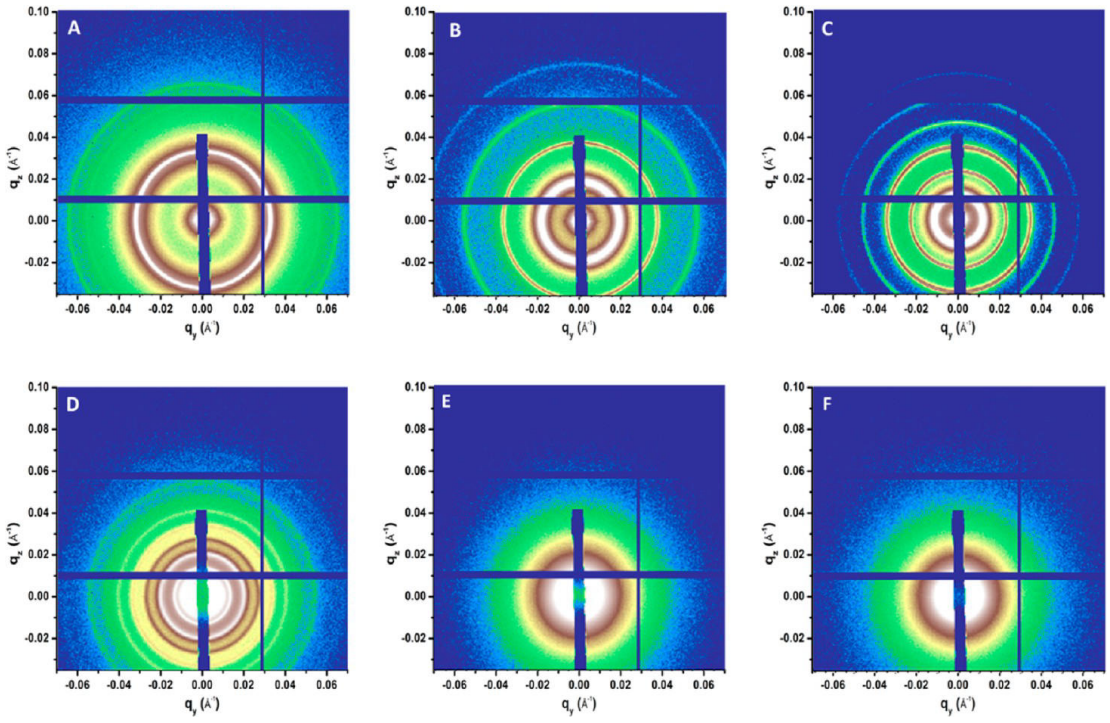

Figure 3-1. Representative 2D SAXS patterns for (A) [*g*-$S_{2.4k}$]$_{19}$-*b*-[*g*-$LA_{2.4k}$]$_{25}$; (B) [*g*-$S_{2.4k}$]$_{35}$-*b*-[*g*-$LA_{2.4k}$]$_{43}$; (C) [*g*-$S_{2.4k}$]$_{51}$-*b*-[*g*-$LA_{2.4k}$]$_{67}$; (D) [*g*-$S_{2.4k}$]$_{98}$-*b*-[*g*-$LA_{2.4k}$]$_{124}$; (E) [*g*-$S_{2.4k}$]$_{189}$-*b*-[*g*-$LA_{2.4k}$]$_{233}$; and (F) [*g*-$S_{2.4k}$]$_{259}$-*b*-[*g*-$LA_{2.4k}$]$_{381}$.

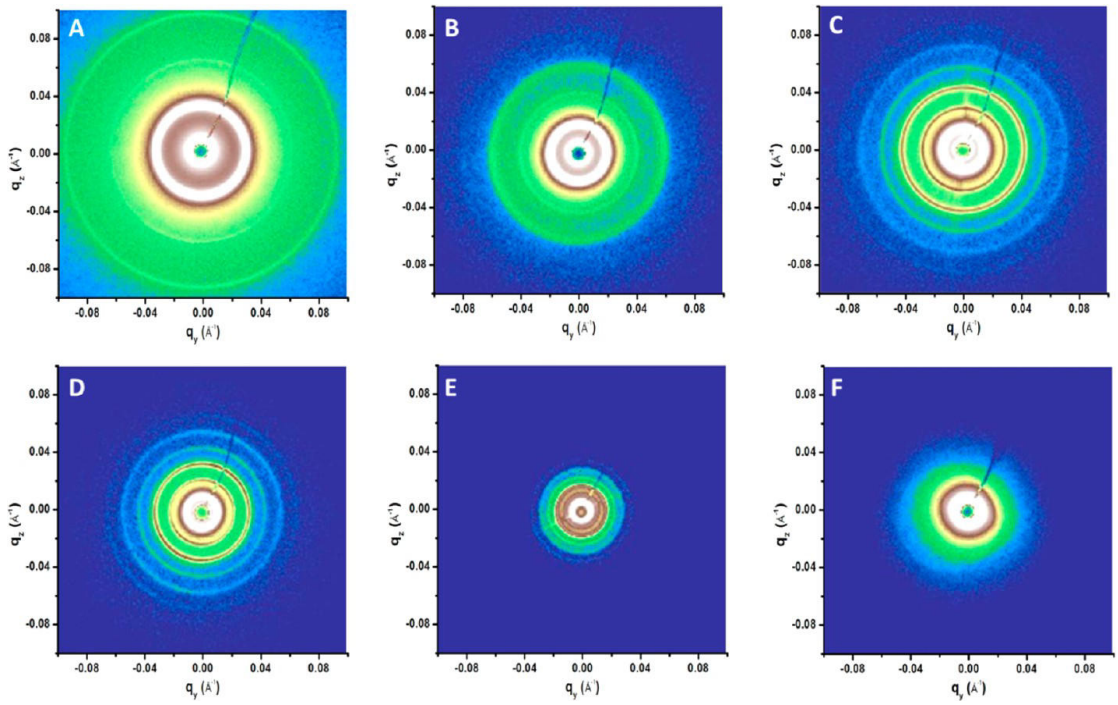

Figure 3-2. Representative 2D SAXS patterns for (A) $[g\text{-}S_{4.3k}]_{11}$-*b*-$[g\text{-}LA_{4.5k}]_{14}$; (B) $[g\text{-}S_{4.3k}]_{19}$-*b*-$[g\text{-}LA_{4.5k}]_{25}$; (C) $[g\text{-}S_{4.3k}]_{32}$-*b*-$[g\text{-}LA_{4.5k}]_{42}$; (D) $[g\text{-}S_{4.3k}]_{42}$-*b*-$[g\text{-}LA_{4.5k}]_{58}$; (E) $[g\text{-}S_{4.3k}]_{93}$-*b*-$[g\text{-}LA_{4.5k}]_{128}$; (F) $[g\text{-}S_{4.3k}]_{206}$-*b*-$[g\text{-}LA_{4.5k}]_{278}$.

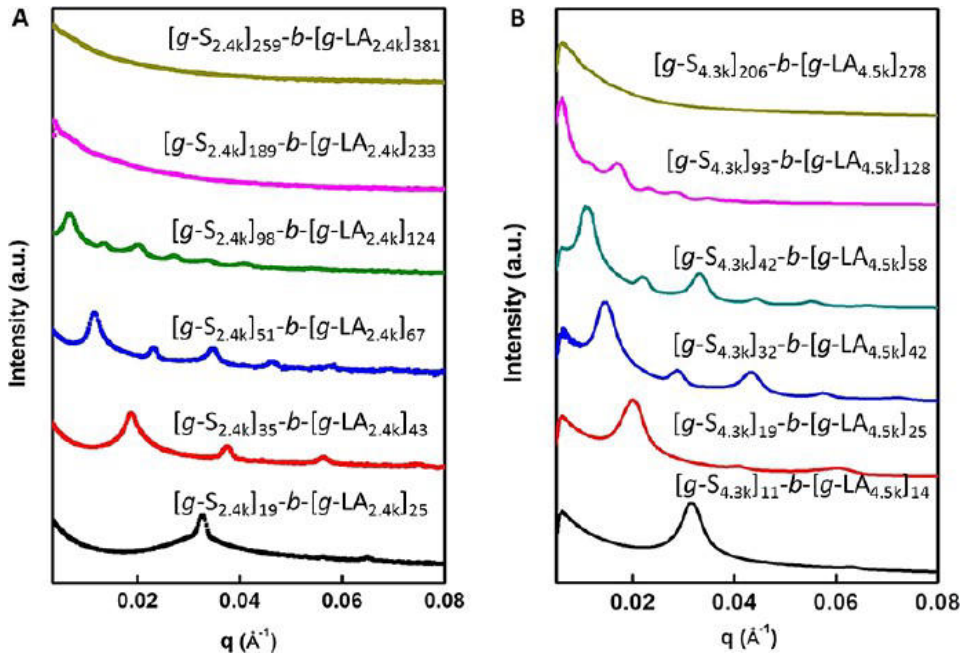

Figure 3-3. One-dimensional SAXS profiles calculated from the 2-D SAXS patterns in Figure 3-1 and Figure 3-2, respectively. (A) Group I. (B) Group II. Profile curves were offset for clarity

To further analyze the relationship between the measured domain spacing, L_0, and DP of the backbone, L_0 was plotted against total DP in a log-log plot (**Figure 3-4**). The exponents v in the scaling form $L_0 \sim DP^v$ for both cases were determined from the slope: $v = 0.84$ for group I, and $v = 0.91$ for group II. Both values are greater than the power law index determined in the SSL region, which is 2/3, and were also even greater than the greatest value previously reported, to the best of our knowledge, for a PS-*b*-PLA based BCP system (0.81).[32,33] This suggests that the backbones of brush BCPs are highly stretched as the PS and PLA side chains are segregated from each other, since the stretching of the backbone decreases the PS/PLA interfacial area per unit volume. Since group II brush BCPs have longer side chains compared with group I, steric hindrance may make the backbone more rigid, and thus cause the v value to be even larger.

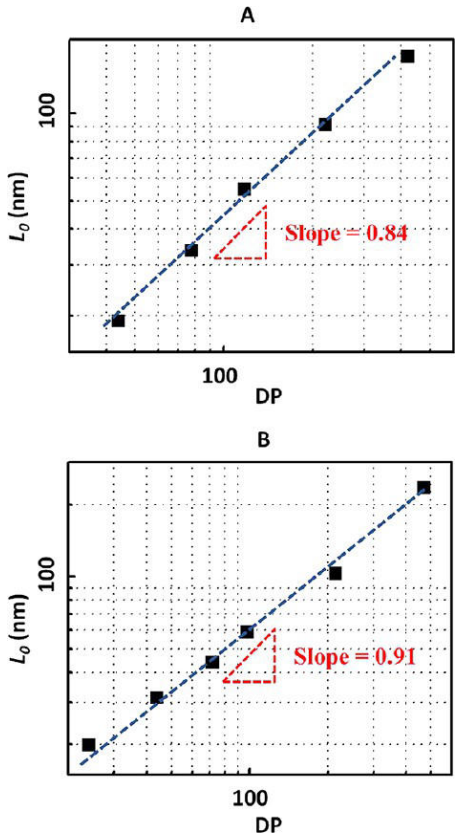

Figure 3-4. Scaling law between L_0 and DP. (A) Group I. (B) Group II.

Samples from group III were also analyzed via SAXS, and the results used to plot L_0 against the DP (**Figure 3-5**). Interestingly, the v value for this series was lower than that for group II even though it had longer side chains. Attempts were also made at analogous analysis of samples from group IV

with limited success so far. This suggests that as the side chains grow longer, it may become increasingly difficult to obtain well-ordered microdomains, at least with the annealing techniques used here. Therefore, there may be an optimal side chain length for these brush polymers to give the highest *v* value while being able to self-assemble into well-ordered microdomains in the bulk.

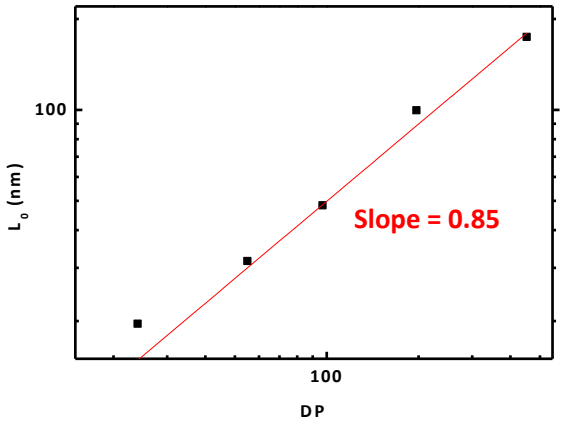

Figure 3-5. Scaling law between L_0 and DP for group III.

SELF-ASSEMBLY OF BRUSH BCPs IN THIN-FILMS

Thin films of brush BCPs were prepared on silicon substrates and, to effectively induce well-developed nanostructures, thin films were then solvent-annealed using either pure tetrahydrofuran (THF) or a mixture of solvents, tetrahydrofuran/chlorobenzene (THF/CBz), by which interfacial interactions were mediated. Scanning force microscopy (SFM) and grazing incidence small angle X-ray scattering (GI-SAXS) were used to characterize thin films of brush BCPs.

Interestingly, when thin films of $[g\text{-}S_{2.4}]_{189}$-*b*-$[g\text{-}LA_{2.4}]_{233}$ (film thickness was measured to be 47nm by ellipsometry), which has an extremely high MW of 1007×10^3 g/mol, were solvent-annealed with THF/CBz, well-developed lamellar microdomains oriented perpendicular to the substrate were obtained within a relatively short solvent-annealing time, as shown in **Figure 3-6**. From the SFM analysis, *L* of $[g\text{-}S_{2.4}]_{189}$-*b*-$[g\text{-}LA_{2.4}]_{233}$ is measured to be 228.5 nm. The microphase separation of the brush BCP is rapid, in comparison to conventional BCPs. This is due to the fact that the brush BCP backbone is more rigid than that of a conventional flexible BCP caused by steric hindrance, and consequently there is a reduction in the number of chain-entanglements when compared to

analogous linear BCPs with the same MW. Therefore, even ultrahigh MW brush BCPs will rapidly self-assemble into well-ordered microphase-separated morphologies that have extremely large feature sizes. Additional SFM images of lamellar-forming $[g\text{-}S_{2.4}]_p$-*b*-$[g\text{-}LA_{2.4}]_q$ and $[g\text{-}S_{4.3}]_p$-*b*-$[g\text{-}LA_{4.5}]_q$ series are shown in **Figure 3-7** and **Figure 3-8**. It was also remarkable that lamellar microdomains formed by those brush BCPs were oriented perpendicular to the substrate without any need of surface modification. As shown in **Scheme 3-2**, the conventional linear BCPs will generally form a layer-by-layer structure, due to the surface energy difference between two blocks and preferential interactions between one block and the substrate or air interface. However, for the brush BCPs used in this study, lamellar microdomains were oriented perpendicular to the substrate, the origin of which was attributed to the entropy gain caused by the unique chain architecture.

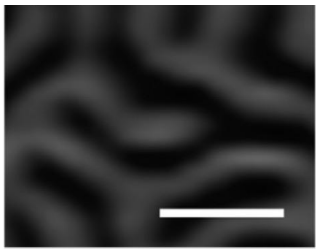

Figure 3-6. SFM height image of solvent-annealed thin film of $[g\text{-}S_{2.4}]_{189}$-*b*-$[g\text{-}LA_{2.4}]_{233}$ on Si substrate. The solvent annealing time was 10 hours. The scale bar is 400 nm.

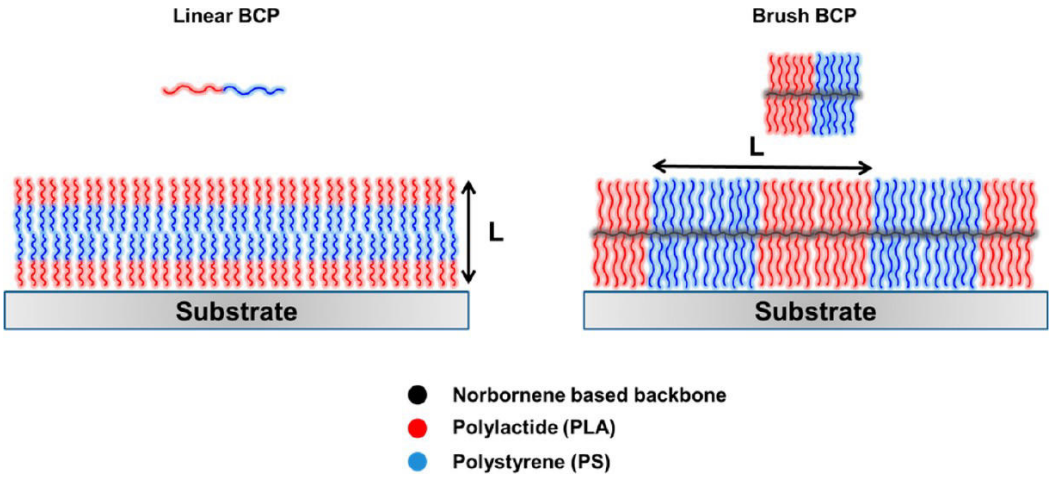

Scheme 3-2. Schematic of lamellar microdomains oriented parallel (left) or perpendicular (right) to the substrate from the self-assembly of linear BCP or brush BCP.

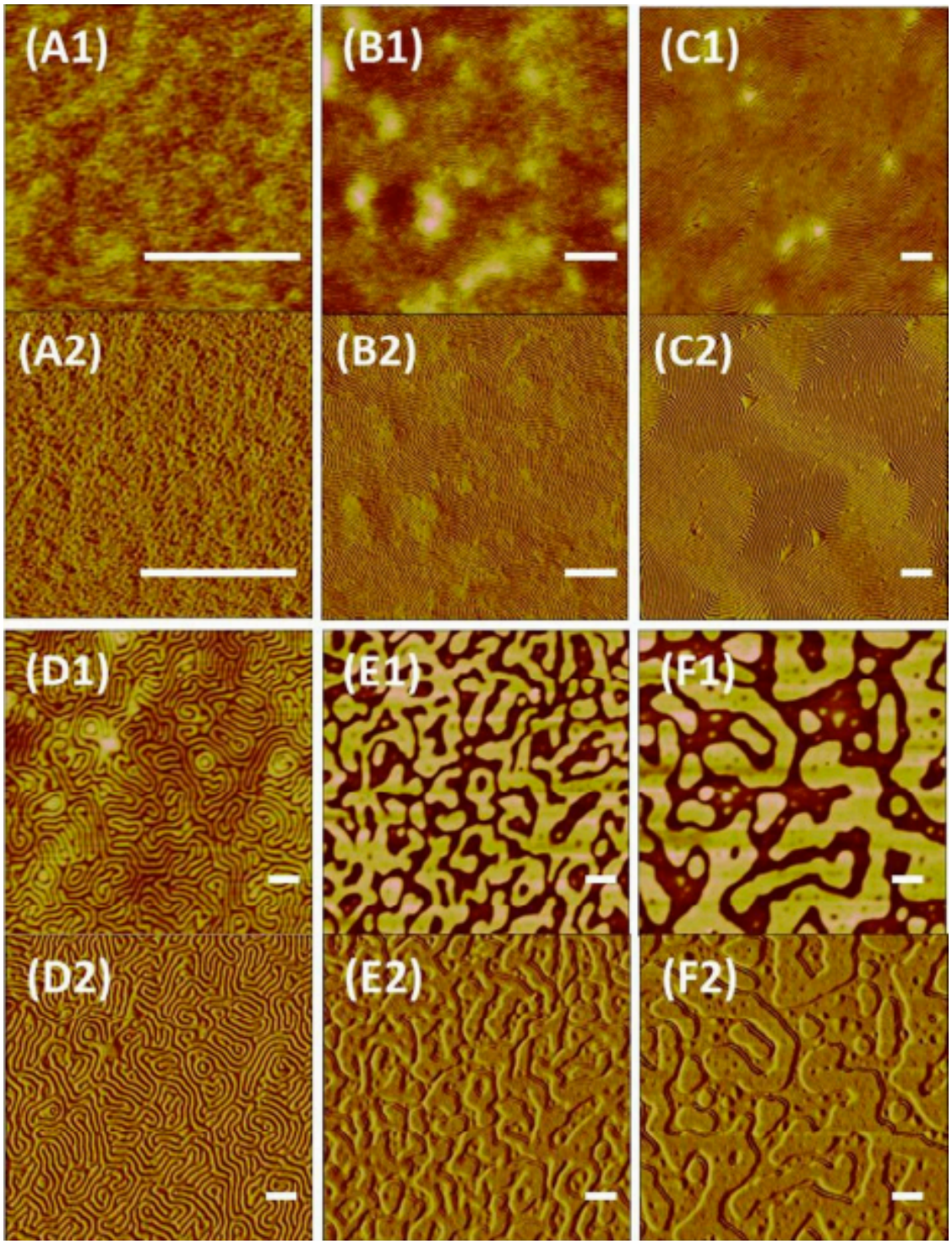

Figure 3-7. SFM height (A1-F1) and phase (A2-F2) images of solvent annealed thin films of $[g\text{-}S_{2.4}]_{19}$-*b*-$[g\text{-}LA_{2.4}]_{25}$, $[g\text{-}S_{2.4}]_{35}$-*b*-$[g\text{-}LA_{2.4}]_{43}$, $[g\text{-}S_{2.4}]_{51}$-*b*-$[g\text{-}LA_{2.4}]_{67}$, $[g\text{-}S_{2.4}]_{98}$-*b*-$[g\text{-}LA_{2.4}]_{124}$, $[g\text{-}S_{2.4}]_{189}$-*b*-$[g\text{-}LA_{2.4}]_{233}$, and $[g\text{-}S_{2.4}]_{259}$-*b*-$[g\text{-}LA_{2.4}]_{381}$, respectively. Scale bars: 500 nm.

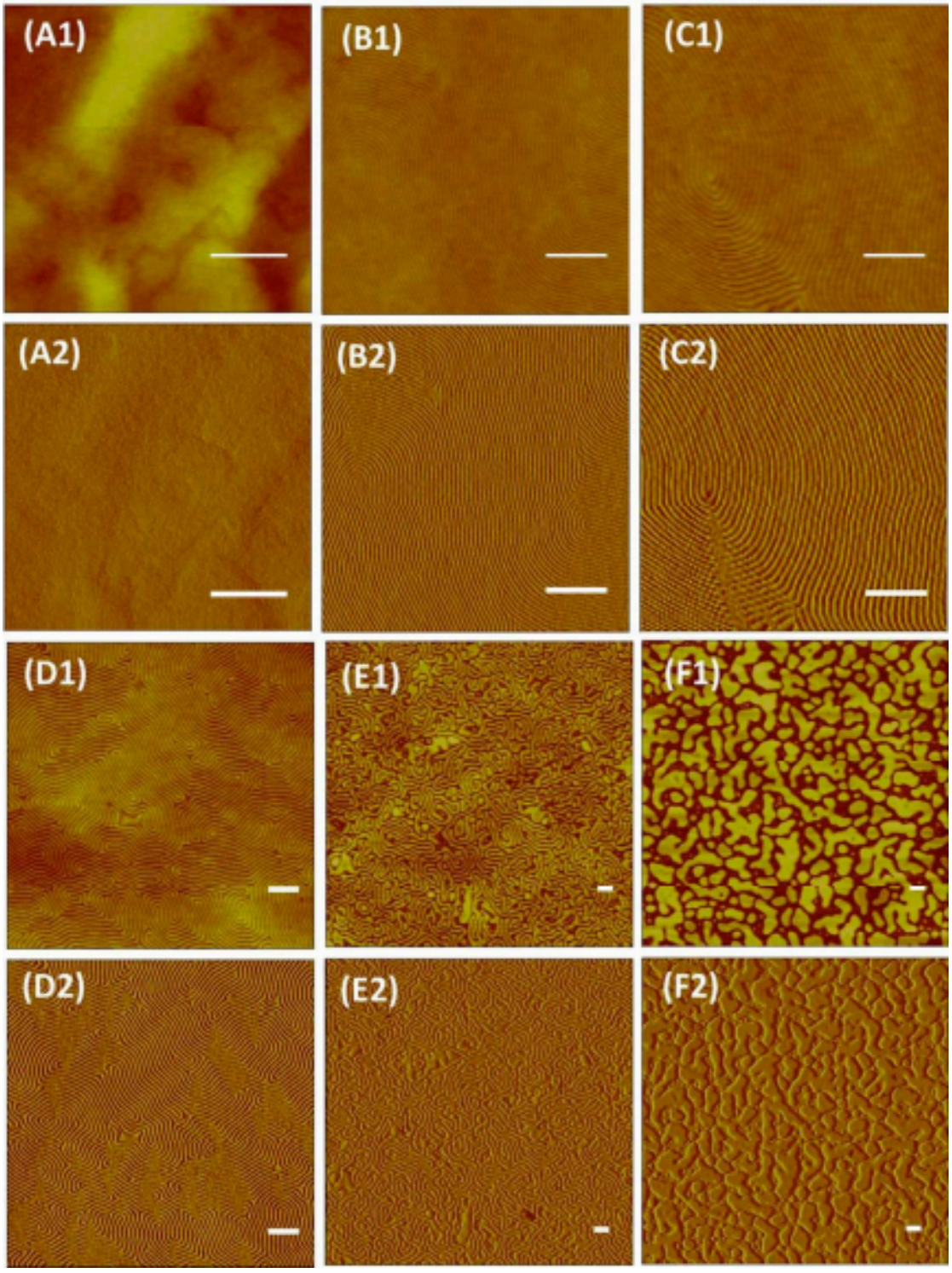

Figure 3-8. SFM height (A1-F1) and phase (A2-F2) images of solvent annealed thin films of $[g\text{-}S_{4.3}]_{11}$-*b*-$[g\text{-}LA_{4.5}]_{14}$, $[g\text{-}S_{4.3}]_{19}$-*b*-$[g\text{-}LA_{4.5}]_{25}$, $[g\text{-}S_{4.3}]_{32}$-*b*-$[g\text{-}LA_{4.5}]_{42}$, $[g\text{-}S_{4.3}]_{42}$-*b*-$[g\text{-}LA_{4.5}]_{58}$, $[g\text{-}S_{4.3}]_{93}$-*b*-$[g\text{-}LA_{4.5}]_{128}$, and $[g\text{-}S_{4.3}]_{206}$-*b*-$[g\text{-}LA_{4.5}]_{278}$, respectively. Scale bars: 500 nm.

The fact that no special steps were taken to modify the substrate in order to control interfacial interactions,[34–37] and the orientation of the lamellar microdomains normal to the substrate, even with solvent annealing, was surprising, because PLA has strongly preferential interactions with the oxide layer on the silicon substrate, and the orientation found requires that the PS block be in contact with the substrate. Consequently, the orientation of the lamellar microdomains normal to the substrate may arise from the screening of the interactions of the blocks with the substrate, coupled with more favored parallel alignment of the sterically hindered, rigid blocks at the polymer/substrate interface, which again is an entropic-type of preferred chain orientation. Unlike linear BCPs, the many chain ends of the side chains attached to the backbone would preferentially segregate to the surface and substrate interfaces. This orientation allows the microphase-separated brush BCPs to have more conformational degrees of freedom, in comparison to the case where microdomains of brush BCPs are oriented parallel to the substrate.

The GI-SAXS studies on the group I and group II series are shown in **Figure 3-9**. From the first order reflection in the GI-SAXS, the period, L, was determined. **Figure 3-10** shows L as a function of DP for both series of brush BCPs (results summarized in **Table 3-1**). From a regression analysis of the data it was found that $L \propto \mathrm{DP}^{0.99}$ for group I, and $L \propto \mathrm{DP}^{1.03}$ for group II. The slight increase in the exponent as the side chain length increases, and the apparent saturation, with a further increase in the side chain molecular weight, arises from the entropic penalty associated with the packing of the side chains. It is evident, though, that the backbone chain is highly stretched, regardless of MW of the side chain, and only the extended contour length of the main chain dictates L. Again, it should be noted that the exponent for the brush BCPs is much larger than that for flexible BCPs in the strong segregation regime,[15] where $L \propto \mathrm{DP}^{2/3}$.

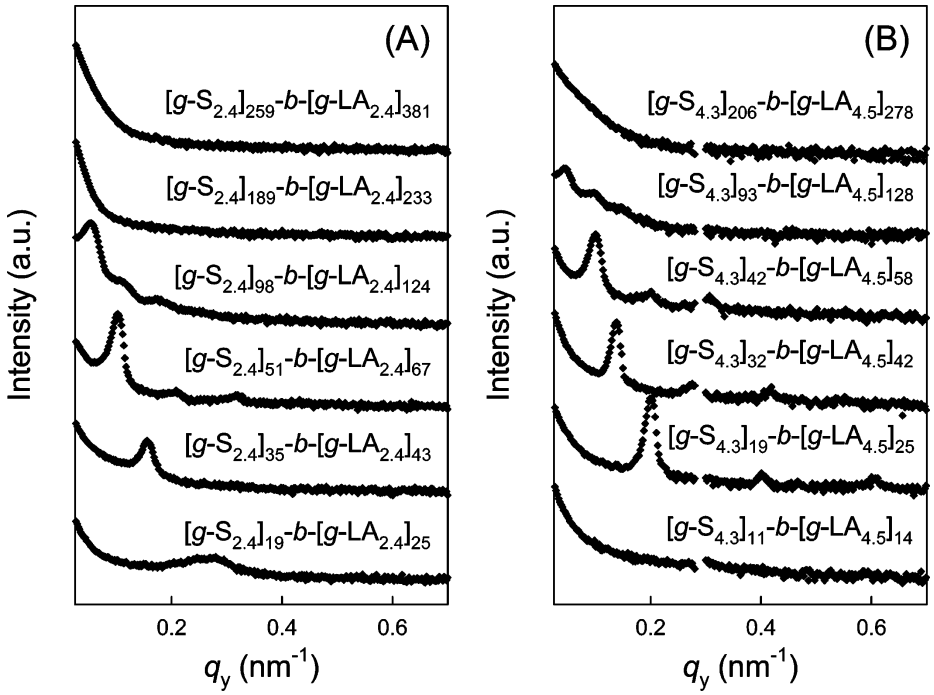

Figure 3-9. GI-SAXS patterns from Brush BCP thin films having different side chains: (A) MW of PS side chain is 2.4×10^3 g/mol and MW of PLA side chain is 2.4×10^3 g/mol; (B) MW of PS side chain is 4.3×10^3 g/mol and MW of PLA side chain is 4.5×10^3 g/mol. Film thicknesses, as measured by ellipsometry, ranged from 38 to 63 nm.

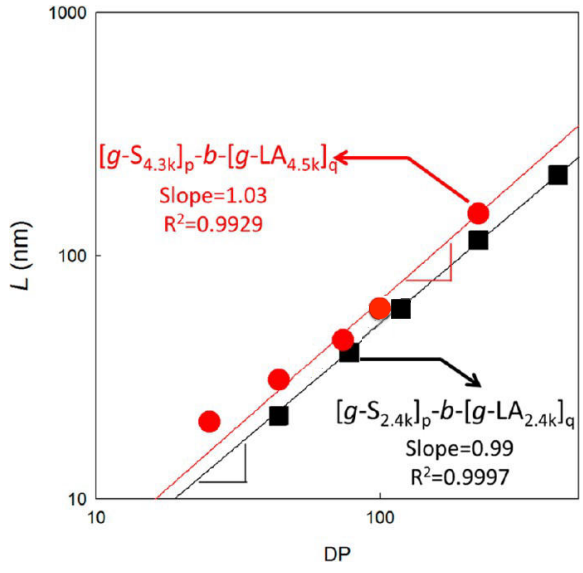

Figure 3-10. Plot of the period (L) as a function of degree of polymerization (DP) of the backbone for brush BCPs with different side chains (2.5×10^3 g/mol for PS and 2.5×10^3 g/mol for PLA (black square), 4.3×10^3 g/mol for PS and 4.5×10^3 g/mol for PLA (red circle)).

As discussed in the previous section, similar results were found in the case of the thermally annealed bulk samples of brush BCPs. In particular, the domain spacing found with solvent annealing is consistently larger than that for thermal annealing, because the swollen domain spacing during solvent annealing is kinetically trapped during the evaporation of the solvent vapor after the sample is removed from the annealing jar. Consequently, the exponents in the bulk state (thermal annealing) are smaller than that in film state (solvent annealing), indicating that the backbone chains are more stretched in solvent-annealed films.

Thin films made from the highest MW brush BCPs showed a very curious surface topography after solvent annealing for 2 hours in THF vapor. The film thickness in **Figure 3-11** was determined by ellipsometry to be 60, 63, and 65 nm, respectively. A uniform height difference between the two microdomains was observed in **Figure 3-11A** and **B**, where representative thin films of brush BCPs with the same side chain MWs, but with different DPs of the backbone ($[g\text{-}S_{2.4}]_{189}$-*b*-$[g\text{-}LA_{2.4}]_{233}$ and $[g\text{-}S_{2.4}]_{259}$-*b*-$[g\text{-}LA_{2.4}]_{381}$), were shown. Analysis of the surface topography shows that terraces formed on the surface, with a step height of only 9 nm for both brush BCPs. This is far less than the step height, *L*, arising from incommensurability between the film thickness and *L*, when the microdomains orient parallel to the surface.[38,39] When the molecular weight of the side chains was increased, as shown in **Figure 3-11C** ($[g\text{-}S_{4.3}]_{206}$-*b*-$[g\text{-}LA_{4.5}]_{278}$), the step changed to being 13 nm. These values correspond roughly to the diameters of the brushes, and suggest that there is a single layer of the brush BCP covering the surface of the film. X-ray photon spectroscopy (XPS) was used to characterize the composition of the surface of the films (**Table 3-2**), which, from an atomic concentration analysis, suggests that the PS-brush block is preferentially covering the surface. This would be consistent with the lower surface energy of the PS-brush block, but also suggests that the brush BCP must assume a rather unusual bent configuration at the surface in order to minimize the surface energy. The exact nature of this configuration is unknown, at present, and is under further study. It is also noted that the difference in film thickness and solvent annealing time can have a significant influence on final morphologies; for example, both **Figure 3-6** and **Figure 3-11A** are from the same sample, but behave differently.

Table 3-2. Carbon:Oxygen Atomic Concentration (According to C 1s and O 1s Peaks in XPS Spectrscopy).

Sample	15°	75°
$[g\text{-}S_{2.4}]_{189}$-*b*-$[g\text{-}LA_{2.4}]_{233}$	80.2:11.5	89.5:7.2
$[g\text{-}S_{2.4}]_{259}$-*b*-$[g\text{-}LA_{2.4}]_{381}$	70.2:24.9	73.9:25
$[g\text{-}S_{4.3}]_{206}$-*b*-$[g\text{-}LA_{4.5}]_{278}$	79.2:20.8	78.8:21.2

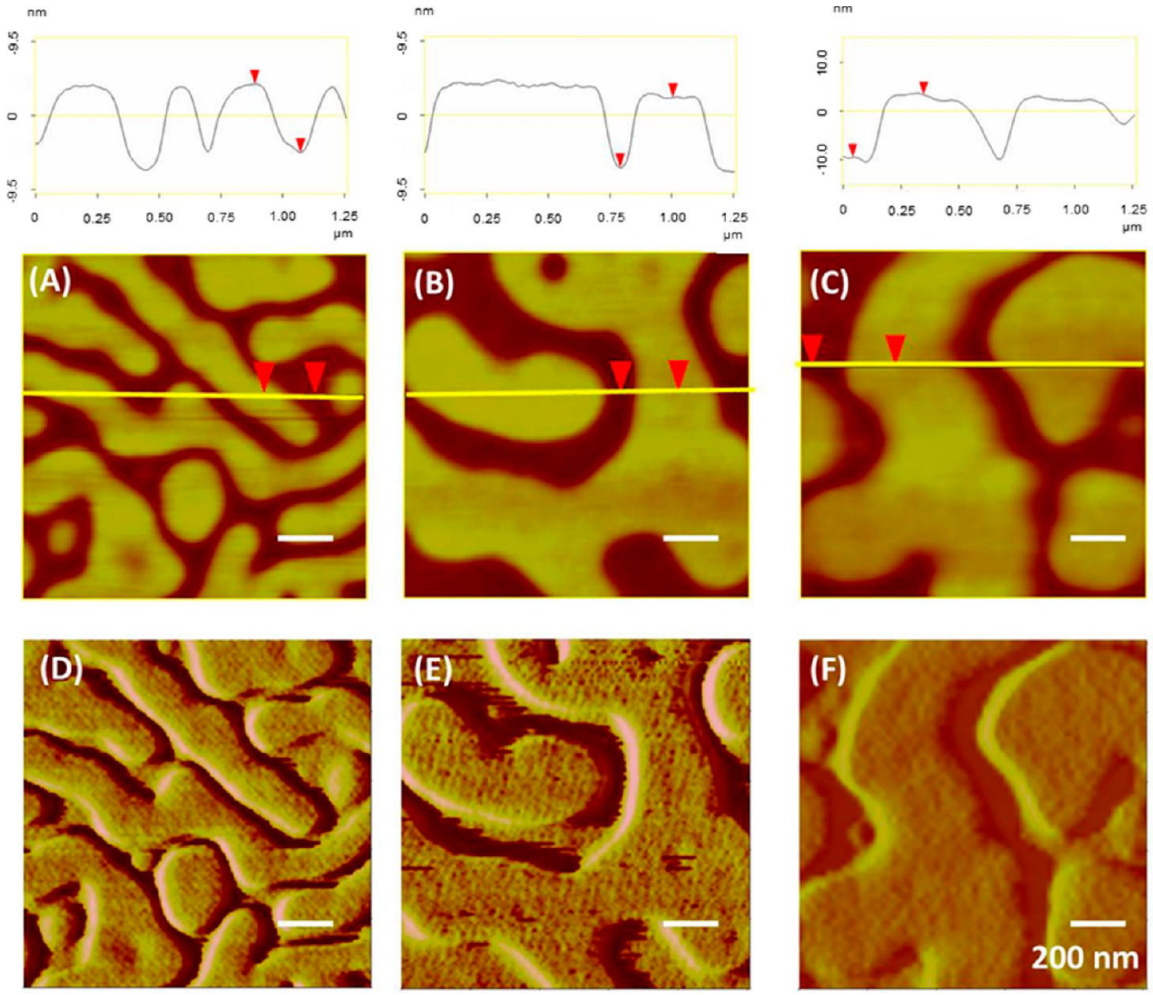

Figure 3-11. SFM height (A-C) and phase (D-F) images obtained from thin films of $[g\text{-}S_{2.4}]_{189}$-*b*-$[g\text{-}LA_{2.4}]_{233}$, $[g\text{-}S_{2.4}]_{259}$-*b*-$[g\text{-}LA_{2.4}]_{381}$, and $[g\text{-}S_{4.3}]_{206}$-*b*-$[g\text{-}LA_{4.5}]_{278}$ on Si substrates, respectively. The plots above SFM images are cross sectional analysis of the corresponding height images below.

FAST KINETICS OF SELF-ASSEMBLY IN THE BULK

Polymer entanglement causes a kinetic barrier for polymers to self-assemble, thus leading to a slow kinetic process of the self-assembly. As the polymers grow bigger, entanglement can have an increased effect on the self-assembly process. Brush polymers have, on the other hand, been reported to show non-entangled dynamics at the high MW regime up to several thousand kilodaltons,[40] which allows us to expect a more rapid self-assembly process even for the ultra-high MW (hundreds to thousands of kilodaltons, as indicated in **Table 3-1**) of brush BCPs. This inspired

us to take a closer look at the unique properties of those brush BCPs and their self-assembly behavior in the bulk state. *In situ* SAXS was used to monitor the kinetics of the self-assembly process. **Figure 3-12** shows representative examples of samples $[g\text{-}S_{2.4}]_{35}$-*b*-$[g\text{-}LA_{2.4}]_{43}$, $[g\text{-}S_{2.4}]_{51}$-*b*-$[g\text{-}LA_{2.4}]_{67}$, and $[g\text{-}S_{2.4}]_{98}$-*b*-$[g\text{-}LA_{2.4}]_{124}$. For instance, in **Figures 3-12B**, the initial state, as indicated by the bottom black curve, did not show any distinct peak and exhibited a gradual decrease in intensity, suggesting that chains of brush BCPs were in random arrangements. A measurement was taken immediately (1 s, red curve) once the temperature was increased to 130 °C and a primary peak at ~ 0.012 $Å^{-1}$ appeared. This implies that a characteristic distance was developed, although it was not too well-defined due to its broad shape. Upon longer annealing time, the primary scattering wavevector q* shifted a little bit to smaller q value (0.011 Å), and higher-order reflections were profoundly enhanced at integral multiples of q*, evidence of improvement in lateral order of lamellar structures. Notably, the low MW brush BCP (**Figure 3-12A**) self-assembled much more rapidly (~5 minutes) in comparison to the high MW (**Figure 3-12C**, ~1 hour) brush BCP. It is understandable that low MW brush BCPs have less entanglement between chains, and thus the mobility is higher. Nevertheless, these results show that well-ordered lamellar structures were formed within an hour for all of the samples shown.

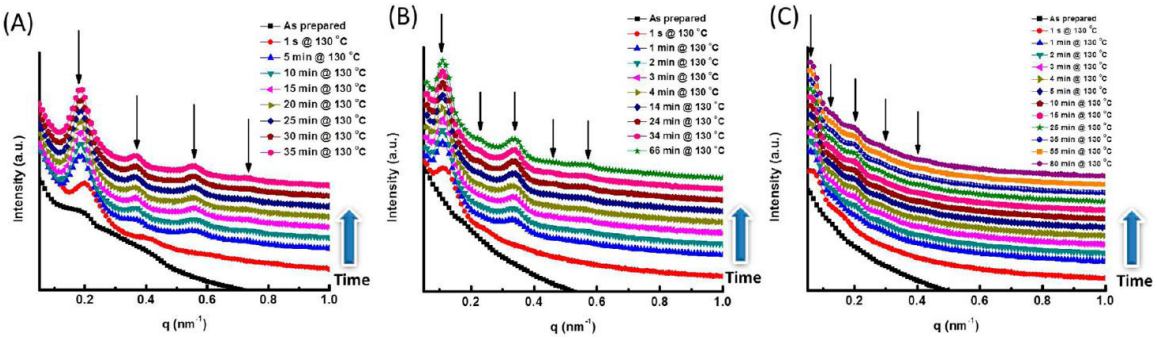

Figure 3-12. *In situ* SAXS of sample (A) $[g\text{-}S_{2.4}]_{35}$-*b*-$[g\text{-}LA_{2.4}]_{43}$, (B) $[g\text{-}S_{2.4}]_{51}$-*b*-$[g\text{-}LA_{2.4}]_{67}$, and (C) $[g\text{-}S_{2.4}]_{98}$-*b*-$[g\text{-}LA_{2.4}]_{124}$.

CONCLUSION AND FUTURE DIRECTIONS

In summary, symmetric brush BCPs of PLA and PS side chains self-assemble rapidly into highly ordered lamellar domains ranging from 20 to 235 nm, as revealed by SAXS, both in bulk and thin films. The domain size increases approximately linearly with the DP of the backbone, which indicates that the backbone is in an extremely extended conformation. The domain spacing was

found to be consistently larger in thin films than in bulk samples, and this was attributed to the swollen domains being kinetically trapped during the evaporation of the solvent vapor after the sample is removed from the annealing jar.

Further analysis of the higher MW samples (group III and group IV) is still underway, but preliminary results suggest that it may be more difficult to obtain well-ordered microdomains as the side chain size increases. Samples have also been synthesized with a few units of deuterated PS (PS(*d*8)) side chains at the end of the brush BCP for small-angle neutron scattering (SANS) studies (**Table 3-3**). The SANS studies will be used to provide evidence to distinguish if these brush polymers undergo a normal head-to-head packing or if they undergo interdigitate packing (**Scheme 3-3**).

Table 3-3. Characteristics of brush BCPs with deuterated PS at the end of the brush BCP.

Sample	M_n [a] (× 10^3 g/mol)	PDI [a]	DP - PLA [b]	DP - PS [c]	DP - PS(*d*8) [d]	Total DP
1	417	1.02	44	40	5	89
2	862	1.03	91	83	9	183
3	1794	1.10	190	172	20	382

[a] Determined by THF GPC using RI and MALLS detectors. [b] DP of the PLA MM (M_n = 4.76 ×10^3 g/mol) as estimated by GPC and mol % of MM used during ROMP. [c] DP of the PS MM (M_n = 4.67 ×10^3 g/mol) as estimated by GPC and mol % of MM used during ROMP. [d] DP of the PS(*d*8) MM (M_n = 4.69 ×10^3 g/mol) as estimated by GPC and mol % of MM used during ROMP.

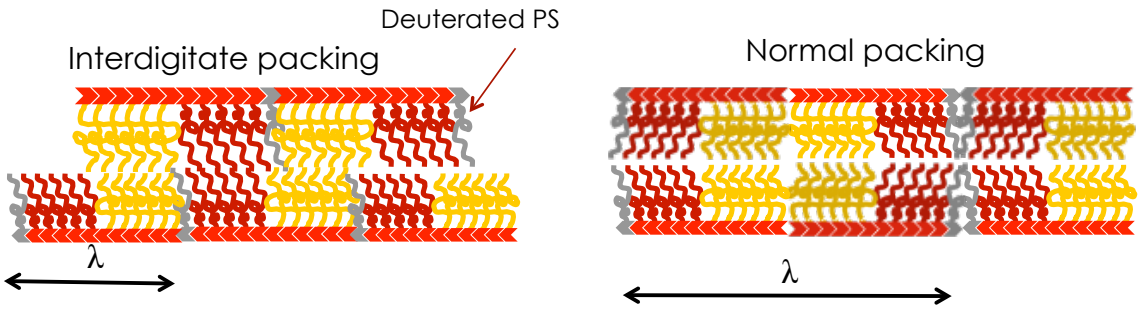

Scheme 3-3. A schematic illustration of the expected self-assembly of brush BCPs with deuterated PS side chains at the end, undergoing either interdigitate packing (left) or normal packing (right).

REFERENCES:

(1) Park, M.; Harrison, C.; Chaikin, P. M.; Register, R. A.; Adamson, D. H. *Science* **1997**, *276*, 1401.

(2) Li, R. R.; Dapkus, P. D.; Thompson, M. E.; Jeong, W. G.; Harrison, C.; Chaikin, P. M.; Register, R. a.; Adamson, D. H. *Appl. Phys. Lett.* **2000**, *76*, 1689.

(3) Thurn-Albrecht, T.; Schotter, J.; Kastle, G. A.; Emley, N.; Shibauchi, T.; Krusin-Elbaum, L.; Guarini, K.; Black, C. T.; Tuominen, M. T.; Russell, T. P. *Science* **2000**, *290*, 2126.

(4) Kim, B. H.; Jia, X.; Stafford, C. M.; Kim, D. H.; Mccarthy, T. J.; Tuominen, M.; Hawker, C. J.; Russell, T. P. *Adv. Mater.* **2001**, *13*, 795.

(5) Cheng, J. Y.; Ross, C. A.; Chan, V. Z.; Thomas, E. L.; Lammertink, R. G. H.; Vancso, G. J. *Adv. Mater.* **2001**, *13*, 1174.

(6) Black, C. T.; Guarini, K. W.; Milkove, K. R.; Baker, S. M.; Russell, T. P.; Tuominen, M. T. *Appl. Phys. Lett.* **2001**, *79*, 409.

(7) Lopes, W. a; Jaeger, H. M. *Nature* **2001**, *414*, 735.

(8) Black, C. T. *Appl. Phys. Lett.* **2005**, *87*, 163116.

(9) Pelletier, V.; Asakawa, K.; Wu, M.; Adamson, D. H.; Register, R. a.; Chaikin, P. M. *Appl. Phys. Lett.* **2006**, *88*, 211114.

(10) Cheng, J. Y.; Ross, C. a.; Smith, H. I.; Thomas, E. L. *Adv. Mater.* **2006**, *18*, 2505.

(11) Kang, Y.; Walish, J. J.; Gorishnyy, T.; Thomas, E. L. *Nat. Mater.* **2007**, *6*, 957.

(12) Luttge, R. *J. Phys. D Appl. Phys.* **2009**, *42*, 123001.

(13) Xu, J.; Hong, S. W.; Gu, W.; Lee, K. Y.; Kuo, D. S.; Xiao, S.; Russell, T. P. *Adv. Mater.* **2011**, *23*, 5755.

(14) Gu, X.; Liu, Z.; Gunkel, I.; Chourou, S. T.; Hong, S. W.; Olynick, D. L.; Russell, T. P. *Adv. Mater.* **2012**, *24*, 5688.

(15) Bates, F. S.; Fredrickson, G. H. *Annu. Rev. Phys. Chem.* **1990**, *41*, 525.

(16) Hamley, I. W. *Nanotechnology* **2003**, *14*, R39.

(17) Park, C.; Yoon, J.; Thomas, E. L. *Polymer* **2003**, *44*, 6725.

(18) Segalman, R. A. *Mater. Sci. Eng. R Rep.* **2005**, *48*, 191.

(19) Stoykovich, M. P.; Nealey, P. F. *Nature* **2006**, *9*, 20.

(20) Park, S.; Lee, D. H.; Xu, J.; Kim, B.; Hong, S. W.; Jeong, U.; Xu, T.; Russell, T. P. *Science* **2009**, *323*, 1030.

(21) Marencic, A. P.; Register, R. A. *Annu. Rev. Chem. Biomol. Eng.* **2010**, *1*, 277.

(22) Albert, J. N. L.; Epps, T. H. *Mater. Today* **2010**, *13*, 24.

(23) Tseng, Y.-C.; Darling, S. B. *Polymers* **2010**, *2*, 470.

(24) Gedde, U. F. *Polymer Physics*; Springer: London, 1995.

(25) RamachandraRao, V. S.; Gupta, R. R.; Russell, T. P.; Watkins, J. J. *Macromolecules* **2001**, *34*, 7923.

(26) Kim, E.; Ahn, H.; Park, S.; Lee, H.; Lee, M.; Lee, S.; Kim, T.; Kwak, E.-A.; Lee, J. H.; Lei, X.; Huh, J.; Bang, J.; Lee, B.; Ryu, D. Y. *ACS Nano* **2013**, *7*, 1952.

(27) Fink, Y.; Urbas, A. M.; Bawendi, M. G.; Joannopoulos, J. D.; Thomas, E. L. *J. Light. Technol.* **1999**, *17*, 1963.

(28) Kang, C.; Kim, E.; Baek, H.; Hwang, K.; Kwak, D.; Kang, Y.; Thomas, E. L. *J. Am. Chem. Soc.* **2009**, *131*, 7538.

(29) Yoon, J.; Mathers, R. T.; Coates, G. W.; Thomas, E. L. *Macromolecules* **2006**, *39*, 1913.

(30) Runge, M. B.; Dutta, S.; Bowden, N. B. *Macromolecules* **2006**, *39*, 498.

(31) Rzayev, J. *Macromolecules* **2009**, *42*, 2135.

(32) Oono, Y.; Bahiana, M. *Phys. Rev. Lett.* **1988**, *61*, 1100.

(33) Zalusky, A. S.; Olayo-Valles, R.; Wolf, J. H.; Hillmyer, M. A. *J. Am. Chem. Soc.* **2002**, *124*, 12761.

(34) Delamarche, E.; Michel, B.; Gerber, C.; Anselmetti, D.; Guntherodt, H.-J.; Wolf, H.; Ringsdorf, H. *Langmuir* **1994**, *10*, 2869.

(35) Mansky, P.; Liu, Y.; Huang, E.; Russell, T. P.; Hawker, C. *Science* **1997**, *275*, 1458.

(36) Ryu, D. Y.; Shin, K.; Drockenmuller, E.; Hawker, C. J.; Russell, T. P. *Science* **2005**, *308*, 236.

(37) Ji, S.; Liu, C.-C.; Son, J. G.; Gotrik, K.; Craig, G. S. W.; Gopalan, P.; Himpsel, F. J.; Char, K.; Nealey, P. F. *Macromolecules* **2008**, *41*, 9098.

(38) Russell, T. P.; Coulon, G.; Deline, V. R.; Miller, D. C. *Macromolecules* **1989**, *22*, 4600.

(39) Anastasiadis, S. H.; Russell, T. P.; Satija, S. K.; Majkrzak, C. F. *J. Chem. Phys.* **1990**, *92*, 5677.

(40) Hu, M.; Xia, Y.; McKenna, G. B.; Kornfield, J. A.; Grubbs, R. H. *Macromolecules* **2011**, *44*, 6935.

Chapter 4

SELF-ASSEMBLY OF ASYMMETRIC BRUSH BLOCK COPOLYMERS

ABSTRACT

Self-assembled structures of asymmetric brush block copolymers (BCPs) with polylactide (PLA) and polystyrene (PS) side chains were studied. The volume fractions of each block were varied in order to observe where morphological transitions took place. AFM and SEM imaging showed a transition from lamellar to a cylindrical-like morphology when the volume fraction of one of the blocks exceeded 70% for samples annealed by either thermal compression or controlled evaporation from tetrahydrofuran (THF). Drop-cast samples were analyzed via small-angle X-ray scattering (SAXS). They were found to be kinetically trapped in their initial morphologies that were best indexed to an undulating lamellar type structure, where the primary structure is a lamellar array, but with small regions possessing short-range hexagonal order.

INTRODUCTION

Block copolymers (BCPs) have attracted tremendous interest from both academia and industry because of their ability to self-assemble into periodic structures with domain spacing ranging from 10 to 100 nm.[1–3] The incompatibility effects arising from the particular chemical structure of block copolymers give them a number of specific morphologies such as spheres, cylinders, lamellae, or gyroid, which leads to numerous technological applications.[4,5] For a noncrystalline A-B diblock copolymer, the bulk morphology is determined by Flory-Huggins parameter, χ, the total degree of polymerizaion, N, and volume fraction of each block, f. When χN exceeds the critical value for the order-disorder transition, the repulsive interactions between the blocks are strong enough for microphase separation to occur.[6] By increasing the asymmetry of the volume fractions of each block in a BCP, the morphology of the microdomains can be shifted from lamellar to hexagonally arranged cylinders to cubically ordered spheres.[6,7] The ability to control the morphology of BCPs is important to tuning the BCP properties for specific application. For example, for photonic materials, the morphology affects in how many dimensions light modes can be localized.[8,9]

Morphological transitions have been well studied for linear BCPs and have resulted in phase diagrams for a number of polymer systems. However, to the best of our knowledge, morphology transitions of brush BCPs have not yet been studied. This chapter describes our initial findings concerning where the morphology transitions of a polylactide (PLA)/polystyrene (PS) based brush BCP system take place.

SYNTHESIS OF ASYMMETRIC BRUSH BCPs

Asymmetric brush BCPs were synthesized in an analogous manner, as described in *Chapter 2*, using a sequential ruthenium-catalyzed ring-opening metathesis polymerization (ROMP) of PLA and PS based macromonomers (MMs).[10] The molar equivalences of the MMs were varied during the sequential ROMP in order to control the asymmetry of the blocks in the resulting brush BCP. Several series of asymmetric brush BCPs were synthesized, as shown in **Table 4-1**. Each series utilized different side chain lengths; within each series, the block length asymmetry was varied while maintaining approximately constant total degree of polymerization (DP). The form of the sample codes, $[g\text{-}S_x]_p\text{-}b\text{-}[g\text{-}LA_y]_q$, is the same as used in *Chapter 3,* where the subscripts x and y are the molecular weights of the side chains of each type (in units of one thousand), and subscripts p and q represent the degree of polymerization of each brush block.

Table 4-1. Sample codes and characteristics of asymmetric brush block copolymers.

Group	Sample codes	Total M_n [a] ($\times 10^3$ g/mol)	PDI [a]	Total DP [b]	PLA% [b]	PS% [b]
I	$[g\text{-}S_{2.4}]_{56}$-*b*-$[g\text{-}LA_{2.4}]_{182}$	565	1.14	238	76	24
	$[g\text{-}S_{2.4}]_{64}$-*b*-$[g\text{-}LA_{2.4}]_{158}$	528	1.07	222	71	29
	$[g\text{-}S_{2.4}]_{118}$-*b*-$[g\text{-}LA_{2.4}]_{137}$	607	1.09	255	54	46
II	$[g\text{-}S_{4.3}]_{26}$-*b*-$[g\text{-}LA_{4.3}]_{174}$	868	1.07	194	87	13
	$[g\text{-}S_{4.3}]_{56}$-*b*-$[g\text{-}LA_{4.3}]_{160}$	934	1.06	209	74	26
	$[g\text{-}S_{4.3}]_{159}$-*b*-$[g\text{-}LA_{4.3}]_{48}$	895	1.09	204	23	77
	$[g\text{-}S_{4.3}]_{195}$-*b*-$[g\text{-}LA_{4.3}]_{24}$	943	1.06	216	11	89
III	$[g\text{-}S_{2.6}]_{332}$-*b*-$[g\text{-}LA_{2.5}]_{17}$	902	1.03	349	5	95
	$[g\text{-}S_{2.6}]_{314}$-*b*-$[g\text{-}LA_{2.5}]_{29}$	885	1.01	342	8	92
	$[g\text{-}S_{2.6}]_{313}$-*b*-$[g\text{-}LA_{2.5}]_{46}$	929	1.02	359	13	87
	$[g\text{-}S_{2.6}]_{343}$-*b*-$[g\text{-}LA_{2.5}]_{68}$	1060	1.02	411	17	83
	$[g\text{-}S_{2.6}]_{278}$-*b*-$[g\text{-}LA_{2.5}]_{73}$	905	1.05	351	21	79
	$[g\text{-}S_{2.6}]_{288}$-*b*-$[g\text{-}LA_{2.5}]_{95}$	988	1.05	383	25	75
	$[g\text{-}S_{2.6}]_{273}$-*b*-$[g\text{-}LA_{2.5}]_{117}$	1005	1.03	390	30	70
	$[g\text{-}S_{2.6}]_{264}$-*b*-$[g\text{-}LA_{2.5}]_{144}$	1049	1.02	408	35	65
IV	$[g\text{-}S_{4.7}]_{370}$-*b*-$[g\text{-}LA_{4.2}]_{19}$	1834	1.21	389	5	95
	$[g\text{-}S_{4.7}]_{364}$-*b*-$[g\text{-}LA_{4.2}]_{38}$	1888	1.18	402	10	90
	$[g\text{-}S_{4.7}]_{348}$-*b*-$[g\text{-}LA_{4.2}]_{63}$	1917	1.11	411	15	85
	$[g\text{-}S_{4.7}]_{332}$-*b*-$[g\text{-}LA_{4.2}]_{79}$	1910	1.10	411	19	81
	$[g\text{-}S_{4.7}]_{308}$-*b*-$[g\text{-}LA_{4.2}]_{102}$	1892	1.06	410	25	75
	$[g\text{-}S_{4.7}]_{283}$-*b*-$[g\text{-}LA_{4.2}]_{121}$	1853	1.06	404	30	70
	$[g\text{-}S_{4.7}]_{263}$-*b*-$[g\text{-}LA_{4.2}]_{143}$	1851	1.05	406	35	65
	$[g\text{-}S_{4.7}]_{268}$-*b*-$[g\text{-}LA_{4.2}]_{179}$	2028	1.06	447	40	60

[a] Determined by THF GPC using RI and MALLS detectors. [b] Degree of polymerization and mol percentages were determined by ^{1}H NMR and THF GPC (as described in *Chapter 2*).

RESULTS AND DISCUSSION

Samples from group I and group II were thermally annealed at 130 °C for 24 hours before being analyzed by atomic force microscopy (AFM). Samples from group I (**Figure 4-1**) showed that when the PS block was 46% of the whole brush BCP ($[g\text{-}S_{2.4}]_{118}$-*b*-$[g\text{-}LA_{2.4}]_{137}$), a lamellar structure was observed by AFM (**Figure 4-1C**). When the PS block was 29% ($[g\text{-}S_{2.4}]_{64}$-*b*-$[g\text{-}LA_{2.4}]_{158}$), a change in morphology was observed, where AFM images showed a structure that could be either a) part cylindrical and part lamellar, or b) cylindrical, where some of the cylinders are perpendicular to the surface and others are parallel to the surface (**Figure 4-1B**). At 24% PS incorporation in the

brush BCP ([*g*-$S_{2.4}$]$_{56}$-*b*-[*g*-$LA_{2.4}$]$_{182}$), a uniform morphology was observed, indicating that the brush BCP may have self-assembled completely into a cylindrical structure (**Figure 4-1A**).

AFM images of [*g*-$S_{4.3}$]$_{26}$-*b*-[*g*-$LA_{4.3}$]$_{174}$ (13% PS) and [*g*-$S_{4.3}$]$_{56}$-*b*-[*g*-$LA_{4.3}$]$_{160}$ (26% PS) from group II (**Figure 4-2A-B**) showed a similar morphology to the 24% PS sample ([*g*-$S_{2.4}$]$_{56}$-*b*-[*g*-$LA_{2.4}$]$_{182}$) from group I, suggesting that these samples had a cylindrical morphology. However, when PLA was the major block in the brush BCPs, the AFM images were not as clear regarding their morphology. [*g*-$S_{2.4}$]$_{150}$-*b*-[*g*-$LA_{2.4}$]$_{48}$ (77% PS) showed some lamellar like structure, but not consistently throughout the sample (**Figure 4-2C**), and while ([*g*-$S_{2.4}$]$_{195}$-*b*-[*g*-$LA_{2.4}$]$_{24}$ (89% PS) displayed a structure that could be suggestive of a somewhat cylindrical morphology (**Figure 4-2D**), the image was not clear enough to make a conclusive conjecture. In order to determine the morphologies of the above-mentioned samples, more data, such as small angle X-ray scattering (SAXS), was required.

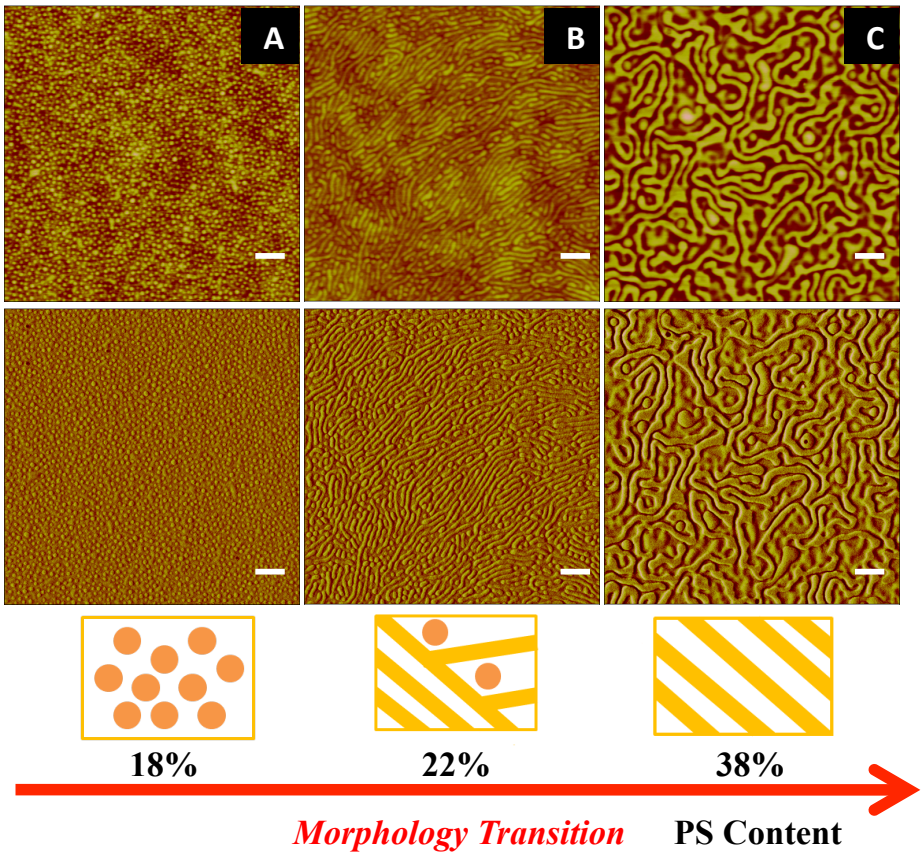

Figure 4-1. AFM height (first row) and phase (second row) images of A) [*g*-$S_{2.4}$]$_{56}$-*b*-[*g*-$LA_{2.4}$]$_{182}$; B) [*g*-$S_{2.4}$]$_{64}$-*b*-[*g*-$LA_{2.4}$]$_{158}$; and C) [*g*-$S_{2.4}$]$_{118}$-*b*-[*g*-$LA_{2.4}$]$_{137}$. Scale bar is 500 nm.

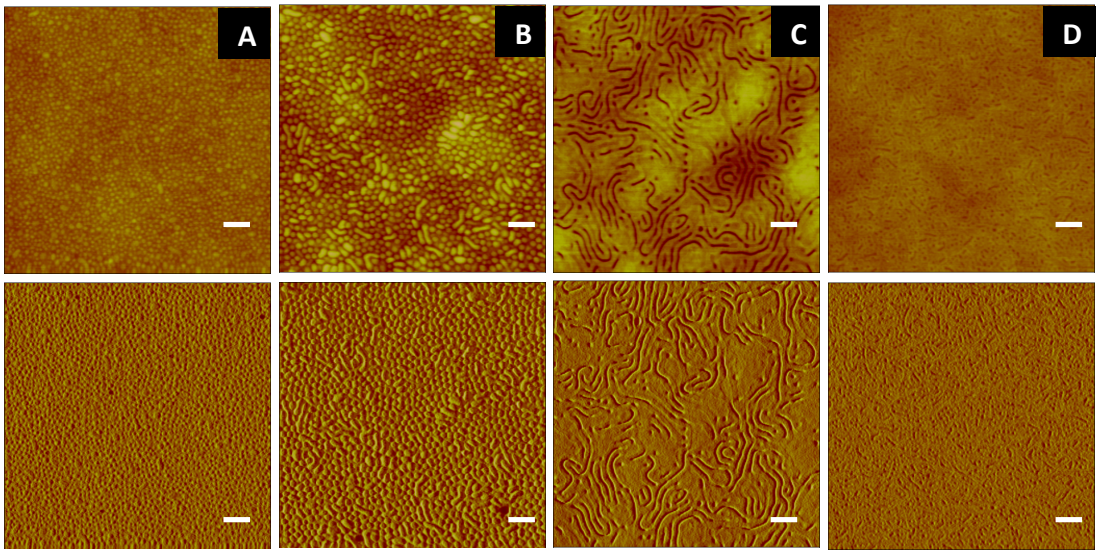

Figure 4-2. AFM height (first row) and phase (second row) images of A) $[g\text{-}S_{4.3}]_{26}$-*b*-$[g\text{-}LA_{4.3}]_{174}$; B) $[g\text{-}S_{4.3}]_{56}$-*b*-$[g\text{-}LA_{4.3}]_{160}$; C) $[g\text{-}S_{4.3}]_{159}$-*b*-$[g\text{-}LA_{4.3}]_{48}$; and D) $[g\text{-}S_{4.3}]_{195}$-*b*-$[g\text{-}LA_{4.3}]_{24}$. Scale bar is 500 nm.

In order to identify the volume fractions of PS/PLA where morphology transitions take place, brush BCPs from group III and group IV were drop-cast onto glass slides and analyzed via SAXS (**Figure 4-3**). These series had smaller increments of volume fractions, making it easier to identify where the morphology started to change. The SAXS profiles of the samples with highest degree of symmetry were best indexed to a lamellar morphology. As the asymmetry increased, the order of the samples decreased, as indicated by the reduced sharpness of the scattering peaks in the SAXS profiles and the reduced number of visible scattering peaks. However, some peaks appeared to be asymmetric, and other peaks were present only in some samples. This is more easily observed when the profiles are offset in order to align the first order scattering peak (**Figure 4-4**) (e.g. the presence/absence of a peak @ $q/q_o \sim 2.8$). This indicates that, in some of the samples, multiple different morphologies may be present, although with limited amount of order. We hypothesize that these results indicate that, since the drop-cast samples do not have adequate time to achieve thermodynamic equilibrium, these structures are kinetically trapped in the initial morphologies. These morphologies are best indexed to an undulating lamellar type structure where the primary structure is a lamellar array, but with small regions possessing short-range hexagonal order.

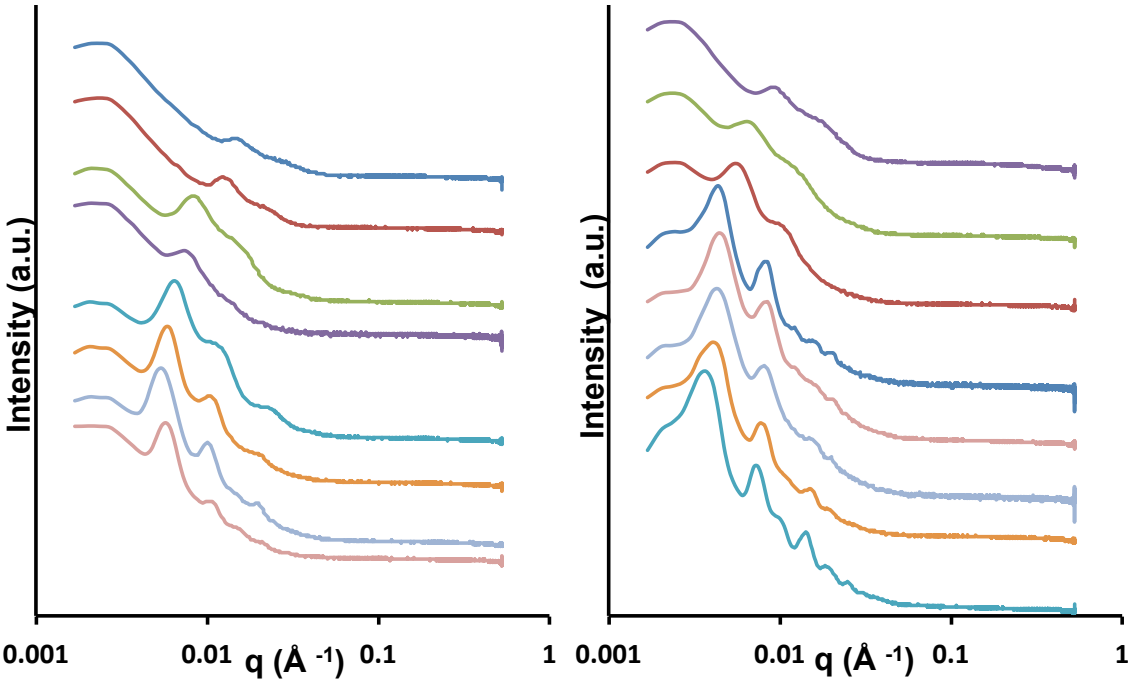

Figure 4-3. SAXS profiles of samples from group III (left) and group IV (right), where higher traces are of increased asymmetry.

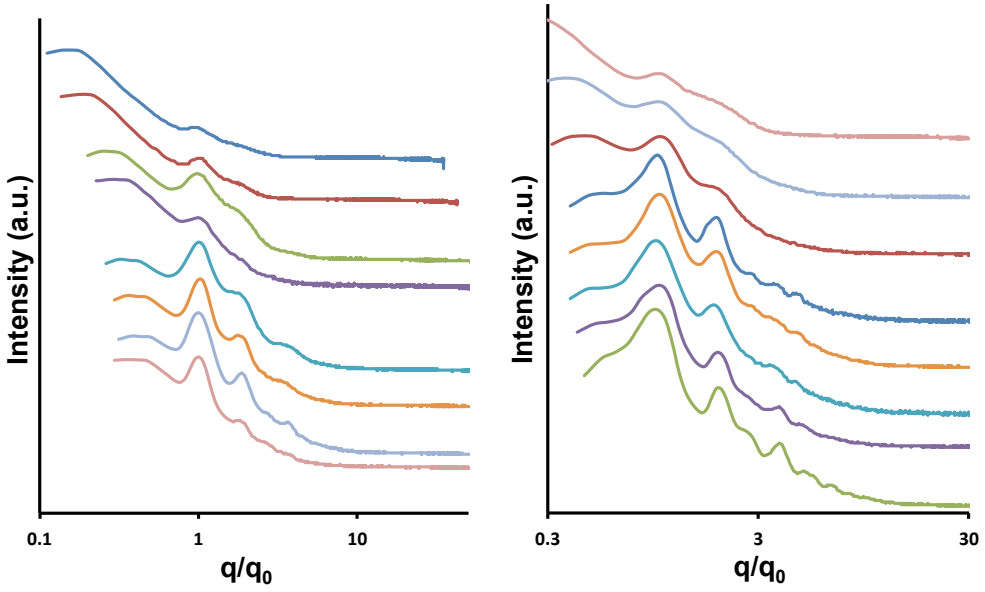

Figure 4-4. Offset SAXS profiles of samples from group III (left) and group IV (right), where higher traces are of increased asymmetry.

The group IV samples were also annealed via controlled evaporation from tetrahydrofuran (THF) on silica substrates, and thermal compression between two glass slides, before being subjected to scanning electron microscopy (SEM) imaging. For the samples annealed via controlled evaporation, it was clear that [*g*-$S_{4.7}$]$_{268}$-*b*-[*g*-$LA_{4.2}$]$_{179}$ (40% PS) and [*g*-$S_{4.7}$]$_{263}$-*b*-[*g*-$LA_{4.2}$]$_{143}$ (35% PS) gave lamellar structure (**Figure 4-5 A-B**). Meanwhile, [*g*-$S_{4.7}$]$_{282}$-*b*-[*g*-$LA_{4.2}$]$_{121}$ (30% PS) (**Figure 4-5C**) seemed to give a structure similar to the one observed in **Figure 4-1B** for [*g*-$S_{2.4}$]$_{64}$-*b*-[*g*-$LA_{2.4}$]$_{158}$, where it could be either a) part cylindrical and part lamellar, or b) cylindrical, in parts parallel and in parts perpendicular to the substrate. This provides further evidence that these brush BCPs seem to start undergoing some transition when one of the volume fractions is around 30%.

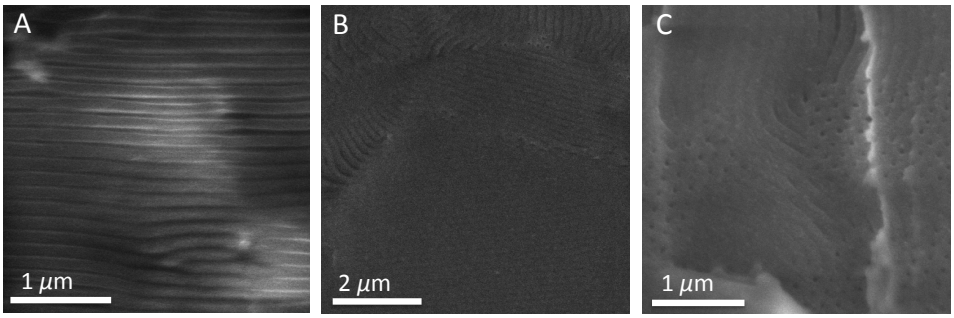

Figure 4-5. SEM images of a) [*g*-$S_{4.7}$]$_{268}$-*b*-[*g*-$LA_{4.2}$]$_{179}$; b) [*g*-$S_{4.7}$]$_{263}$-*b*-[*g*-$LA_{4.2}$]$_{143}$; and c) [*g*-$S_{4.7}$]$_{282}$-*b*-[*g*-$LA_{4.2}$]$_{121}$.

The thermally compressed samples did not give as clear morphologies. Nevertheless, there was a clear morphology change observed from [*g*-$S_{4.7}$]$_{263}$-*b*-[*g*-$LA_{4.2}$]$_{143}$ (35% PS) (**Figure 4-6A**) to [*g*-$S_{4.7}$]$_{282}$-*b*-[*g*-$LA_{4.2}$]$_{121}$ (30% PS) (**Figure 4-6B**). Other samples with more asymmetry showed somewhat similar structures that might suggest some cylindrical morphology for samples with up to 85% PS incorporation (**Figure 4-6C-D**). Clear SEM images were not obtained for other samples.

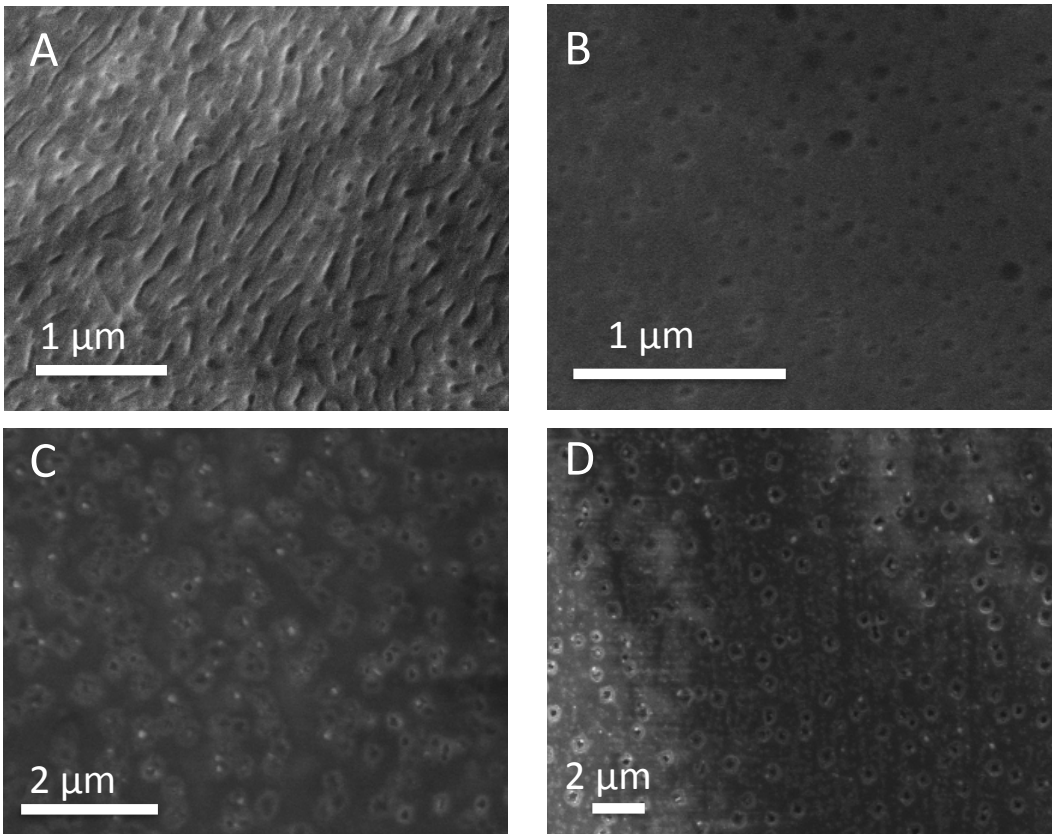

Figure 4-6. SEM images of a) [*g*-$S_{4.7}$]$_{263}$-*b*-[*g*-$LA_{4.2}$]$_{143}$; b) [*g*-$S_{4.7}$]$_{282}$-*b*-[*g*-$LA_{4.2}$]$_{121}$; c) [*g*-$S_{4.7}$]$_{332}$-*b*-[*g*-$LA_{4.2}$]$_{79}$; and d) [*g*-$S_{4.7}$]$_{348}$-*b*-[*g*-$LA_{4.2}$]$_{63}$.

CONCLUSIONS AND FUTURE DIRECTIONS

These results indicate that under thermal equilibrium, brush BCPs with similarly sized side chains undergo a morphology transition when the volume fraction of one of the blocks exceeds 70%. Asymmetric brush BCPs can also be kinetically trapped into a (undulating) lamellar morphology where the order of the sample decreases with increased asymmetry. In order to make more conclusive statements about the morphology transitions of asymmetric brush BCPs, it will be important to obtain SAXS data from samples that have achieved thermal equilibrium. Furthermore, it may prove valuable to explore the effect of the backbone length on the self-assembly of these macromolecules, as lower molecular weight brush BCPs have been shown to achieve thermal equilibrium more rapidly than those with higher molecular weights.[11]

REFERENCES:

(1) Bates, F. S.; Hillmyer, M. A.; Lodge, T. P.; Bates, C. M.; Delaney, K. T.; Fredrickson, G. H. *Science* **2012**, *336*, 434.

(2) Bates, F. S.; Fredrickson, G. H. *Annu. Rev. Phys. Chem.* **1990**, *41*, 525.

(3) Hamley, I. W. *The Physics of Block Copolymers*; Oxforrd University Press: New York, 1998.

(4) Segalman, R. A. *Mater. Sci. Eng. R Rep.* **2005**, *48*, 191.

(5) Tsui, O. K. C.; Russell, T. P. *Polymer Thin Films*; World Scientific: Singapore, 2008.

(6) Kim, H.-C.; Park, S.-M.; Hinsberg, W. D. *Chem. Rev.* **2010**, *110*, 146.

(7) Grubbs, R. B. *J. Polym. Sci. Part A Polym. Chem.* **2005**, *43*, 4323.

(8) Edrington, A. C.; Urbas, A. M.; DeRege, P.; Chen, C. X.; Swager, T. M.; Hadjichristidis, N.; Xenidou, M.; Fetters, L. J.; Joannopoulos, J. D.; Fink, Y.; Thomas, E. L. *Adv. Mater.* **2001**, *13*, 421.

(9) Joannopoulos, J. D. *Photonic Crystals: Molding The Flow of Light*; Princeton University Press, 2008.

(10) Sveinbjörnsson, B. R.; Weitekamp, R. A.; Miyake, G. M.; Xia, Y.; Atwater, H. A.; Grubbs, R. H. *Proc. Natl. Acad. Sci. USA* **2012**, *109*, 14332.

(11) Gu, W.; Huh, J.; Hong, S. W.; Sveinbjornsson, B. R.; Park, C.; Grubbs, R. H.; Russell, T. P. *ACS Nano* **2013**, *7*, 2551.

C h a p t e r 5

STEREOCOMPLEXATION OF BRUSH POLYMERS

Reproduced with permission from:
Sveinbjörnsson, B. R.; Miyake, G. M.; El-Batta, A.; Grubbs, R. H. *ACS Macro Letters* **2014**, *3*, 26-29.

ABSTRACT

In this chapter, we explore the capability of macromolecules to interdigitate into densely grafted molecular brush copolymers. We demonstrate that by using the tendency for stereocomplexation between poly(L-lactide) and poly(D-lactide) as a driving force, complementary linear polymers and brush copolymers can form a stereocomplex. However, stereocomplex formation between complementary brush copolymers is restricted, and only partially observed when the side chains are of a critical molecular weight.

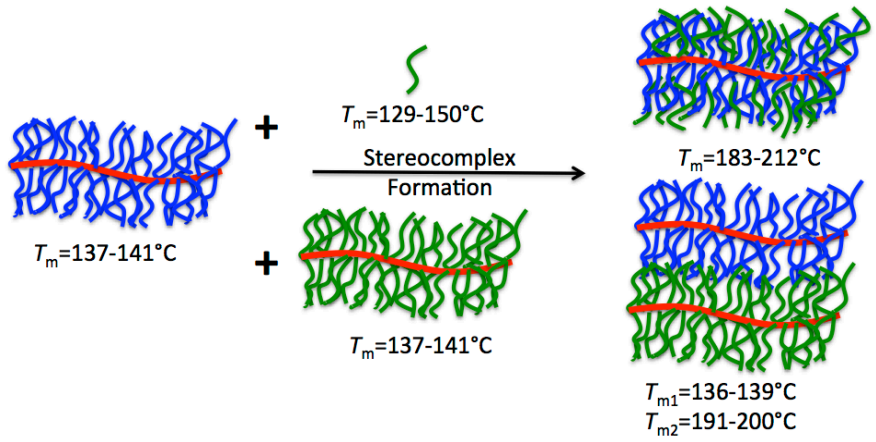

INTRODUCTION

As discussed before, one of the advantages of using the self-assembly of brush polymers for applications, such as for photonic material, is that these polymers undergo very rapid self-assembly compared to the linear analogs. This is in part due to the reduced degree of entanglement for brush polymers compared to their linear analogs, as well as because of their rigid structure. Previous studies, using racemic densely grafted brush polymers with racemic poly(lactic acid) side chains, verified that neither the side chains nor the whole polymer showed evidence of entanglement.[1] Furthermore, due to the high density of the grafted polymers, densely grafted brush polymers restrict diffusion of polymers to their backbone while being permeable for small molecules.[2] To the best of our knowledge, this resistance to allowing macromolecules to diffuse through them has only been studied when there was not a strong driving force for the polymer to interact with the brush polymer side chains.

The stereoisomers poly-L-lactide (PLLA) and poly-D-lactide (PDLA) have been reported to show a strong tendency to interact with each other to form stereocomplexes,[3,4] even with certain topological restraints such as in cyclic polymers.[5] Stereocomplexes made from polylactides have a variety of uses, including biodegradable films,[6] fibers,[7,8] hydrogels,[9,10] and as nucleation agents.[11,12] Sparsely grafted polymers have also shown stereocomplex formation,[13] as well as graft polymers with oligomeric side chains.[14] This chapter describes our investigation on whether the propensity for stereocomplexation between PLLA and PDLA could act as an adequately strong driving force to allow macromolecules, both linear and brush, to diffuse through densely grafted brush side chains of various sizes to form the stereocomplexes.

RESULTS AND DISCUSSION

We utilized the macromonomer (MM) approach for the synthesis of the brush polymers, which ensures quantitative grafting density.[15–18] The MMs, PLLA, and PDLA were synthesized through modified literature procedures by ring-opening polymerization from a norbornene-based alcohol initiator catalyzed by a N-heterocyclic carbene (**Scheme 5-1**).[5,19,20] In order to study the side-chain size effect on stereocomplex formation, four pairs of PLLA and PDLA MMs were synthesized, with molecular weights ranging from 5.9-17.4 × 10^3 g/mol (**Table 5-1**). Brush copolymers were subsequently synthesized from each of the MMs via ring-opening metathesis polymerization (ROMP) using a Ruthenium-based third generation initiator (**Scheme 5-1**). The brush polymers

were synthesized with a degree of polymerization through the main chain from 100-200 MM units, yielding brush copolymers with molecular weights ranging from 1.07-2.55 × 10^6 g/mol (**Table 5-1**).

Organocatalyzed polymerization of the enantiomeric lactide monomers produces polylactide MMs that are highly isotactic.[5,21,22] The brush copolymers derived from these MMs exhibit similar optical rotations as their respective MMs, while showing consistently lower melting temperatures and heats of melting than their corresponding MMs (**Table 5-1**). In fact, differential scanning calorimetry (DSC) analysis did not reveal a melting transition temperature for the brush polymers with the shortest side chains. We attribute this to the confinement of the side chains by the brush copolymer architecture, which inhibits their mobility and capability for crystallization.

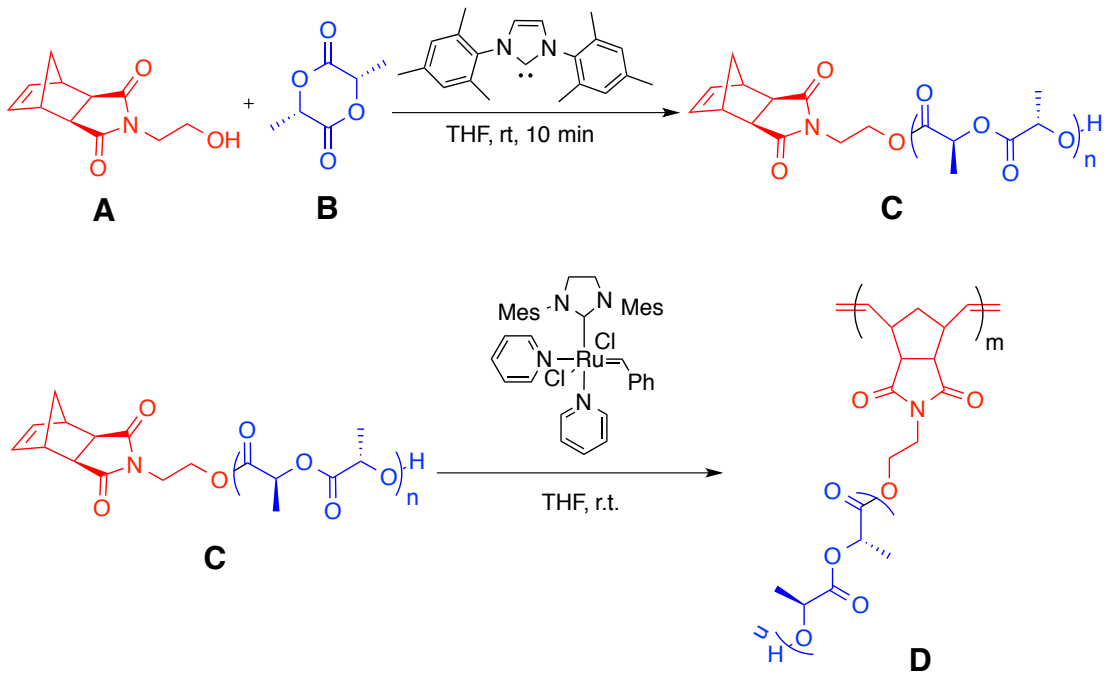

Scheme 5-1. General reaction scheme for the synthesis of the macromonomers (**C**) from a norbornene initiator (**A**) and lactide (**B**) (top) and for the synthesis of the brush copolymer (**D**) form the macromonomer (**C**) (bottom).

Table 5-1. Results for the Macromonomers and Brush Copolymers.

Sample	M_n (10^3 g/mol)[a]	PDI[b]	(Yield)/Conversion (%)[b]	[α][c]	T_m (°C)[d]	ΔH_m (J/g)[d]
L_{MM}-1	5.9	1.18	(63)	-133	129	16
L_{MM}-2	8.6	1.16	(72)	-140	148	34
L_{MM}-3	11.7	1.24	(46)	-140	150	31
L_{MM}-4	13.0	1.11	(63)	-132	144	42
D_{MM}-1	6.6	1.17	(49)	+126	128	20
D_{MM}-2	8.6	1.15	(82)	+142	149	36
D_{MM}-3	10.6	1.08	(63)	+139	149	32
D_{MM}-4	17.4	1.05	(27)	+153	149	43
L_{Br}-1	1.07 10^3	1.02	100	-139	-	-
L_{Br}-2	1.22 10^3	1.06	91	-146	139	24
L_{Br}-3	1.53 10^3	1.03	92	-147	141	13
L_{Br}-4	2.15 10^3	1.05	77	-135	137	14
D_{Br}-1	1.19 10^3	1.03	100	+121	-	-
D_{Br}-2	1.18 10^3	1.04	94	+143	138	23
D_{Br}-3	1.07 10^3	1.16	89	+140	139	25
D_{Br}-4	2.55 10^3	1.03	78	+156	139	18

[a] Measured by NMR for MMs and GPC for brush polymers. [b] M_w/M_n as measured by GPC. [c] Measured with a polarimeter (c = 3 mg/mL, $CHCl_3$). [d] Measured by DSC.

Blends of the MMs were formed by pairing similar molecular weight stereoisomers in equal weight ratios. The mixtures were dissolved in dichloromethane and stereocomplexation was achieved via controlled evaporation. Blends of the MMs with their complementary brush polymer, as well as blends of brush/brush copolymers, were prepared in an analogous manner (**Table 5-2**). After annealing, the samples were dried under vacuum and analyzed by DSC.

As expected, the MM blends (**A1-A4**) formed distinct stereocomplexes, as evidenced by the DSC analysis that showed higher melting temperatures (192-213°C) and heats of melting (37-46 J/g) (**Table 5-2**) than their pristine counterparts. The MM/brush copolymer blends (**B1-B8**) also formed distinct stereocomplexes with similar melting temperatures as the corresponding MM blends, albeit with lower heats of melting. Therefore, we infer that the MMs are able to sufficiently diffuse into the brush copolymer in order to interact with the side chains to form a stereocomplex. Interestingly, although the highest molecular weight MM/brush blends (**B4, B8**) showed stereocomplex formation, they also showed a smaller peak corresponding to the non-stereocomplexed polylactides, suggesting non-quantitative stereocomplex formation.

Table 5-2. DSC Results for the Polymer Blends.

Blend	PLLA	PDLA	T_m (°C) [a]	ΔH_m (J/g) [a]
A1	L_{MM}-1	D_{MM}-1	192	37
A2	L_{MM}-2	D_{MM}-2	212	46
A3	L_{MM}-3	D_{MM}-3	213	39
A4	L_{MM}-4	D_{MM}-4	202	43
B1	L_{MM}-1	D_{Br}-1	183	25
B2	L_{MM}-2	D_{Br}-2	211	31
B3	L_{MM}-3	D_{Br}-3	212	27
B4	L_{MM}-4	D_{Br}-4	205, 141	24, 1.9
B5	L_{Br}-1	D_{MM}-1	192	29
B6	L_{Br}-2	D_{MM}-2	210	27
B7	L_{Br}-3	D_{MM}-3	212	17
B8	L_{Br}-4	D_{MM}-4	204, 143	21, 5.8
C1	L_{Br}-1	D_{Br}-1	-	-
C2	L_{Br}-2	D_{Br}-2	137	4.3
C3	L_{Br}-3	D_{Br}-3	138	6.0
C4	L_{Br}-4	D_{Br}-4	139, 192	12, 6.5
D1 [b]	L_{Br}-2	D_{Br}-2	136, 200	18, 5.1
D2 [b]	L_{Br}-3	D_{Br}-3	136, 196	18, 5.9
D3 [b]	L_{Br}-4	D_{Br}-4	138, 191	23, 5.5

[a] Measured by DSC. [b] Blends heated at 150°C for 4 days after controlled evaporation.

The brush/brush polymer blends (**C1-C4**) showed varied properties. The blend with the shortest side chains (**C1**) did not show any transition peak in its DSC traces, like its parent brush polymers, while the two brush blends with the intermediate length side chains (**C2-C3**), showed melting temperatures close to their parent brushes but with lower heats of melting. The brush blend with the longest side chains (**C4**) showed two transition peaks, corresponding to a major melting transition temperature (138.5°C), and a weaker melting transition temperature at 191.8°C, indicative of some stereocomplex formation. We believe that longer side chains provide more conformational freedom, as the longer side-chains can extend further from the sterically congested core brush off the main chain (**Figure 5-1a**). This may allow for some interaction between brush copolymers at the chain end of the side chains, enabling some stereocomplex formation (**Figure 5-1b**). As previously noted, the brush polymers tend to have lower melting transition temperature than their corresponding MMs or blends involving MMs (both MM/MM and MM/brush blends). This leads us to conjecture that this is a result from true brush/brush interactions.

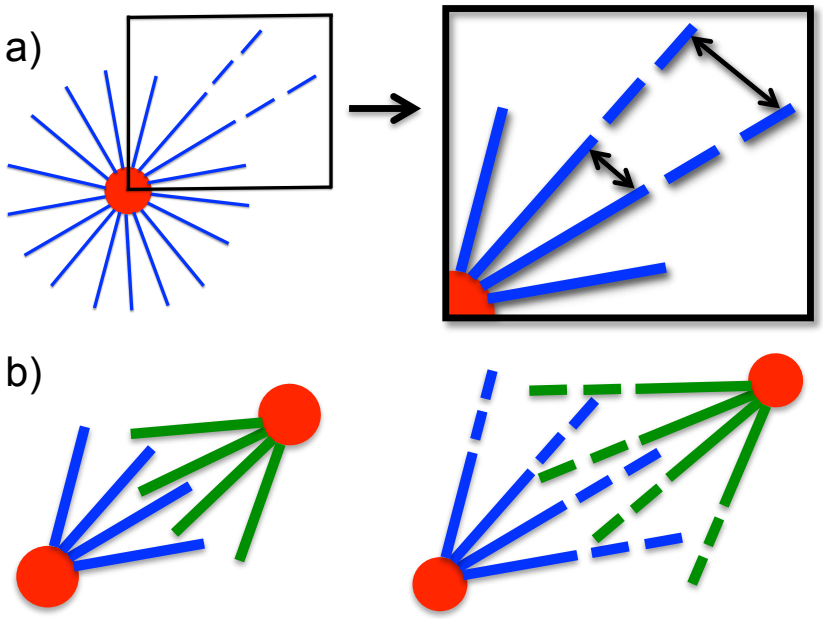

Figure 5-1. Schematics showing that a) longer side chains (where dashed lines represent extended side chain lengths) will have more conformational freedom further from the brush copolymer core, which can result in b) a potentially bigger overlap of side chains to enable stereocomplex formation

To investigate if we could thermally induce stereocomplexation, we thermally annealed the three biggest blendsunder vacuum at 150°C for 4 days after controlled evaporation (**D1-D3**, **Table 5-2**). The sample with the longest side chain (**D3**) did not show an increase in stereocomplexation, but instead the ratio between the heats of melting from before and after thermal annealing became skewed towards the non-stereocomplexed transition temperature. Meanwhile, the other two samples (**D1-D2**) started revealing evidence of some stereocomplex formation. This suggests that with heating, the benefit of the stereocomplex forming interactions can overcome the tendency of these brush copolymers to evade entangling, although only to a limited extent.

A brush statistical copolymer sample was also synthesized via ROMP by polymerizing a mixture of the lowest molecular weight MM pairs, yielding a polymer with M_n of 4.87 × 10^5 g/mol (PDI = 1.09). This polymer exhibited a melting transition temperature (175.8°C) and heat of melting (12 J/g) that suggested a weak stereocomplex formation, while the analogous brush/brush blend (C1) had not shown any stereocomplex formation. Since the other brush/brush blends did not show much stereocomplex formation either, we hypothesize that the intramolecular interactions between the PLLA and PDLA side chains in the brush statistcial copolymer must play an important role in the stereocomplex properties of the brush statistical copolymer sample.

CONCLUSION

In conclusion, we have shown that when there is an adequately strong driving force, brush polymers can allow for diffusion of macromolecules into their side chains, and we have found that at sufficient distance from the brush polymer main chain, some entanglement may begin to take place at the edges of the side chains. These results add to the intriguing properties of brush polymers and may aid in extending the scope of applications for these macromolecules.

SUPPORTING INFORMATION

Materials

$(H_2IMes)(pyr)_2(Cl)_2RuCHPh$[23] and *N*-(hydroxyethanyl)-*cis*-5-norbornene-*exo*-2,3-di-carboximide,[24] were prepared as described previously. All solvents were purchased from VWR or Sigma-Aldrich. Ruthenium-based metathesis catalyst was obtained from Materia Inc. and stored in a drybox. D(+)-Lactide was obtained from BOC Sciences, while other chemicals were bought from Sigma-Aldrich. Dry solvents were purified by passing them through solvent purification columns. Lactide monomers were purified by sublimation under vacuum. All other solvents and chemicals were used without further purification unless otherwise stated.

General Information

^{1}H NMR spectra were recorded at room temperature on a Varian Inova 500 (at 500 MHz). The NMR spectra were analyzed on MestReNova software and are reported relative to CDCl3 (δ 7.26). NMR abbreviations: s = singlet, d = doublet, t = triplet, m = multiplet, br = broad, dt = doublet of triplets.

Gel permeation chromatography (GPC) was carried out in THF on two Plgel 10 μm mixed-B LS columns (Polymer Laboratories) connected in series with a miniDAWN TREOS multiangle laser light scattering (MALLS) detector, a ViscoStar viscometer, and Optilab rex differential refractometer (all from Wyatt Technology). The dn/dc values used for the poly(lactide) macromonomers were 0.050.

Differential Scanning Calorimetry (DSC) was performed on a Perkin-Elmer DSC 7. Samples were heated to 125°C at 20°C/min, held at 25°C for 5 minutes, and then cooled to 20°C at 10°C/min. The temperature was held at 20°C for 5 minutes before being reheated to 250°C at 10°C to determine the melting transition temperature. Finally, the samples were cooled back to room temperature at 20°C/min.

Optical rotations were measured in a solution of chloroform with a Jasco P-2000 polarimeter operating on a sodium D-line (589 nm) at 25°C, using a 10 cm path-length cell.

Synthesis

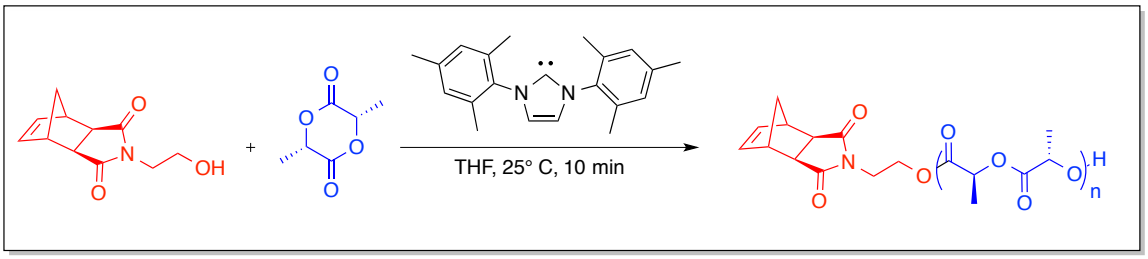

Representative procedure for the synthesis of Norbornene-Poly(lactide) (**L_{MM}-4**)

The monomer, L-Lactide (2.00 g, 13.9 mmol) was added to a 40 mL scintillation vial and dissolved in 15 mL of dry THF. The initiator, N-(hydroxyethanyl)-cis-5-norbornene-exo-2,3-di-carboximide (35.7 mg, 0.172 mmol, 1 equiv) and the catalyst, 1,3-dimesitylimidazol-2-ylidene (9.6 mg, 31.5 μmol) were added to a separate vial and dissolved in 3 mL of dry THF. Then the initiator/catalyst solution was added rapidly to the monomer solution and the whole solution allowed to stir for 10 minutes before being precipitated into MeOH. 1H NMR (500 MHz, CDCl3): δ (ppm) 6.29 (br t, 2H), 5.32-5.00 (m, 177 H), 4.40-4.24 (m, 3H), 3.83-3.69 (m, 2H), 3.27 (s, 2H), 2.70 (br q, 2H), 1.73-1.39 (m, 532H), 1.25-1.23 (m, 1H). M_n (NMR) = 13.0 kg/mol. GPC: M_n = 12.4 kg/mol, M_w/M_n = 1.11.

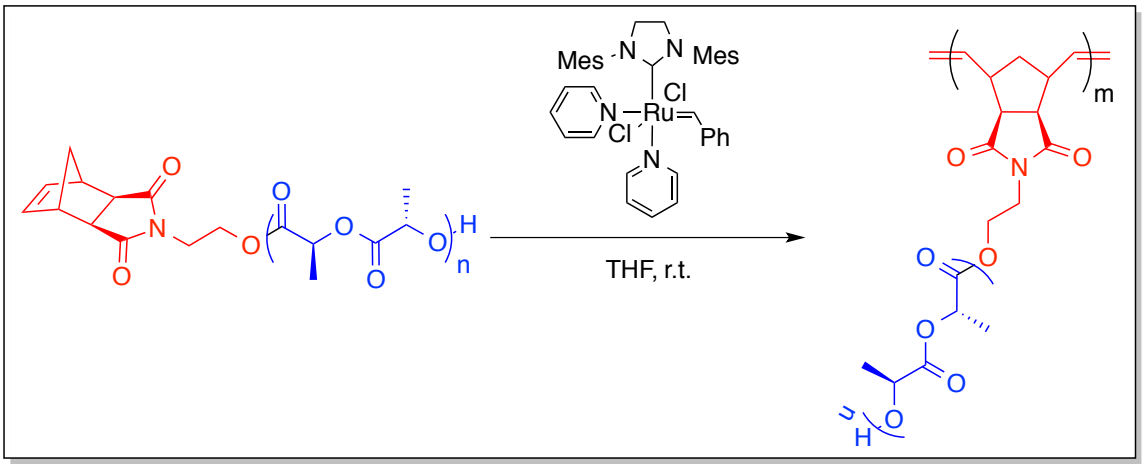

Representative procedure for the synthesis of a poly(lactide) brush copolymers (**L_{Br}-4**)

The poly(lactide) macromonomer (157.8 mg, 12.1 μmol) was weighed into a vial. The catalyst (2.8 mg, 3.85 μmol) was added to a separate vial. The vials were brought into the drybox and the poly(lactide) macromonomer was dissolved in THF (500 μL), while the catalyst was dissolved in

1.00 mL of THF. The catalyst solution (21 μL, 0.081 μmol) was injected via a microsyringe to the solution of macromonomers and the solution allowed to stir for 2 hours. The reaction was moved out of the dry box, quenched with butyl vinyl ether and isolated by precipitation into MeOH. GPC: M_n = 2.15 x 10^6 g/mol, M_w/M_n = 1.05.

General procedure for preparation of blends:

Equal amounts (w/w) of the complementary polymers (≈20 mg of each) were added to a small vial and subsequently dissolved in dichloromethane (≈2 mL). This solution was allowed to evaporate in the vial at room temperature, and after drying under air, it was put under high vacuum to ensure removal of the solvent.

Supplementary Tables

Table 5-3. GPC results for the macromonomers.

Sample	M_n (10^3 g/mol)	PDI
L_{MM}-1	8.16	1.18
L_{MM}-2	10.6	1.16
L_{MM}-3	14.9	1.24
L_{MM}-4	12.4	1.11
D_{MM}-1	8.54	1.17
D_{MM}-2	10.5	1.15
D_{MM}-3	10.5	1.08
D_{MM}-4	16	1.05

Supplementary Figures

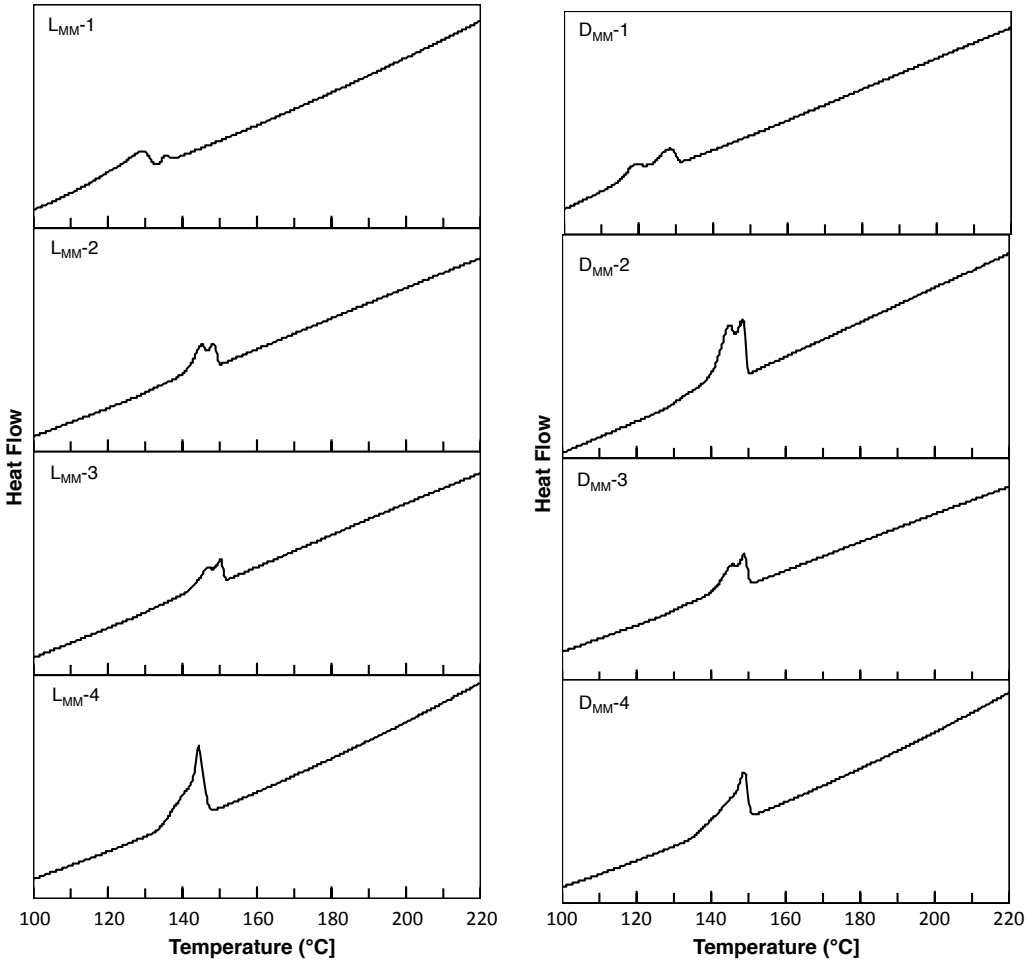

Figure 5-2. DSC traces of the pure macromonomers.

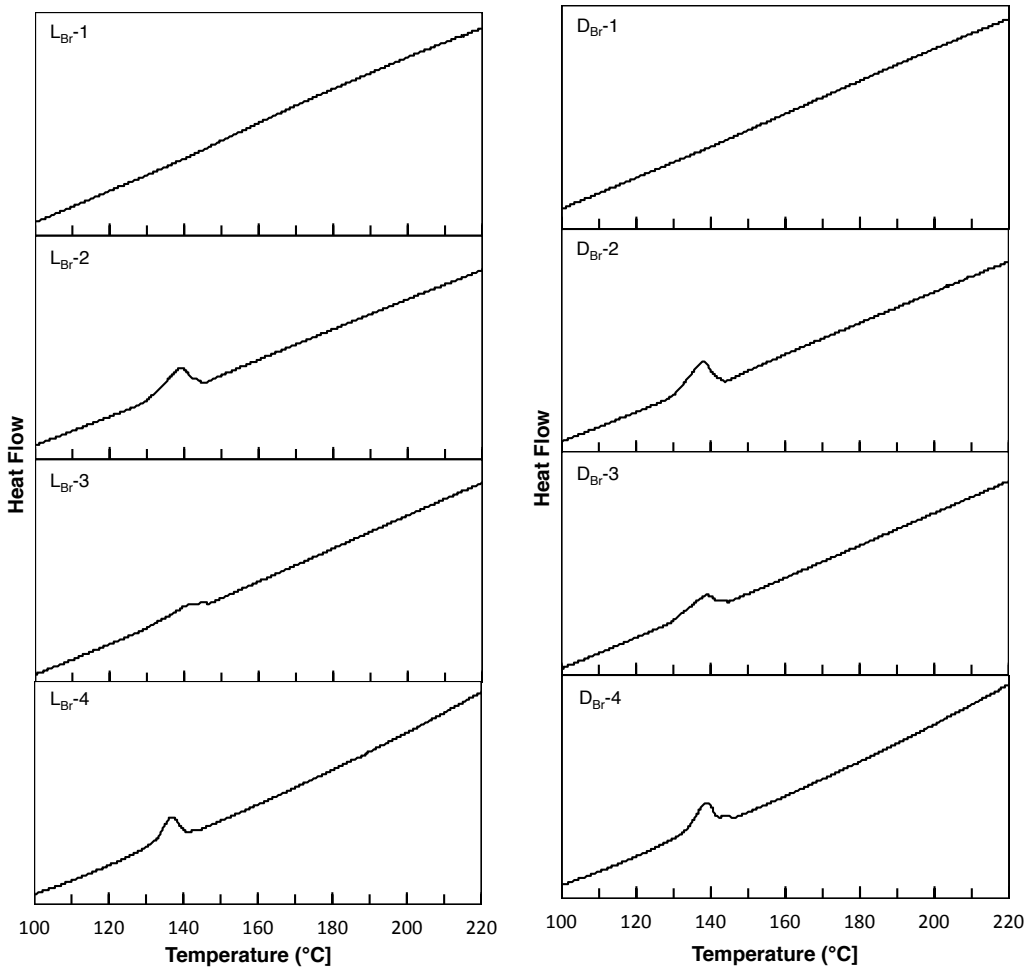

Figure 5-3. DSC traces of the pure brush copolymers.

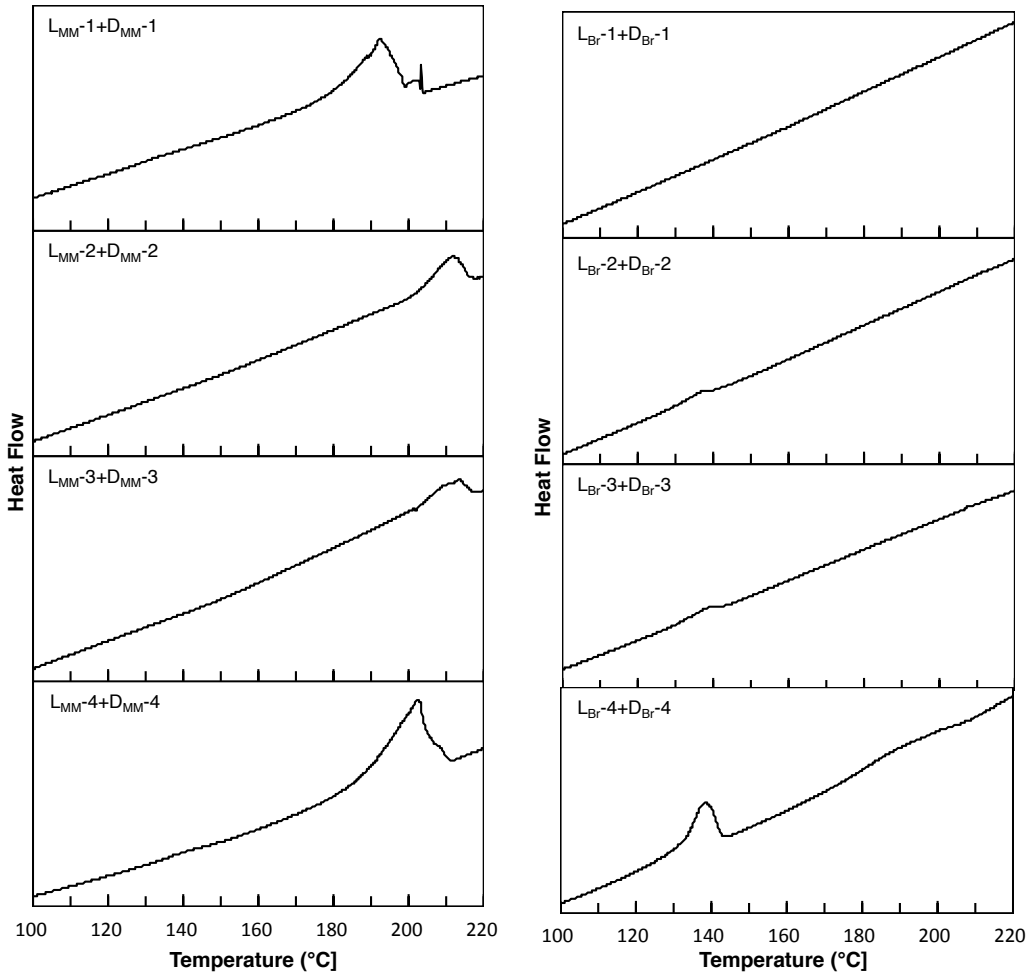

Figure 5-4. DSC traces of the MM/MM blends (left) and the brush/brush blends (right)

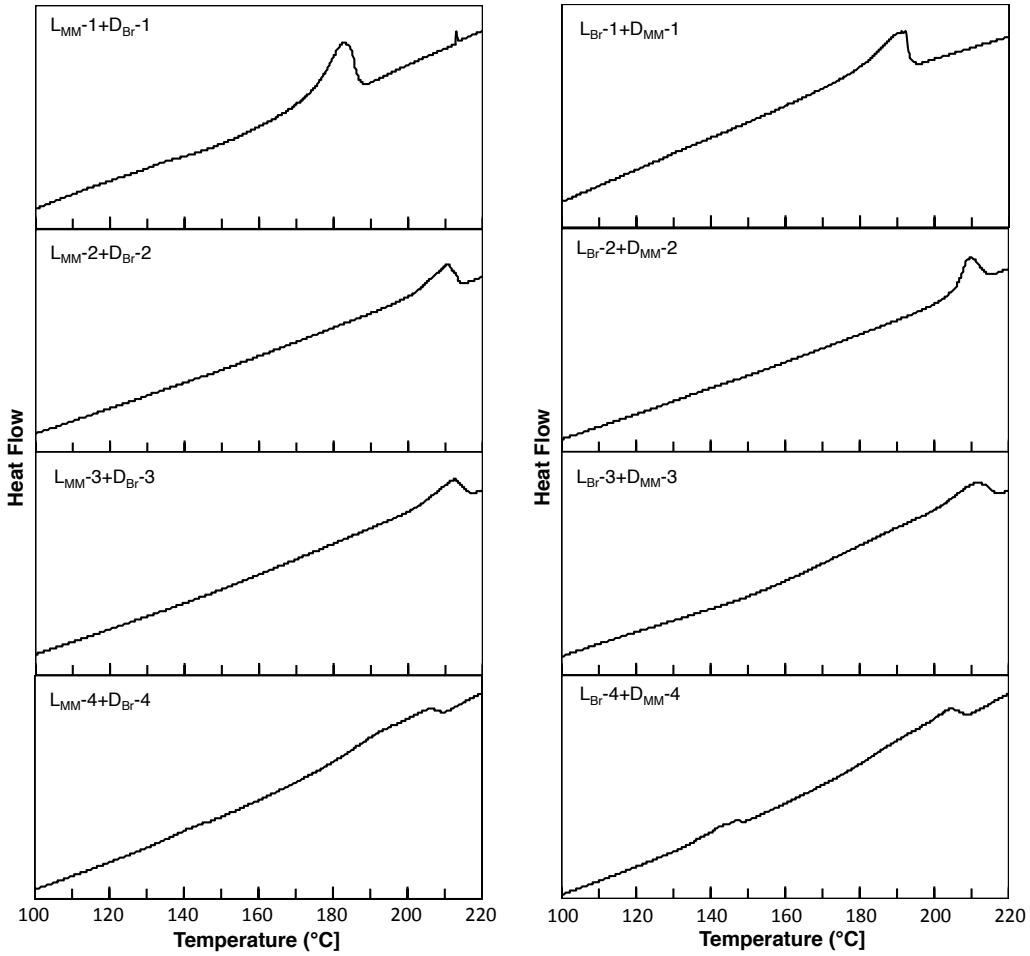

Figure 5-5. DSC traces of the MM/brush blends.

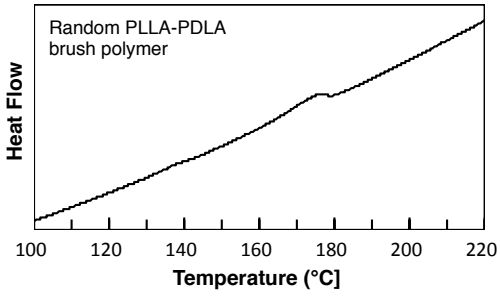

Figure 5-6. DSC trace of the random PLLA-PDLA brush copolymer.

REFERENCES

(1) Hu, M.; Xia, Y.; McKenna, G. B.; Kornfield, J. A.; Grubbs, R. H. *Macromolecules* **2011**, *44*, 6935–6943.

(2) Xia, Y.; Li, Y.; Burts, A. O.; Ottaviani, M. F.; Tirrell, D. A.; Johnson, J. A.; Turro, N. J.; Grubbs, R. H. *J. Am. Chem. Soc.* **2011**, *133*, 19953–19959.

(3) Ikada, Y.; Jamshidi, K.; Tsuji, H.; Hyon, S.-H. *Macromolecules* **1987**, *20*, 904–906.

(4) Tsuji, H. *Macromol. Biosci.* **2005**, *5*, 569–597.

(5) Shin, E. J.; Jones, A. E.; Waymouth, R. M. *Macromolecules* **2012**, *45*, 595–598.

(6) Tsuji, H.; Hyon, S.-H.; Ikada, Y. *Macromolecules* **1991**, *24*, 5651–5656.

(7) Tsuji, H.; Ikada, Y.; Hyon, S.-H.; Kimura, Y.; Kitao, T. *J. Appl. Polym. Sci.* **1994**, *51*, 337–344.

(8) Takasaki, M.; Ito, H.; Kikutani, T. *J. Macromol. Sci., Part B Phys.* **2003**, *B42*, 403.

(9) Li, S.; Vert, M. *Macromolecules* **2003**, *36*, 8008–8014.

(10) Li, S. *Macromol. Biosci.* **2003**, *3*, 657–661.

(11) Schmidt, S. C.; Hillmyer, M. A. *J. Polym. Sci., Part B Polym. Phys.* **2001**, *39*, 300–313.

(12) Yamane, H.; Sasai, K. *Polymer* **2003**, *44*, 2569–2575.

(13) Fukushima, K.; Pratt, R. C.; Nederberg, F.; Tan, J. P. K.; Yang, Y. Y.; Waymouth, R. M.; Hedrick, J. L. *Biomacromolecules* **2008**, *9*, 3051–3056.

(14) Van Nostrum, C. F.; Veldhuis, T. F. J.; Bos, G. W.; Hennink, W. E. *Macromolecules* **2004**, *37*, 2113–2118.

(15) Hadjichristidis, N.; Pitsikalis, M.; Pispas, S.; Iatrou, H. *Chem. Rev.* **2001**, *101*, 3747–3792.

(16) Neiser, M. W.; Okuda, J.; Schmidt, M. *Macromolecules* **2003**, *36*, 5437–5439.

(17) Rizmi, A. C. M.; Khosravi, E.; Feast, W. J.; Mohsin, M. A.; Johnson, A. F. *Polymer* **1998**, *39*, 6605–6610.

(18) Heroguez, V.; Breunig, S.; Gnanou, Y.; Fontanille, M. *Macromolecules* **1996**, *29*, 4459–4464.

(19) Nyce, G. W.; Glauser, T.; Connor, E. F.; Möck, A.; Waymouth, R. M.; Hedrick, J. L. *J. Am. Chem. Soc* **2003**, *125*, 3046–3056.

(20) Csihony, S.; Culkin, D. A.; Sentman, A. C.; Dove, A. P.; Waymouth, R. M.; Hedrick, J. L. *J. Am. Chem. Soc* **2005**, *127*, 9079–9084.

(21) Chabot, F.; Vert, M.; Chapelle, S.; Granger, P. *Polymer* **1983**, *24*, 53–59.

(22) Miyake, G. M.; Chen, E. Y. *Macromolecules* **2011**, *44*, 4116–4124.

(23) Love, J. A.; Morgan, J. P.; Trnka, T. M.; Grubbs, R. H. *Angew. Chem. Int. Ed.* **2002**, *41*, 4035–4037.

(24) Matson, J. B.; Grubbs, R. H. *J. Am. Chem. Soc.* **2008**, *130*, 6731–6733.

A p p e n d i x A

PROGRESS TOWARDS THE TOTAL SYNTHESIS OF CHRYSOPHAENTIN F

ABSTRACT

The progress towards the total synthesis of chrysophaentin F is herein reported. Chrysophaentin F is a recently isolated antimicrobial natural product from the chrysophyte alga *Chrysophaeum taylori* and has been shown to strongly inhibit the bacterial cell division protein FtsZ. The synthetic strategy involves a tandem cross-metathesis/ring-closing metathesis of the bisdiarylbutene macrocycles as the key step.

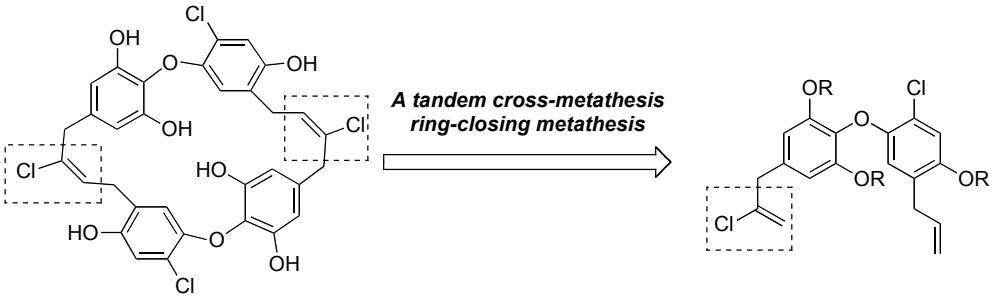

Chrysophaentin F

INTRODUCTION

One of the leading causes of death worldwide today is infectious diseases,[1,2] and in the United States it has been estimated that more people die due to methicillin-resistant *Staphylococcus aureus* (MRSA) bacterium than from HIV.[3] The increased amount of multidrug resistant bacteria results in more expensive treatments that can also be more uncertain and sometimes ineffective.[4] Therefore, there is clearly a need to identify new compounds with the potential to treat infections caused by multidrug resistant bacteria, as well as to find new ways to approach this growing problem.

The bacterial cell division protein FtsZ is a fairly new and attractive target in antimicrobial drug discovery, since it is both vital for cell division as well as highly conserved among most bacteria.[5] There are already some compounds that have been reported to inhibit the function of FtsZ. These compounds include the phenolic natural products totarol,[6] berberine,[7] viriditoxin,[8] and cinnamaldehyde.[9] Another potential source for new FtsZ inhibitors is marine natural products, because of their strong antimicrobial activities and unique structures.

Eight new antimicrobial natural products were recently isolated from the chrysophyte alga *Chrysophaeum taylori*, and they were termed chrysophaentin A-H.[10] The structure of these compounds (see **Figure A-1** for chrysophaentin A and F) was determined by thorough spectroscopic analysis, including mass spectrometry (MS) and nuclear magnetic resonance (NMR). Some of these compounds were found to strongly inhibit the growth of *S. aureus*, MRSA, *Enterococcus faecium*, and vancomycin-resistant *E. faecium*. Of these compounds, chrysophaentin A was the most potent antibiotic, and chrysophaentin F and H were found to be the next most potent compounds. Through studies of chrysophaentin A it was observed that it inhibited the GTPase activity and polymerization of FtsZ.[10]

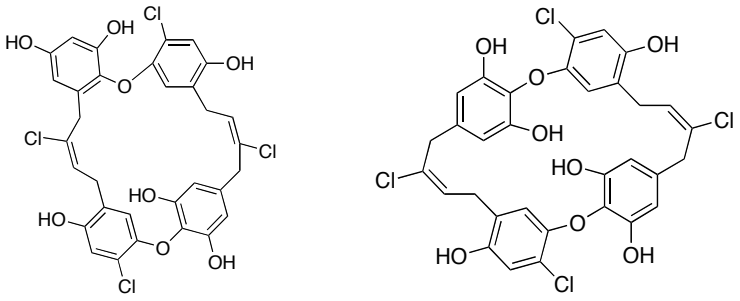

Figure A-1. The structures of Chrysophaentin A (left) and Chrysophaentin F (right).

The antibiotic potential of these compounds made them ideal synthetic targets and thus, it was decided to pursue the total synthesis of the symmetrical chrysophaentin F using metathesis as the key step to form the macrocycle.

SYNTHETIC STRATEGY

The synthetic strategy for this target was organized towards using a tandem olefin cross-metathesis/ ring-closing metathesis as the key step to combine two fragments of biaryl ether symmetrically. The following retrosynthetic analysis was aimed at making the biaryl ether with a coupling reaction between an aryl halide and a phenol, which could each be synthesized from readily available starting materials (**Scheme A-1**).

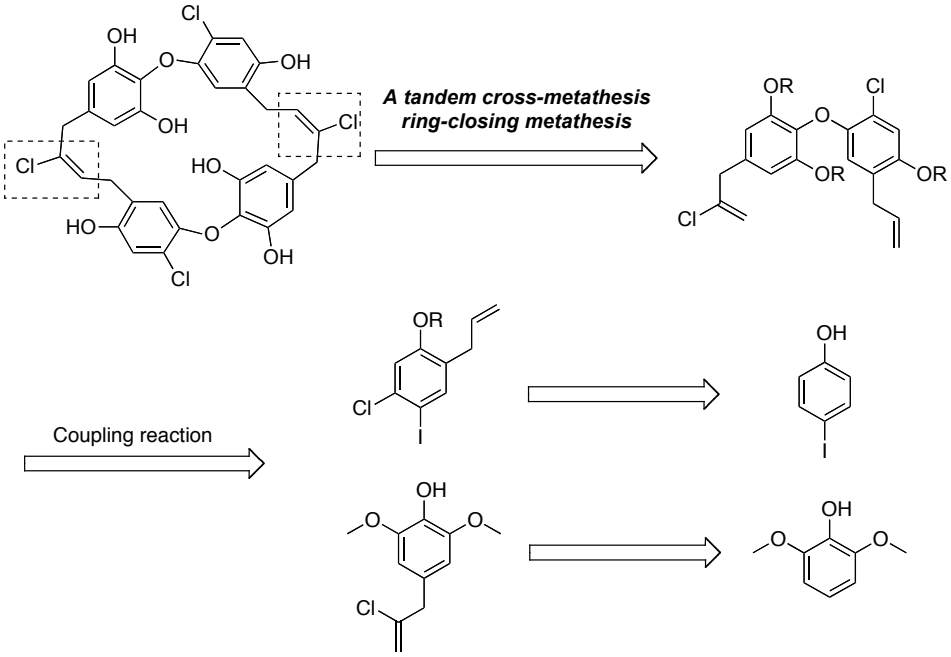

Scheme A-1. Retrosynthetic analysis of Chrysophaentin F, leading to readily available starting materials.

For the forward synthesis of the aryl halide it was required that we find a way to introduce the chlorine to the meta-position and an allyl group to the ortho-position of the molecule, as well as protect the hydroxyl group. We decided to start with a Williamson ether synthesis,[11–13] followed by a Claisen rearrangement[11–15] in a microwave reactor,[11,16] to insert the allyl group to the desired position. To prepare the molecule for the chlorination, we decided to protect the ortho/para-directing hydroxyl group as an acetyl.[17–19] Since iodine is an ortho/para-directing group[20] and the

allyl group is ortho/para-directing as well, we believed that even though phenyl acetate is also ortho/para-directing on its own,[21] the combined effect would yield the desired chlorinated product in some amount.[22,23]

The forward synthesis of the phenol was based on an analogous approach starting with a Williamson ether synthesis[11–13] and followed by a Claisen rearrangement, resulting in the 2-chloroallyl group at the para-position since both ortho-positions were occupied.[24,25]

With both A and B synthesized the next step would be a coupling reaction. The conditions of the Ullmann biaryl ether synthesis seemed suitable for the reactants.[26–28] Since there would only be one available hydroxyl group and the reactivity trend of the halides follows I > Br > Cl >>F,[29] this reaction was expected to give the appropriate biaryl ether.

Inspired by the progress made in metathesis of vinyl halides in the past decade, its application in the synthesis of chrysophaentin F was appealing. Recent reports have shown that vinyl halides can undergo both ring-closing metathesis[30–32] and cross-metathesis[33,34] with appropriate catalysts. Since metathesis has also been used to close macrocycles[35,36] it was deemed desirable to accomplish a ring-closing metathesis of a macrocycle through a vinyl halide.

Seeing that vinyl halides are less reactive than monosubstituted alkenes, it was expected that the cross metathesis of the monosubstituted alkenes would be observed first. Since this step would be reversible in a closed system, that would be acceptable. In addition, it would also be unlikely that the two remaining vinyl halides would undergo metathesis to close the macrocycle due to their relatively low reactivity.

It was presumed that some cross metathesis of the vinyl halide with the monosubstituted alkene would eventually be observed, and that step would be irreversible due to the lack of metathesis reactivity expected of the product formed. The metathesis of the remaining alkenes in the newly formed molecule would lead to a ring-closing of the macrocycles, and thus give the desired product (**Scheme A-2**).

When the metathesis step would be completed, all that would remain would be to deprotect the acetyl groups[37] as well as the methyl ether groups.[38] The success of this synthetic strategy would

lead to an effective route to synthesize chrysophaentin F from commercially available starting materials in 10 steps, where the longest linear sequence would include 7 steps (**Scheme A-3**).

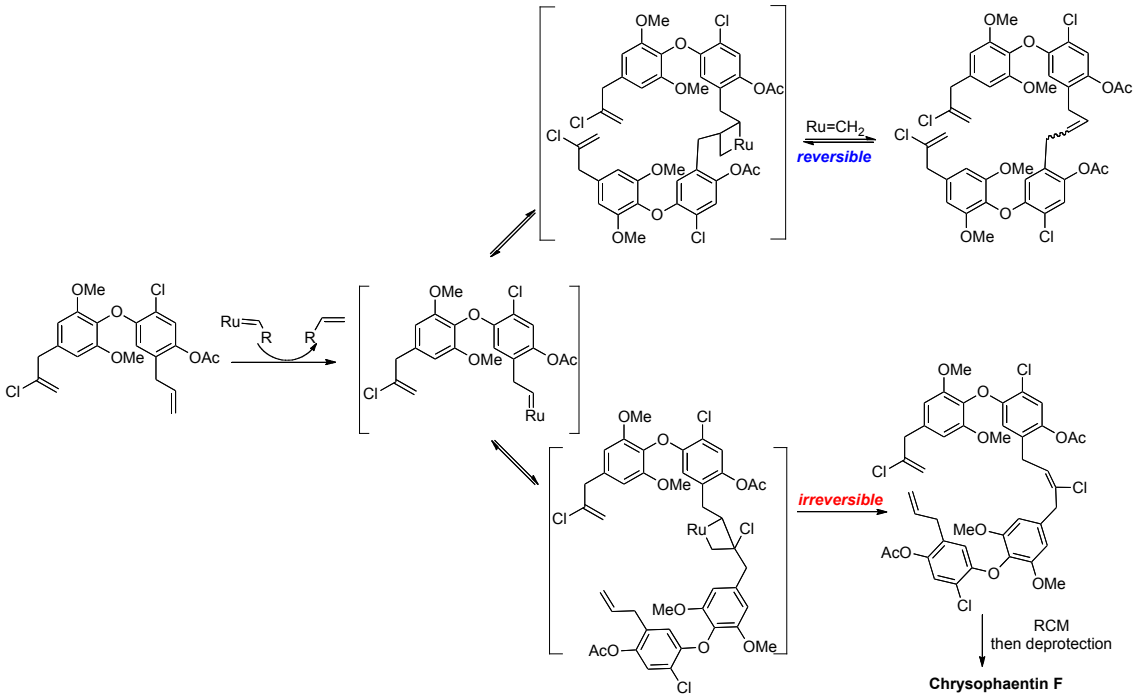

Scheme A-2. The expected route of the tandem cross-metathesis/ring-closing metathesis step.

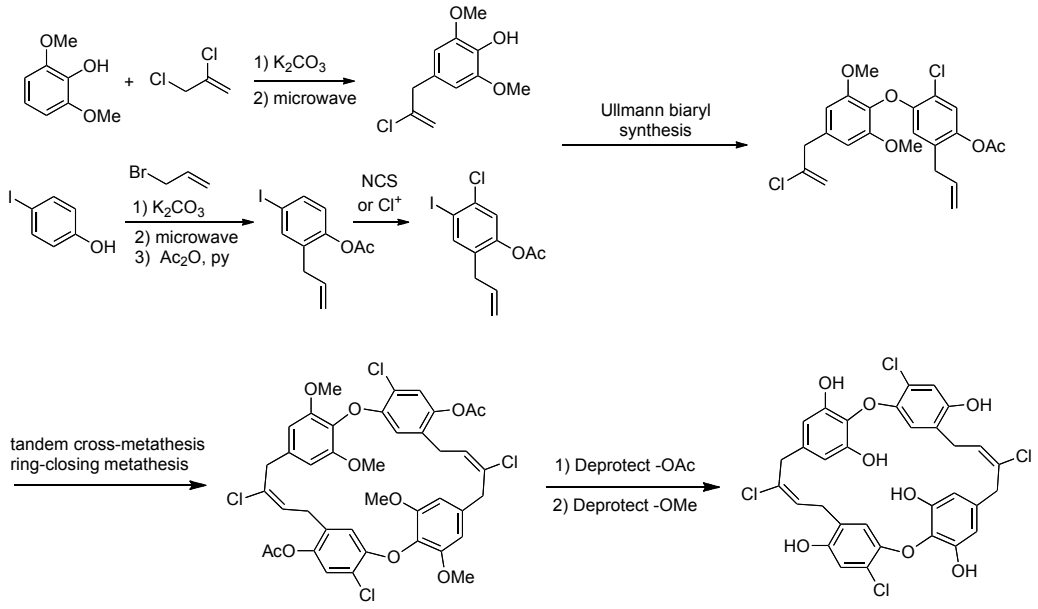

Scheme A-3. The synthetic strategy from available starting material to Chrysophaentin F.

RESULTS AND DISCUSSION

The synthesis commenced with a simple substitution reaction to introduce the chloro-substituted allyl group to the 2,6-dimethoxy-phenol. This reaction was followed by a Claisen rearrangement to advance the allyl group to the desired para position. These two steps worked well and gave 93% and 70% yields, respectively (**Scheme A-4**).

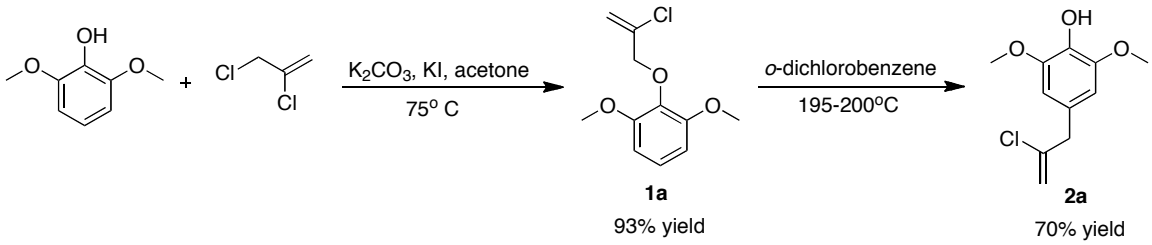

Scheme A-4. Synthesis of intermediat **2a**, 4-(2-chloroallyl)-2,6-dimethoxyphenol.

The next steps were analogous with a 4-iodophenol to introduce a non-substituted allyl group via a substitution reaction, followed by a Claisen rearrangement to shift the allyl group to the desired ortho position. The Claisen rearrangement did not give good yields since it was not allowed to run to full conversion, and thus a lot of the starting material was recovered. Then the phenol was reacted with acetic anhydride in pyridine at room temperature to protect the hydroxyl group as an acetate before attempting to chlorinate the compound (**Scheme A-5**).

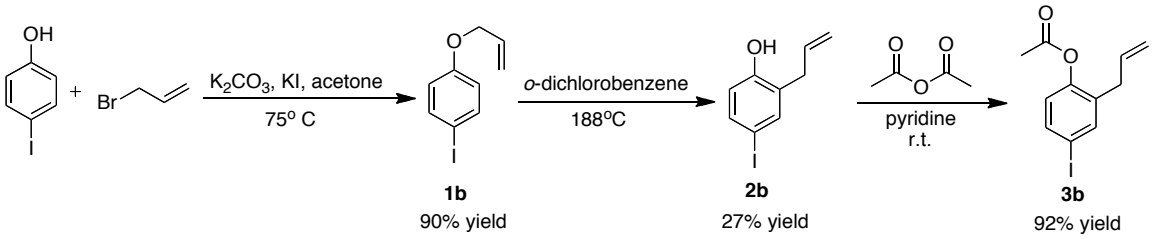

Scheme A-5. Synthesis of intermediat **3b**, 2-allyl-4-iodophenyl acetate.

The following step was to chlorinate the 2-allyl-4-iodophenyl acetate. That was first attempted utilizing the chlorinating agent N-chlorosuccinimide (NCS). These attempts were unsuccessful, and either resulted in the degradation of the essential allyl group (possibly through chlorination of the alkene) or no apparent reaction, depending on the reaction conditions (**Scheme A-6**).

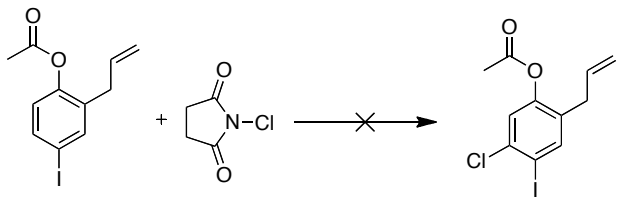

Scheme A-6. The unsuccessful synthesis of 2-allyl-5-chloro-4-iodophenyl acetate. Attempted conditions were a) dichloromethane, r.t.; b) methanol, 55° C; c) acetic acid, acetonitrile; d) acetic acid, acetonitrile, $FeCl_3$.

While searching for other appropriate reaction conditions and chlorinating agents, it was discovered that 4-bromo-3-chlorophenol was commercially available and therefore it was decided to pursue the synthesis using that compound as the starting material instead. That was done to evade the chlorination step, which could have required stronger and more dangerous chlorinating agents.

Thus, the same approach was executed using the new starting material (**Scheme A-7**). The substitution reaction gave excellent yields while the Claisen rearrangement did not, but instead showed an inclination towards the non-desired isomer product.

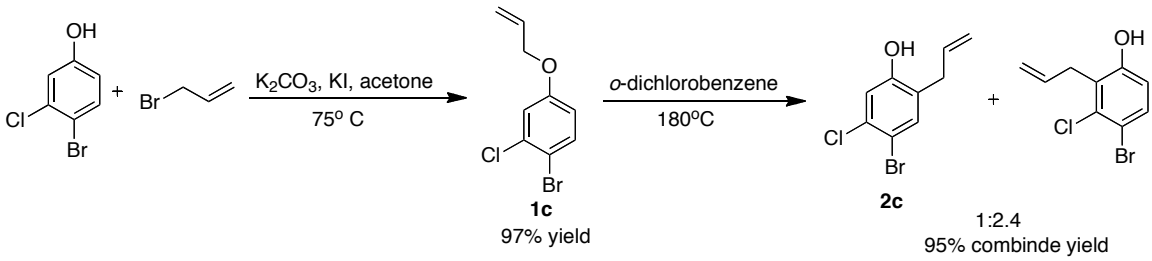

Scheme A-7. Synthesis of 2-allyl-4-bromo-5-chlorophenol.

A short study was done on the solvent effect on the regioselectivity of the Claisen rearrangement. Approximately 40 mg of the allyloxy compound were dissolved in 0.5 mL of solvent, followed by 2-3 freeze-pump-thaw cycles to degas the solvents. The mixture was subsequently heated under argon in a microwave reactor at 170°C for 90 minutes. Due to the small conversion of the reaction, the NMR results may have been somewhat inaccurate, but still gave a rough aspect on the solvent effect (**Table A-1**).

Table A-1. Effect of solvent on the ratio between products of the Claisen rearrangement of 4-(allyloxy)-1-bromo-2-chlorobenzene.

Solvent	2-allyl-4-bromo-5-chlorophenol	2-allyl-4-bromo-3-chlorophenol
o-dichlorobenzene	1	2.4
Pyridine	1	2.7
Acetonitrile	1	2.2
DMF	1	2.3
Water	1	2.3
No solvent	1	2.8

The results showed some effect where more polar solvents seemed to favor the desired product. The greatest improvement observed was roughly 20% between acetonitrile and no solvent.

It was also observed in this short study that the conversion of the reaction differed greatly depending on whether solvent was used or not. In all the cases when solvent was used the observed conversion was less than 5% after 90 minutes, while when the reaction was run neat the conversion was 45% after the same amount of time. This unexpected result might be due to some concentration effect, but still it was not expected to have any effect for this reaction, which is generally unimolecular.

After isolation of the desired Claisen product, it was protected with an acetyl group and then reacted with **2a** using Ullmann biaryl ether synthesis conditions.[26] Unfortunately, this reaction did not give the desired biaryl product. Instead it seems that the hydroxyl group of **2a** reacted with the acetyl group of **3c**, giving 4-(2-chloroallyl)-2,6-dimethoxyphenyl acetate. (**Scheme A-8**).

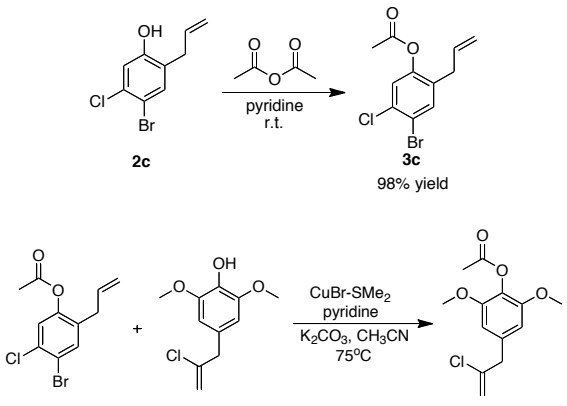

Scheme A-8. The acetyl protection of **2c** (top). The result of the attempted Ullman biaryl ether synthesis (bottom).

The observed reaction can be explained by the proposed mechanism shown in **Scheme A-9** where a base deprotonates the phenol, enabling it to attack the acetyl group and eventually relocate it.

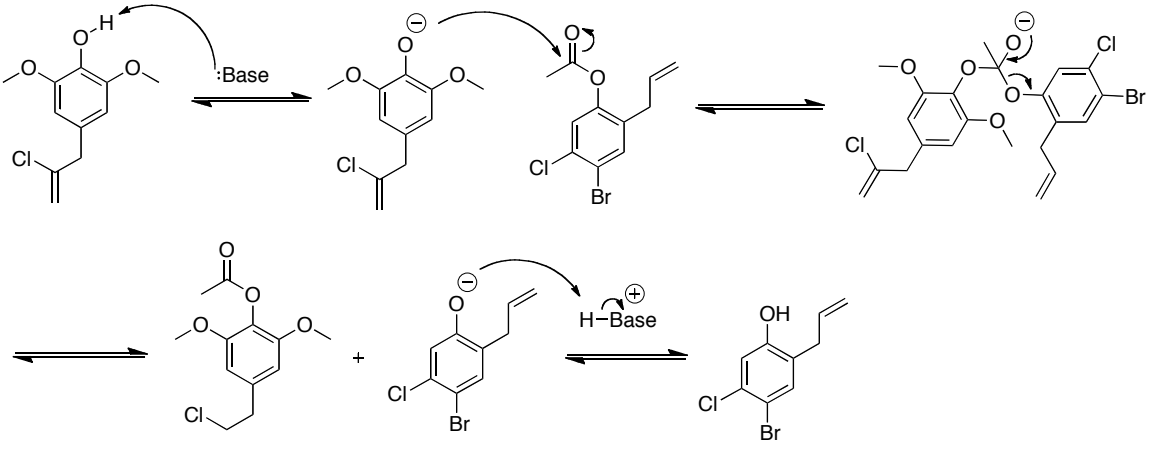

Scheme A-9. Proposed mechanism for the acyl relocation.

To overcome the coupling obstacle, it was decided to use a methyl ether protecting group instead of acetyl, especially since the 4-(2-chloroallyl)-2,6-dimethoxyphenol already had methoxy protecting groups. That way, only one deprotection step would be required at the end of the synthesis, rather than two. This approach was successful in giving the desired biaryl ether compound (**Scheme A-10**), although current yields are low.

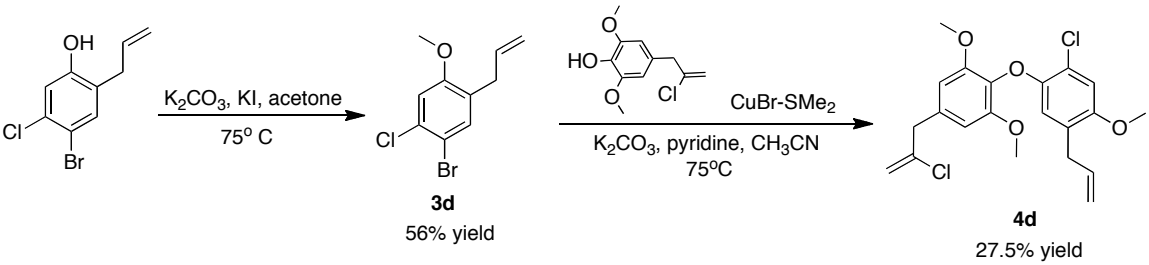

Scheme A-10. Synthesis of the biaryl ether intermediate, **4d**.

Attempts were made at the tandem cross metathesis/ring-closing metathesis reaction with the second generation Grubbs catalyst, but to no avail (**Scheme A-11**).

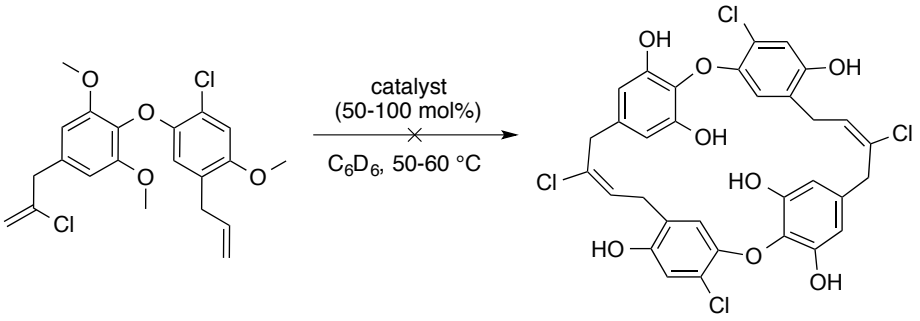

Scheme A-11. Attempts at the tandem cross-metathesis/ring-closing metathesis step have been unsuccessful with the 2nd generation Grubbs catalyst.

CONCLUSION AND FUTURE DIRECTIONS

Further efforts were not made towards finishing the total synthesis of *Chrysophaentin F* at this point in time. The next steps would be to test out other catalyst for the key reaction. A few potential candidates have been identified and are shown in **Figure A-2**.

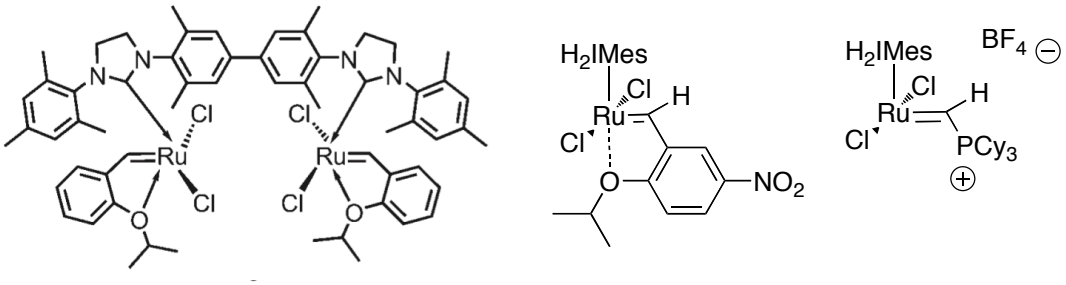

Figure A-2. Examples of ruthenium catalysts yet to be screened.

Alternatively, it would be possible to reverse the order of the cross metathesis reaction and the Ullmann biaryl ether coupling reaction in order to attempt finishing the synthesis. The cross-metathesis step would still be expected to be the main challenge, and it is expected that the yields for that step would be low due to the competing homometathesis reaction.

EXPERIMENTAL SECTION

General information

NMR spectra were recorded on a Varian Inova 500 (at 500 MHz). The NMR spectra were analyzed on MestReNova software and are reported relative to CDCl3 (δ 7.26). High-resolution mass spectra were provided by the California Institute of Technology Mass Spectrometry Facility. IR spectra were recorded on a Perkin Elmer Paragon 1000 Spectrometer and are reported in frequency of absorption (cm-1). Microwave reactions were conducted in a Biotage Initiator Microwave Synthesizer. NMR abbreviations: s = singlet, d = doublet, t = triplet, q = quartet, m = multiplet, bs = broad singlet, bd = broad doublet, dd = doublet of doublets, dt = doublet of triplet, dq = doublet of quartet, ddt = doublet of doublet of triplet.

Materials

All solvents were purchased from EMD Chemicals and Sigma-Aldrich. 4-iodophenol was bought from Acros chemicals, 4-bromo-3-chlorophenol was purchased from Alfa Aesar, sodium sulfate was acquired from Mallinckrodt, and potassium iodide and potassium carbonate were purchased from EM Science. Other chemicals were purchased from Sigma-Aldrich. All solvents and chemicals were used without further purification.

2-((2-chloroallyl)oxy)-1,3-dimethoxybenzene (**1a**)

0.6286 g of 2,6 dimethoxy-phenol (4.104 mmol) was dissolved in 46 mL of acetone in a 100 mL round bottom flask. 1.3392g of K_2CO_3 (9.69 mmol) and 75.4 mg of KI (0.45 mmol) were added to the solution as well as 0.491 g of 2,3-dichloroprop-1-ene (4.425 mmol). This mixture was allowed to reflux for 17 hours. The solution was filtered through celite and the solvent evaporated off. The product was dissolved in ethyl acetate (25 mL) and washed with a solution of KH_2PO_4 (10 mL), Na_2CO_3 (10 mL), and water (10 mL). Then it was dried over sodium sulfate and filtered, and the solvent evaporated off. Finally, the product was dried under high-vacuum and the product obtained as a red-brown oil in 93% yield. (872.9 mg, 3.83 mmol). ^{1}H NMR (500 MHz, $CDCl_3$): δ 7.00 (t, J = 8.4 Hz, 1H), 6.58 (d, J = 8.4 Hz, 2H), 5.73 (q, J =1.4 Hz, 1H), 5.39 (m, 1H), 4.57 (dd, J = 1.3, 0.9 Hz 2H), 3.85 (s, 6H). ^{13}C NMR (500 MHz, $CDCl_3$): δ 153.36, 137.44, 136.48, 123.98, 113.67, 105.33, 74.76, 56.13. IR (Thin Film, NaCl): 3002, 2939, 2838, 1637, 1598, 1495, 1479, 1379, 1298,

1254, 1215, 1185, 1173, 1113, 1031, 895, 839, 775, 733, 718 cm^{-1}. HRMS (EI+) m/z calculated for $C_{11}H_{13}O_3Cl$ $[M+H]^+$: 228.0553, found 228.0552.

4-(2-chloroallyl)-2,6-dimethoxyphenol (**2a**)

314 mg of **1a** (1.38 mmol) was added to a 2 mL microwave vial and dissolved in 1.3 mL of 1,2-dichlorobenzene. This solution was heated in a microwave reactor at 200°C for 30 minutes and at 195°C for an additional 40 minutes. The product was purified by silica gel chromatography (10:90 ethyl acetate:hexanes, R_f = 0.23) and isolated as a dark red oil in 70 % yield (221 mg, 0.97 mmol). ^{1}H NMR (500 MHz, $CDCl_3$): δ 6.46 (s, 2H), 5.44 (s, 1H), 5.26 (m, 1H), 5.14 (q, J = 1.2 Hz, 1H), 3.88 (s, 6H), 3.56-3.55 (m, 2H). ^{13}C NMR (500 MHz, $CDCl_3$): δ 147.0, 141.8, 133.7, 127.8, 113.5, 105.7, 56.3, 45.6. IR (Thin Film, NaCl): 3514, 2938, 2840, 1615, 1518, 1461, 1429, 1366, 1330, 1242, 1216, 1115, 1039, 976, 889, 832, 803, 723 cm^{-1}. HRMS (EI+) m/z calculated for $C_{11}H_{13}O_3Cl$ $[M+H]^+$: 228.0553, found 228.0554.

1-(allyloxy)-4-iodobenzene (**1b**)

1.3064 g of 4-iodophenol (5.94 mmol) was dissolved in 75 mL of acetone in a 100 mL round bottom flask. 1.8327g of K_2CO_3 (13.3 mmol) and 132 mg of KI (0.80 mmol) were added to the solution as well as 1.3 mL of allyl bromide (15.0 mmol). This mixture was refluxed for 3 hours. After that the solution was filtered through celite and the solvent evaporated off. The product was dissolved in ethyl acetate (30 mL) and washed with a solution of KH_2PO_4 (15 mL), Na_2CO_3 (15 mL), and water (15 mL). Then it was dried over sodium sulfate and filtered, and solvent evaporated off. Finally, the product was dried under high-vacuum and the product obtained as a light yellow oil in 90 % yield. (1.3862 g, 5.33 mmol). ^{1}H NMR (500 MHz, $CDCl_3$): δ 7.55 (d, J = 9.0 Hz, 2H), 6.69 (d, J = 9.0 Hz, 2H), 6.03 (ddt, J = 17.3, 10.5, 5.3 Hz, 1H), 5.40 (dq, J = 17.3, 1.6 Hz, 1H), 5.29 (dq, J = 10.5, 1.4 Hz, 1H), 4.50 (dt, J = 5.3, 1.5 Hz, 2H). ^{13}C NMR (500 MHz, $CDCl_3$): δ 158.4, 138.2, 132.8, 117.9, 117.2, 82.9, 68.8.

2-allyl-4-iodophenol (**2b**)

515.5 mg of **1b** (1.98 mmol) was dissolved in 1.4 mL of o-dichlorobenzene in a 2 mL microwave. This solution was heated in a microwave reactor at 188°C for 4.5 hours. The product was purified by silica gel chromatography (1:9 → 2:8 ethyl acetate:hexanes, R_f = 0.42 in 2:8 ethyl

acetate:hexanes) and isolated as a light yellow oil in 27% yield (141.3 mg, 0.54 mmol). ^{1}H NMR (500 MHz, $CDCl_3$): δ 7.42-7.40 (m, 2H), 6.59 (d, J = 8.9 Hz, 1H), 5.96 (ddt, J = 16.6, 10.3, 6.4 Hz, 1H), 5.20-5.14 (m, 2H), 4.98 (s, 1H), 3.35 (dt, J = 6.3, 1.4 Hz, 2H). ^{13}C NMR (500 MHz, $CDCl_3$): δ 154.0, 138.9, 136.6, 135.5, 128.1, 118.1, 117.2, 82.9, 34.7.

2-allyl-4-iodophenyl acetate (**3b**)

22.5 mg of **2b** (0.087 mmol) was dissolved in a 0.4 mL of pyridine in a small vial. 0.4 mL of acetic anhydride (4.2 mmol) was added to the vial and the solution allowed to stir at room temperature for 18 hours. The solvent was evaporated off under high vacuum and the product purified by silica gel chromatography (1:9 ethyl acetate:hexanes) and isolated as a clear oil in 92% yield (24 mg, 0.079 mmol). ^{1}H NMR (500 MHz, $CDCl_3$): δ 7.57-7.54 (m, 2H), 6.80 (d, J = 8.3 Hz, 1H), 5.85 (ddt, J = 16.8, 10.1, 6.6 Hz, 1H), 5.12-5.05 (m, 2H), 3.24 (bd, J = 6.6 Hz, 2H), 2.29 (s, 3H). ^{13}C NMR (500 MHz, $CDCl_3$): δ 169.0, 148.8, 139.2, 136.4, 134.9, 134.5, 124.4, 117.0, 90.4, 34.3, 20.9.

4-(allyloxy)-1-bromo-2-chlorobenzene (**1c**)

1.04 g of 4-bromo-3-chloro-phenol (5.01 mmol) was dissolved in 30 mL of acetone in a 100 mL round bottom flask. 1.1232g of K_2CO_3 (8.13 mmol) and 71.4 mg of KI (0.43 mmol) were added to the solution as well as 0.65 mL of allyl bromide (7.51 mmol). This mixture was refluxed for 3.5 hours, cooled to room temperature, filtered through celite, and purified by silica gel chromatography (10:90 ethyl acetate:hexanes, R_f = 0.66). The product was isolated as clear oil in 97 % yield (1.2079 g, 4.88 mmol). ^{1}H NMR (500 MHz, $CDCl_3$): δ 7.47 (d, J = 8.9 Hz, 1H), 7.02 (d, J = 2.9 Hz, 1H), 6.71 (dd, J = 8.9, 2.9 Hz, 1H), 6.05-5.97 (m, 1H), 5.43-5.38 (m, 1H), 5.33-5.30 (m, 1H), 4.52-4.50 (m, 2H). ^{13}C NMR (500 MHz, $CDCl_3$): δ 158.3, 134.8, 133.8, 132.4, 118.2, 116.7, 115.2, 113.0, 69.2. IR (Thin Film, NaCl): 3085, 2867, 1588, 1566, 1469, 1424, 1381, 1362, 1295, 1282, 1263, 1223, 1110, 1025, 1012, 999, 929, 902, 861, 839, 800 cm^{-1}. HRMS (EI+) m/z calculated for $C_9H_8OBr^{37}Cl$ [M+H]+: 247.9418, found 247.9420.

2-allyl-4-bromo-5-chlorophenol (**2c**)

1.4545 g of **1c** (5.9 mmol) was added to a 5 mL microwave vial and dissolved in 3 mL of dichlorobenzene. This solution was put under three vacuum-argon cycles and then heated in a microwave reactor at 180°C for 24 hours. The reaction produced the desired product along with its

isomer, 2-allyl-4-bromo-3-chlorophenol in a ratio of 1:2.4. The product was purified by silica gel chromatography (0:100 → 20:80 ethyl acetate:hexanes, R_f = 0.47 in 10:90 ethyl acetate: hexanes) and obtained as a light yellow oil after drying under high-vacuum. This reaction gave 28% yield of the desired product (0.41 g, 1.64mmol). ^{1}H NMR (500 MHz, $CDCl_3$): δ 7.32 (s, 1H), 6.94 (s, 1H), 5.99-5.91 (m, 1H), 5.42 (s, 1H), 5.20-5.14 (m, 1H), 5.18-5.17 (m, 1H), 3.36-3.33 (m, 2H). ^{13}C NMR (500 MHz, $CDCl_3$): δ 153.8, 135.1, 134.5, 132.6, 126.4, 117.6, 117.4, 112.8, 34.2. IR (Thin Film, NaCl): 3500, 3081, 2918, 1639, 1595, 1575, 1562, 1481, 1464, 1431, 1381, 1267, 1246, 1201, 1123, 997, 923, 879, 843, 798 cm^{-1}. HRMS (EI+) m/z calculated for $C_9H_8OBr^{37}Cl$ $[M+H]_+$: 247.9418, found 247.9414.

2-allyl-4-bromo-3-chlorophenyl acetate (**3c**)

85.1 mg of **2c** (0.344 mmol) was dissolved in a 0.5 mL of pyridine in a small vial. 0.5 mL of acetic anhydride (5.3 mmol) was added and the solution allowed to stir at room temperature for 22 hours. The solvent was evaporated off under high vacuum and the product purified by silica gel chromatography (1:9 ethyl acetate:hexanes) and isolated as a clear oil in 98% yield (96.4 mg, 0.333 mmol). ^{1}H NMR (500 MHz, $CDCl_3$): δ 7.48 (s, 1H), 7.19 (s, 1H), 5.87-5.79 (m, 1H), 5.14-5.11 (m, 1H), 5.10-5.06 (m, 1H), 3.24 (bd, J = 6.6 Hz, 2H), 2.29 (s, 3H).

1-allyl-5-bromo-4-chloro-2-methoxybenzene (**3d**)

49.9 mg of **2c** (0.202 mmol) was dissolved in 2.5 mL of acetone in a round bottom flask. Then 67.6 mg of K_2CO_3 (0.489 mmol) and 6.5 mg of KI (0.04 mmol) were added to the solution as well as 31 μL of iodomethane (0.50 mmol). This mixture was refluxed overnight, cooled to room temperature, filtered, and concentrated *in vacuo*, followed by purification by silica gel chromatography (10:90 ethyl acetate:hexanes). The product was isolated as clear oil in 56% yield (29.5 mg, 0.11 mmol). ^{1}H NMR (500 MHz, $CDCl_3$): δ 7.32 (s, 1H), 6.92 (s, 1H), 5.95-5.87 (m, 1H), 5.09-5.04 (m, 1H), 5.08-5.07 (m, 1H), 3.81 (s, 3H), 3.31-3.29 (m, 2H). ^{13}C NMR (500 MHz, $CDCl_3$): δ 156.9, 135.5, 133.8, 132.3, 129.4, 116.4, 112.5, 112.4, 55.8, 33.4.

2-(5-allyl-2-chloro-4-methoxyphenoxy)-5-(2-chloroallyl)-1,3-dimethoxy-benzene (**4d**)

16.7 mg of **3d** (63.9 μmol) was added to a small vial along with 15.2 mg of CuBr•SMe_2 (74 μmol) and 14.9 mg of K_2CO_3 (108 μmol). The vial was closed and put under three vacuum-argon cycles. 15.3 mg of **2a** (66.9 μmol) was dissolved seperately in 0.15 mL of pyridine and 0.30 mL of acetonitrile, and that solution was added to the small vial under a constant flow of argon via syringe. The reaction mixture was allowed to stir in a pre-heated oil bath at 75°C for 45 hours. The product was purified by silica gel chromatography (0:10 → 2:8 ethyl acetate:hexanes, R_f, product = 0.62 in 2:8 ethyl acetate:hexanes). The product was isolated as a white solid in 27.5% yield (7.2 mg, 17.6 μmol). ^{1}H NMR (500 MHz, $CDCl_3$): δ 6.89 (s, 1H), 6.51 (s, 2H), 6.35 (s, 1H), 5.85-5.77 (m, 1H), 5.30 (d, J = 0.8 Hz, 1H), 5.17 (dd, J = 2.1, 0.8 Hz, 1H), 4.94-4.87 (m, 1H), 4.92-4.91 (m, 1H), 3.78 (s, 3H), 3.76 (s, 6H), 3.62 (s, 2H), 3.20 (m, 2H). ^{13}C NMR (500 MHz, $CDCl_3$): δ 153.2, 152.0, 147.8, 141.3, 136.4, 134.3, 131.8, 127.6, 119.6, 116.1, 115.4, 113.8, 112.6, 106.5, 56.4, 56.1, 45.8, 33.7. HRMS (EI+) m/z calculated for $C_9H_8OBr^{37}Cl$ $[M+H]^+$: 408.0895, found 408.0888.

Attempted synthesis of 2-allyl-5-chloro-4-(4-(2-chloroallyl)-2,6-dimethoxyphenoxy)-phenyl acetate (**4c**) *that gave 4-(2-chloroallyl)-2,6-dimethoxyphenyl acetate*

30 mg of **3c** (0.104 mmol) was added to a small vial, along with 23.0 mg of CuBr•SMe_2 (0.112 mmol) and 20.8 mg of K_2CO_3 (0.15 mmol). The vial was then closed and put under three vacuum-argon cycles. 24.2 mg of **2a** (0.105 mmol) was dissolved seperately in 0.23 mL of pyridine and 0.46 mL of acetonitrile, and that solution was added to the small vial under a constant flow of Ar. The reaction mixture was allowed to stir in a pre-heated oil bath at 75°C for 48 hours. None of the desired product was isolated, but instead some 4-(2-chloroallyl)-2,6-dimethoxyphenyl acetate was observed by NMR. ^{1}H NMR (500 MHz, $CDCl_3$): δ 6.48 (s, 2H), 5.29 (bs, 1H), 5.19-5.18 (m, 1H), 3.81 (s, 6H), 3.59 (bs, 2.20), 2.33 (s, 3H).

REFERENCES

(1) Rasko, D. A; Sperandio, V. *Nat. Rev. Drug Discov.* **2010**, *9*, 117.

(2) World Health Organization. The Top 10 Causes of Death http://www.who.int/mediacentre/factsheets/fs310/en/index.html (accessed Mar 5, 2010).

(3) Payne, D. J. *Science* **2008**, *321*, 1644.

(4) Levy, S. B.; Marshall, B. *Nat. Med.* **2004**, *10*, S122.

(5) Lock, R. L.; Harry, E. J. *Nat. Rev. Drug Discov.* **2008**, *7*, 324.

(6) Jaiswal, R.; Beuria, T. K.; Mohan, R.; Mahajan, S. K.; Panda, D. *Biochemistry* **2007**, *46*, 4211.

(7) Domadia, P. N.; Bhunia, A.; Sivaraman, J.; Swarup, S.; Dasgupta, D. *Biochemistry* **2008**, *47*, 3225.

(8) Wang, J.; Galgoci, A.; Kodali, S.; Herath, K. B.; Jayasuriya, H.; Dorso, K.; Vicente, F.; González, A.; Cully, D.; Bramhill, D.; Singh, S. *J. Biol. Chem.* **2003**, *278*, 44424.

(9) Domadia, P.; Swarup, S.; Bhunia, A.; Sivaraman, J.; Dasgupta, D. *Biochem. Pharmacol.* **2007**, *74*, 831.

(10) Plaza, A.; Keffer, J. L.; Bifulco, G.; Lloyd, J. R.; Bewley, C. A. *J. Am. Chem. Soc.* **2010**, *132*, 9069.

(11) Choi, P. J.; Rathwell, D. C. K.; Brimble, M. A. *Tetrahedron Lett.* **2009**, *50*, 3245.

(12) Brimble, M. A.; Flowers, C. L.; Trzoss, M.; Tsang, K. Y. *Tetrahedron* **2006**, *62*, 5883.

(13) Van, T. N.; Debenedetti, S.; De Kimpe, N. *Tetrahedron Lett.* **2003**, *44*, 4199.

(14) An, J.; Bagnell, L.; Cablewski, T.; Strauss, C. R.; Trainor, R. W. *J. Org. Chem.* **1997**, *62*, 2505.

(15) Richey, Jr., H. G.; Domalski, M. S. *J. Org. Chem.* **1981**, *46*, 3780.

(16) Lin, Y.-L.; Cheng, J.-Y.; Chu, Y.-H. *Tetrahedron* **2007**, *63*, 10949.

(17) Tyman, J. H. P.; Payne, P. B. *J. Chem. Res.* **2006**, *2006*, 691.

(18) Gresser, M. J.; Wales, S. M.; Keller, P. A. *Tetrahedron* **2010**, *66*, 6965.

(19) Roy, B.; Dasgupta, S.; Rajput, V. K.; Mukhopadhyay. *J. Carbohydr. Chem.* **2008**, *27*, 1.

(20) Prakash, G. K. S.; Mathew, T.; Hoole, D.; Esteves, P. M.; Wang, Q.; Rasul, G.; Olah, G. A. *J. Am. Chem. Soc.* **2004**, *126*, 15770.

(21) Smith, J. R. L.; McKeer, L. C.; Taylor, J. M. *J. Chem. Soc. Perkin Trans. II* **1988**, 385.

(22) Emmanuel-Giota, A. A.; Fylaktakidou, K. C.; Hadjipavlou-Litina, D. J.; Litinas, K. E.; Nicolaides, D. N. *J. Heterocycl. Chem.* **2001**, *38*, 717.

(23) Murphy, J. M.; Liao, X.; Hartwig, J. F. *J. Am. Chem. Soc.* **2007**, *129*, 15434.

(24) Rudroff, F.; Rydz, J.; Ogink, F. H.; Fink, M.; Mihovilovic, M. D. *Adv. Synth. Catal.* **2007**, *349*, 1436.

(25) Ren, X.; She, X.; Peng, K.; Su, Y.; Xie, X.; Pan, X. *J. Chem. Res.* **2003**, *2003*, 358.

(26) Nicolaou, K. C.; Chu, X.-J.; Ramanjulu, J. M.; Natarajan, S.; Brase, S.; Rubsam, F.; Boddy, C. N. C. *Angew. Chem. Int. Ed.* **1997**, *36*, 1539.

(27) Boger, D. L.; Sakya, S. M.; Yohannes, D. *J. Org. Chem.* **1991**, *56*, 4204.

(28) Wipf, P.; Jung, J. K. *J. Org. Chem.* **2000**, *65*, 6319.

(29) Kurti, L.; Czakó, B. *Strategic Applications of Named Reactions in Organic Synthesis*; Elsevier Inc.: Burlington, 2005.

(30) Chao, W.; Weinreb, S. M. *Org. Lett.* **2003**, *5*, 2505.

(31) Chao, W.; Meketa, M. L.; Weinreb, S. M. *Synthesis* **2004**, 2058.

(32) White, D. E.; Stewart, I. C.; Grubbs, R. H.; Stoltz, B. M. *J. Am. Chem. Soc.* **2008**, *130*, 810.

(33) Macnaughtan, M. L.; Gary, J. B.; Gerlach, D. L.; Johnson, M. J. A.; Kampf, J. W. *Organometallics* **2009**, *28*, 2880.

(34) Sashuk, V.; Samojłowicz, C.; Szadkowska, A.; Grela, K. *Chem. Commun.* **2008**, 2468.

(35) Dixon, D. J.; Foster, A. C.; Ley, S. V. *Org. Lett.* **2000**, *2*, 123.

(36) Banwell, M. G.; McRae, K. J. *Org. Lett.* **2000**, *2*, 3583.

(37) Moreau, S.; Varache-Lembege, M.; Larrouture, S.; Fall, D.; Neveu, A.; Deffieux, G.; Vercauteren, J.; Nuhrich, A. *Eur. J. Med. Chem.* **2002**, *37*, 237.

(38) Tipparaju, S. K.; Muench, S. P.; Mui, E. J.; Ruzheinikov, S. N.; Lu, J. Z.; Hutson, S. L.; Kirisits, M. J.; Prigge, S. T.; Roberts, C. W.; Henriquez, F. L.; Kozikowski, A. P.; Rice, D. W.; McLeod, R. L. *J. Med. Chem.* **2010**, *53*, 6287.